

Argonne National Laboratory

**AN EXPERIMENTAL INVESTIGATION
OF TWO-PHASE, TWO-COMPONENT FLOW
IN A HORIZONTAL,
CONVERGING-DIVERGING NOZZLE**

by

Joseph A. Vogrin, Jr.

LEGAL NOTICE

This report was prepared as an account of Government sponsored work. Neither the United States, nor the Commission, nor any person acting on behalf of the Commission:

- A. Makes any warranty or representation, expressed or implied, with respect to the accuracy, completeness, or usefulness of the information contained in this report, or that the use of any information, apparatus, method, or process disclosed in this report may not infringe privately owned rights; or*
- B. Assumes any liabilities with respect to the use of, or for damages resulting from the use of any information, apparatus, method, or process disclosed in this report.*

As used in the above, "person acting on behalf of the Commission" includes any employee or contractor of the Commission, or employee of such contractor, to the extent that such employee or contractor of the Commission, or employee of such contractor prepares, disseminates, or provides access to, any information pursuant to his employment or contract with the Commission, or his employment with such contractor.

ARGONNE NATIONAL LABORATORY
9700 South Cass Avenue
Argonne, Illinois 60440

AN EXPERIMENTAL INVESTIGATION OF TWO-PHASE,
TWO-COMPONENT FLOW IN A HORIZONTAL,
CONVERGING-DIVERGING NOZZLE

by

Joseph A. Vogrin, Jr.
Reactor Engineering Division
and
Associated Midwest Universities

July 1963

This report is one of a series that describes heat-transfer and fluid-flow studies performed at Argonne under a program sponsored jointly by the Associated Midwest Universities and the Argonne National Laboratory.

The earlier reports in this series are ANL-6625, ANL-6667, ANL-6674, ANL-6710, ANL-6734, and ANL-6738.

Reproduced from Thesis Submitted in Partial Fulfillment of the Requirements for the Degree of Master of Science in Mechanical Engineering in the Graduate School of Illinois Institute of Technology.

Operated by The University of Chicago
under
Contract W-31-109-eng-38
with the
U. S. Atomic Energy Commission

TABLE OF CONTENTS

	Page
LIST OF TABLES.	iv
LIST OF ILLUSTRATIONS.	v
PREFACE.	vii
CHAPTER	
I. INTRODUCTION.	1
Purpose of the Investigation	1
Literature Survey	2
II. EXPERIMENTAL APPARATUS AND PROCEDURE	6
Water-supply System	6
Air-injection System	6
Air-Water Mixer	6
Experimental Nozzle	9
Air-Water Separator	9
Air- and Water-metering Orifices	9
Temperature Measurements	9
Pressure Measurements	12
Equipment for Void Fraction Measurement	12
1. Radioactive Source	14
2. Scintillation Crystal and Photomultiplier Tube Assembly	14
3. Instrumentation	14
4. The Traversing Drive Mechanism	21
Experimental Procedure	21
III. PROBLEM DISCUSSION AND ANALYTICAL DEVELOPMENT	23
Analytical Development - General	23
Measurement of the Void Fraction	26
IV. DATA ANALYSIS, RESULTS AND DISCUSSION . . .	29
Data Analysis	29
Pressure Profiles	31

TABLE OF CONTENTS

	Page
Slip Ratios along the Nozzle Length	31
Data Repetition	36
Flow Mechanisms, Void Distribution, and Change of Flow Regime	42
Exit Characteristics	46
Correlation of Data - Empirical Relationships	54
Optimum Nozzle Design	60
Theoretical Models Used in Predicting Nozzle Characteristics	61
Nozzle Efficiency	63
Critical Mass Velocity and Critical Pressure	65
Conclusions	70
Suggested Further Considerations	72
APPENDICES	
A. FLOW RATE DETERMINATION	73
B. ANALYTICAL DEVELOPMENT - GAMMA-RAY- ATTENUATION METHOD	74
C. DETERMINATION OF INSTRUMENTATION CONSTANT K.	82
D. ANALYSIS OF DENSITY EFFECT ON FULL AND EMPTY READINGS FOR VOID FRACTION DETERMINATION.	84
E. DETERMINATION OF THE TRUE VOID FRACTION DISTRIBUTION ALONG THE NOZZLE CENTERLINE.	87
F. ANALYTICAL DEVELOPMENT OF ELLIOTT'S NOZZLE EFFICIENCY.	90
G. CRITICAL MASS VELOCITY	98
H. TABULATED DATA AND RESULTS.	102
 BIBLIOGRAPHY.	 124
NOMENCLATURE	127

LIST OF TABLES

Table	Subject	Page
1-39	Tabulated Data and Results	102-121
40	Mass Velocities	122
41	Nozzle Efficiencies	123

LIST OF ILLUSTRATIONS

Figure	Title	Page
1	Overall View of Test Facility	7
2	Schematic Diagram of Experimental Loop.	8
3	Converging-Diverging Nozzle	10
4	Nozzle and Traverse Equipment	11
5	Manometer Layout	13
6	Schematic Diagram of Gamma-Ray Attenuation Equipment - Elevation View	15
7	Holder and Shield for Thulium-170 Source	16
8	Scintillation Crystal and Photomultiplier Tube Assembly	17
9	Lead Shielding for Scintillation Crystal and Photomultiplier Tube Assembly	18
10	$\frac{1}{16}$ by $\frac{1}{8}$ -in. Lead Window	19
11	Negative High-voltage Supply, Linear Current Amplifier, and Brown Electronik Recorder	20
12	Typical Empty, Full, and Two-phase Tracings.	27
13	Typical Compressible-type Pressure Profiles; $M_\ell \cong 0.7$	32
14	Typical Compressible-type Pressure Profiles; $M_\ell \cong 0.5$	33
15	Typical Compressible-type Pressure Profiles; $M_\ell \cong 0.3$	34
16	Comparison of Compressible- and Incompressible- type Pressure Profiles	35
17	Slip Ratios along the Nozzle Length; $M_\ell \cong 0.7$	37
18	Slip Ratios along the Nozzle Length; $M_\ell \cong 0.5$	38
19	Slip Ratios along the Nozzle Length; $M_\ell \cong 0.3$	39
20	Data Repetition Comparison - Pressure Profile.	40
21	Data Repetition Comparison - Void Fractions	41
22	Steam-Water System Flow Pattern Chart	43

LIST OF ILLUSTRATIONS (Continued)

Figure	Title	Page
23	Exit Half-cross-sectional Void Fraction Distribution.	45
24	Nozzle Exit Characteristics for Water Flow Rate = 0.701 lb/sec	47
25	Nozzle Exit Characteristics for Water Flow Rate = 0.498 lb/sec	48
26	Nozzle Exit Characteristics for Water Flow Rate = 0.303 lb/sec	49
27	Nozzle Exit Characteristics for Water Flow Rate = 0.219 lb/sec	50
28	Nozzle Exit Characteristics for Water Flow Rate = 0.155 lb/sec	51
29	Nozzle Exit Acceleration Factors	53
30	Exit Quality-Pressure Ratio Correlation	55
31	Exit Slip Ratio-Pressure Ratio Correlation; $\alpha < 0.85$	57
32	Exit Slip Ratio-Pressure Ratio Correlation; $\alpha > 0.85$	59
33	Faletti and Moulton ⁽²⁰⁾ Results - Effect of Back Pressure on the Profile, 20.5% Steam	68
34	Comparison of Vogrin and Faletti's Results	69
35	Gas, Liquid, and Wall Thicknesses as Seen by Radiation through the $\frac{1}{16}$ -in. Lead Window in a Typical Nozzle Cross Section.	76
36	Two-phase Cross Section; Annular Distribution Shown for Analysis Simplicity Only	80
37	Cross Section of a Circular Channel	88
38	Elliott's Schematic Diagram for a Two-Component Power Conversion Cycle	91

PREFACE

This investigation was conducted to determine the effects of accelerating a liquid phase by a gaseous phase in a converging-diverging nozzle in the low-quality region for a two-component (air-water) system. The project was initiated under the auspices of Argonne National Laboratory in conjunction with the Associated Midwest Universities.

The author expresses his gratitude to his advisor, Dr. R. A. Budenholzer, to Dr. M. Petrick and the Heat Engineering Section of Argonne National Laboratory, to Dr. J. H. Roberson of the Associated Midwest Universities, to E. Gunchin, S. Bonk, and D. Quinn for their assistance in constructing the test apparatus, and to M. Gats and Argonne's Graphic Arts Division for their photographic assistance.

CHAPTER I INTRODUCTION

Purpose of the Investigation

A considerable amount of effort is now being expended in the two-phase (liquid-gas) flow area. Two-phase mixtures are met repeatedly in everyday applications such as refrigeration cycles, power plants, and, more precisely, in compressors, condensers, evaporators, and boilers. More recently, the study of two-phase mixtures has become a very important portion of nuclear reactor research and space rocket technology.

Two-phase studies have been performed involving many various geometrical configurations. One of these configurations, a converging-diverging nozzle, has been thoroughly investigated in the high-quality region, but very little information is available in the low-quality region. Interest in low quality, one- and two-component two-phase flow in converging-diverging nozzles has recently been stimulated by space applications, two of which are: 1) jet pumps for rocket engines, and 2) a magnetohydrodynamic electrical power conversion cycle proposed by Elliott.^{(1)*}

This report describes an investigation of the flow characteristics in a horizontal, converging-diverging nozzle for a two-phase, two-component system. The working media tested were systems of air and water. The primary consideration was to determine the effects of accelerating the liquid phase by the gaseous phase. These effects were measured experimentally in terms of nozzle exit water velocity, exit slip ratio, and exit acceleration factor. The slip ratio is defined as the ratio of gas velocity to liquid velocity, and the acceleration factor as the ratio of the two-phase exit water velocity to the exit water velocity that would have been obtained if the water phase only had been accelerated through the nozzle at the same water mass rate of flow as the

*For all numbered references see bibliography.

two-phase condition. In order to determine these values, however, an accurate method had to be employed to determine the average cross-sectional void fraction (ratio of gas volume to total mixture volume). The method used here was a gamma-ray-attenuation technique.

For either laminar, turbulent, or transition-type flow, the velocity at the center of a channel tends to be greater than the velocity in a region close to the wall because of viscosity effects. However, no attempt was made in this investigation to determine velocity profiles and, therefore, slip ratio and acceleration factor profiles across the cross section. Thus average cross-sectional values only were determined.

Literature Survey

Rapid advances have been accomplished in the study of two-phase, low-quality flow in the past twenty years. Study in this area is being accelerated in connection with nuclear reactor technology. Recently, study has been directed toward actual flow mechanisms and the experimental measurement of existing void fractions. No attempt will be made to survey all the literature on two-phase studies, but only that which is most directly concerned with the scope of this report.

Numerous methods have been employed to measure void fractions experimentally. McManus⁽²⁾ inserted a probe into the flow path in an attempt to determine the position of the interface between a gas and a liquid in annular-type flow. Griffith, *et al.*⁽³⁾ investigated voids for boiling water in a transparent channel by photographing the two-phase flow and determining the void fraction from the bubble size. Johnson and Abou-Sabe⁽⁴⁾ used simultaneously closing valves at the entrance and exit sections of a channel and determined the average void by measuring the volume of each phase present. Petrick⁽⁵⁾ developed a traversing technique for measuring void fractions by the gamma-ray-attenuation method. He applied this technique to rectangular flow channels and found that the measured voids differed from the

actual voids by an average of 7.3 per cent, the measured voids being determined by the use of Lucite mockups to represent various types of flow regimes. Richardson⁽⁶⁾ furthered the work of Petrick and investigated circular channels, also using Lucite mockups of various flow regimes, and was able to measure voids within an average of 10.6 per cent for one-in.-diameter channels and 11.1 per cent for $\frac{1}{2}$ -in.-diameter channels.

Research efforts at Purdue's Jet Propulsion Laboratory on rocket engine jet pumps included some study of two-phase flow in nozzles. Reese and Richard⁽⁷⁾ investigated liquid nitrogen-gaseous nitrogen and liquid nitrogen-gaseous helium flow media. They injected the two phases at an approximately 400°F temperature differential and assumed: 1) perfect thermal mixing with no temperature differential between phases throughout the expansion process, 2) isentropic, adiabatic flow, 3) slip ratio equal to unity (that is, liquid local velocity equal to gaseous local velocity), and 4) steady, one-dimensional flow so that the energy and continuity equation apply between nozzle inlet and exit. Applying these assumptions, they predicted the nozzle exit mixture velocity. A liquid exit velocity was calculated from experimental thrust measurements assuming all the thrust was a result of the liquid momentum. The ranges investigated were 1-14 per cent quality at a constant liquid inlet pressure of 500 psig. They found the measured liquid exit velocity to be within 88-90 per cent of the predicted value for the helium-liquid nitrogen system and within 70-80 per cent of the predicted value for the nitrogen-liquid nitrogen system. On the basis of these results, they claimed that thermal equilibrium or a condition very close to thermal equilibrium existed throughout the expansion process.

Richard⁽⁸⁾ continued the work on an air-water mixture, injecting at a constant liquid pressure of 500 psig and a quality range of 1-30 per cent, with the liquid temperature initially at 70°F and the air

temperature initially at 50°F. For the air-water system he was able to predict within 80-90 per cent the measured liquid exit velocity.

Elliott^(1,9) also experimented with two-phase flow through nozzles at Purdue's Jet Propulsion Laboratory with an air-hot water system. He proposed an ideal nozzle based on an isentropic expansion and a slip ratio of unity, and calculated exit velocities by means of the energy equation and the First Law of Thermodynamics. Velocities were measured experimentally (for expansions from 500 psig to atmospheric conditions) and ranged from 450 ft/sec for a water-air ratio of 25 to 900 ft/sec for a ratio of 5. A nozzle efficiency was defined as the ratio of the measured energy to the energy calculated for the ideal nozzle, and for the conditions tested this ratio was about 0.70.

Recently, four theses were published by the University of California's Ernest O. Lawrence Radiation Laboratory. Neusen,⁽¹⁰⁾ Maneely,⁽¹¹⁾ Brown,⁽¹²⁾ and Fiedler⁽¹³⁾ conducted experiments with two-phase, steam-water flow through converging-diverging nozzles. Test inlet conditions ranged from 100-1300 psia. Neusen, Maneely, and Fiedler varied the inlet qualities from 0 to 28 per cent, and Brown investigated subcooled inlet conditions from 0 to 254°F subcooling. The flow continued to expand past the throat area for all of the quality ranges investigated. An attempt was made to predict mass flow rates, based on inlet conditions, by means of various flow models. The best agreement with actual flow rates was obtained from a homogeneous model which assumed 1) slip ratio of unity, 2) cross-sectional thermal and pressure equilibrium, and 3) isentropic expansion. This model led to predictions of mass flow rates within 15 per cent for qualities above 5 per cent. The various flow models were also used to predict thrust, but were not very accurate for low qualities. Fiedler was unsuccessful in an attempt to predict the location of the compression zone in the pressure profiles by relating it to perfect gas theory.

Hering and Vogrin⁽¹⁴⁾ conducted air-water nozzle experiments and attempted to determine actual water and air exit velocities by

employing a "one-shot," gamma-ray-attenuation method of measuring void fractions for conditions of 10-100 psig inlet pressures and qualities of 0.3-1.8 per cent. They were unsuccessful because of the nozzle design, poor mixing, and considerable error introduced by the "one-shot" method.

Recently, Muir and Eichhorn⁽¹⁵⁾ investigated air-water flow in a converging-diverging nozzle. The ranges investigated were inlet pressures from 20-90 psia and qualities from 0.013-0.548 per cent. The throat pressure was maintained close to atmospheric for all tests. The nozzle design consisted of a rectangular cross section, the top walls being made of aluminum and the side walls of Plexiglas. A Fastax camera (exposing 500 frames/sec) filmed the flow through the nozzle. Primary interest was at the throat region. For the conditions tested, a bubble-flow regime was reported up to qualities of 0.154 per cent, after which an annular-type flow existed. For the bubble-flow regime, bubble velocity and air velocity were determined from the high-speed pictures, and this velocity was compared with a velocity calculated from the continuity equation based on a slip ratio of one. The agreement was excellent. From the measured air velocities, the average cross-sectional water velocities, slip ratios, and void fractions were calculated by the continuity equation. Slip ratios ranged from 1.2 to 1.4.

Except for the latter two investigations,^(14,15) a search of the literature revealed that no attempts have been made to investigate the flow mechanism in a two-phase nozzle, that is, with regard to flow regimes, existing voids, or slip ratios.

CHAPTER II

EXPERIMENTAL APPARATUS AND PROCEDURE

An experimental apparatus was designed and constructed for the purpose of analyzing two-phase, air-water flow in a converging-diverging nozzle. The equipment consisted of a water-supply system, an air-injector system, a mixing chamber, a two-phase nozzle, a water reservoir with separator, and equipment for measuring temperatures, mass flow rates, pressures, and void fractions. An overall view of the experimental facility is shown in Fig. 1, and the schematic diagram in Fig. 2.

Water-supply System

A 100-gal reservoir which served as the water source and sink for the test procedures was supplied with ordinary tap water. The water was circulated through the loop by a centrifugal pump of 40-gpm capacity. Water flow rates were regulated by a pump bypass valve and a more sensitive valve in the pump-discharge line. The pump was internally cooled by the circulating water which, in turn, was cooled by laboratory water through cooling coils in the reservoir.

Air-injection System

The air was supplied by compressed laboratory air with a maximum supply pressure of 100 psig. The air pressure was regulated by two control valves with a constant upstream pressure maintained by a 125-psi Nogren air-regulator valve.

Air-Water Mixer

Air was injected and very finely dispersed in a horizontal direction through a 4-in.-diameter porous glass disk into a 4-in.-diameter mixing chamber. The water entered the chamber at a 45° angle with the plane of the air stream and in an upward direction, so that it deflected off the top wall of the chamber and then down at all angles into the dispersed air stream, where sufficient mixing occurred.

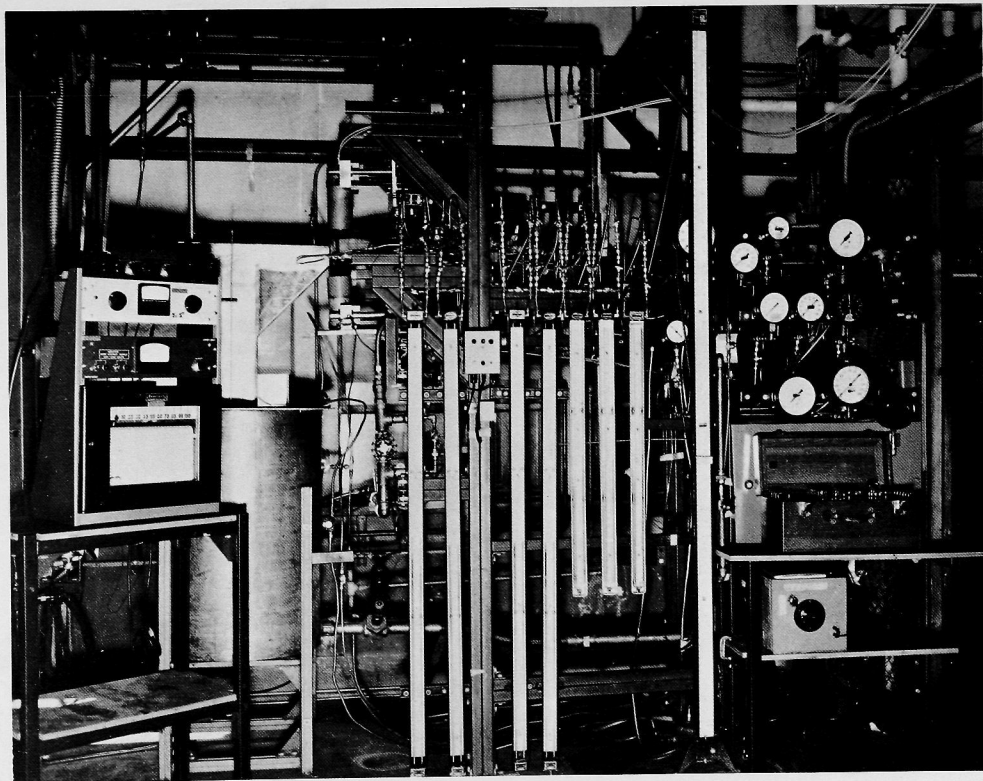


Fig. 1. Overall View of Test Facility

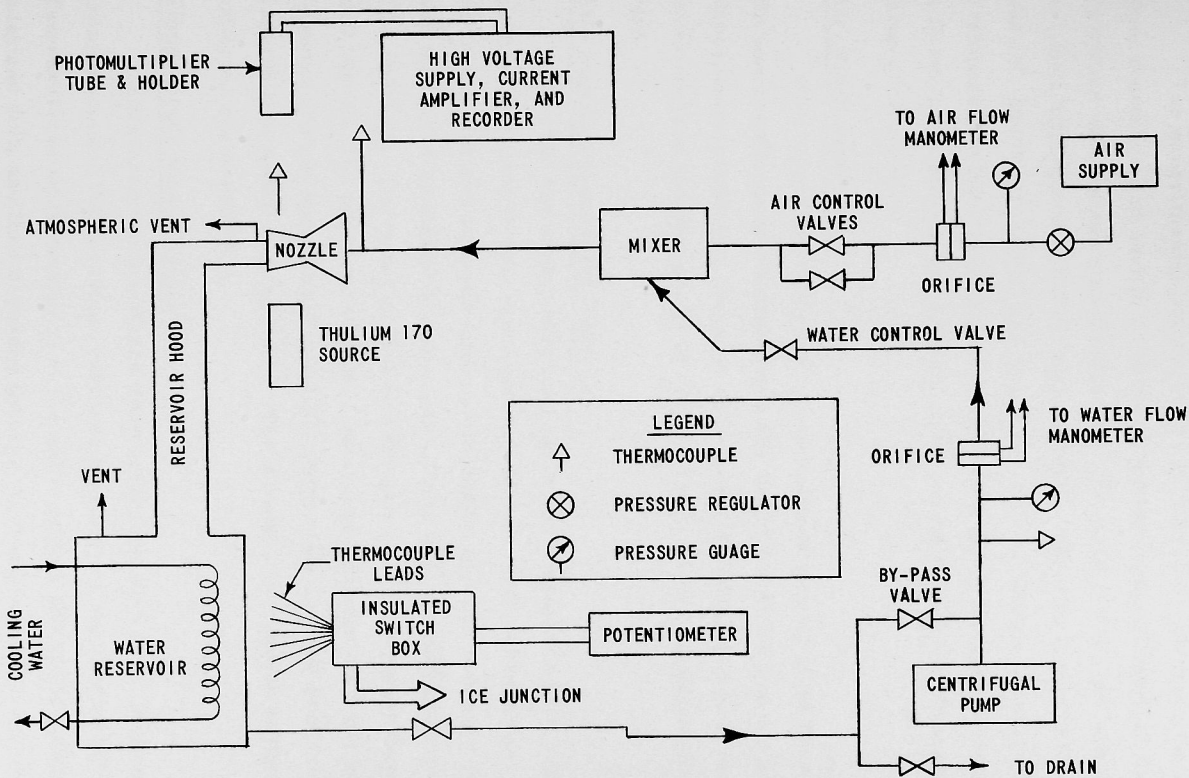


Fig. 2. Schematic Diagram of Experimental Loop

Experimental Nozzle

The experimental nozzle, shown in Figs. 3 and 4, was a DeLaval type, constructed of stainless steel and having a conical internal configuration with the internal diameters of the inlet, throat, and exit equal to 1.002, 0.2034, and 0.502 in., respectively. The converging half angle was 15° , and the diverging half angle was 3.5° . Thirteen pressure and 2 temperature taps were located horizontally along the nozzle length. A Pyrex glass viewer was located at the nozzle exit so that flow patterns could be seen.

Air-Water Separator

The separation of the two-phase mixture flowing from the nozzle was readily accomplished, since the water reservoir was always at atmospheric conditions. Because of its lower density, air rose above the water surface and passed out of the reservoir through an atmospheric vent.

Air- and Water-metering Orifices

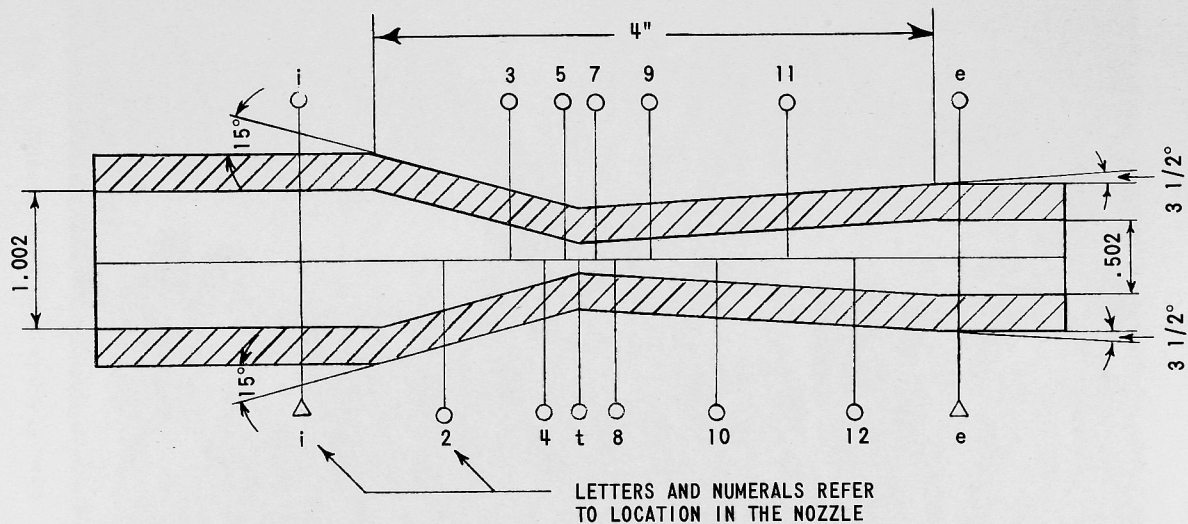
The air and water mass flow rates were measured with thin-plate orifices and U-tube manometers. The air orifice had vena-contracta taps and an inner diameter of 0.2705 in. The pressure drop was measured by means of manometer fluids with specific gravities of 1.25 and 2.95. The water orifice had flanged taps and an inner diameter of 0.343 in. The pressure drop was measured with mercury and manometer fluid of specific gravity 2.95. Both orifices were fabricated according to ASME standards.⁽¹⁶⁾ For a further discussion of these orifices, see Appendix A.

Temperature Measurements

All system temperatures were measured with 24 or 30 gauge iron-constantan thermocouple wire with a reference junction of 32°F . Temperatures were measured at the water orifice and at the nozzle inlet and exit, and then recorded through an insulated switch box on a

○ REFERS TO PRESSURE MEASURING STATION

△ REFERS TO THERMOCOUPLE LOCATION



FULL SCALE

THROAT DIAMETER = .2034
ALL DIMENSIONS ARE IN INCHES

Fig. 3. Converging-Diverging Nozzle

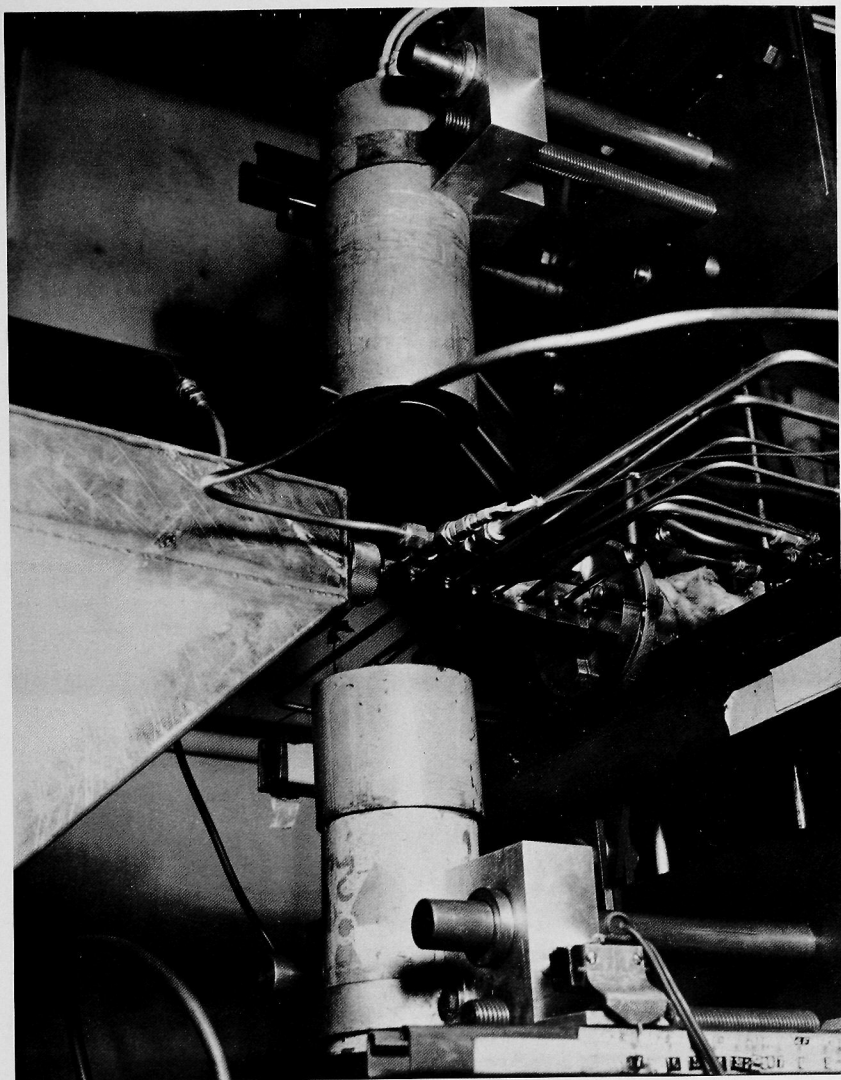


Fig. 4. Nozzle and Traverse Equipment

manually operated potentiometer. All thermocouples were calibrated in a hypsometer at temperatures corresponding to regulated steam-saturation pressures.

Pressure Measurements

Pressures were measured with Bourdon-type gauges at the following locations: water-pump discharge, air orifice, and positions i, 2, 3, 4, 5, t, and 7 (see Fig. 3) along the nozzle length. U-tube manometers were installed to measure pressure differentials at positions 8, 9, 10, 11, 12, and e along the nozzle length. The reference leg of each manometer was connected to a pressure vessel, as shown in Fig. 5. Pressure was built up in the vessel through the laboratory water-supply line. When the desired pressure was obtained in the vessel, the water supply was closed off and a constant pressure was maintained in the vessel. The pressure in the vessel was measured by a U-tube manometer with one leg open to the atmosphere. Thus system pressures were determined by the following relationship:

$$P_n = P_{\text{vessel}} + P_{\text{atm}} - 0.453\Delta H \quad ,$$

where

P_n = pressure at a specific nozzle location

P_{vessel} = pressure in the pressure vessel

P_{atm} = atmospheric pressure

0.453 = conversion factor from inches to psi for mercury under water

ΔH = manometer differential in inches of mercury.

Equipment for Void Fraction Measurement

The equipment for measuring voids consisted of: 1) a radioactive thulium-170 source, 2) a thulium-activated sodium iodide scintillation crystal and photomultiplier tube, 3) instrumentation, and 4) the traversing drive mechanism. The gamma rays emitted from the

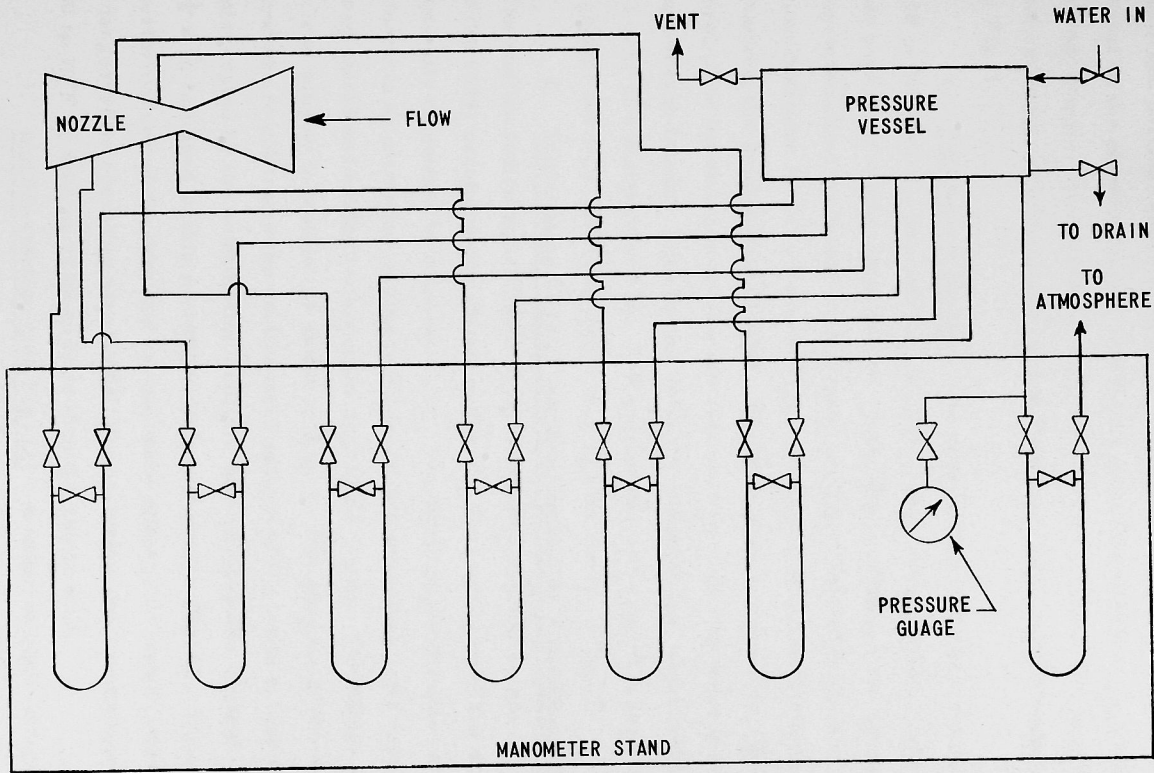


Fig. 5. Manometer Layout

radioactive source were absorbed in part by the test section. The unabsorbed portion impinged upon the scintillation crystal, producing a signal in the photomultiplier tube which received voltage from a high-voltage supply. The signal was amplified by a linear current amplifier and recorded on a Brown Elektronik Recorder, as shown schematically in Fig. 6.

1. Radioactive Source - The source material was a thulium-170 pellet having a half-life of 129 days. The energy spectrum showed two peaks, at 53 kev and at 84 kev. Since the accuracy of the gamma-ray-attenuation technique is dependent upon the transmission of a monoenergetic beam, all low-energy rays had to be prevented from reaching the scintillation crystal. This was done by inserting a $\frac{1}{32}$ -in. steel plate between the source and test section to absorb most of the low-energy beams. Initially the strength of the thulium source was 12 r/hr at a distance of 2 in. The source was contained in a lead cylinder (of 4-in. diameter and 6 in. long), as shown in Fig. 7.

2. Scintillation Crystal and Photomultiplier Tube Assembly - The sodium iodide scintillation crystal and photomultiplier tube (RCA 5819) assembly are shown in Fig. 8. The crystal and tube were optically connected by a Lucite plate. The whole assembly was enclosed in an aluminum casing to block out any impinging light rays. A lead shield and holder enclosed the aluminum casing. The holder with a lead window in position is shown in Fig. 9. The purpose of the window was to collimate the unattenuated portion of the beam before it was intercepted by the scintillation crystal. The rectangular window ($\frac{1}{8} \times \frac{1}{16}$ in.) used in this investigation is pictured in Fig. 10. Since the performances of the tube and crystal were affected by temperature changes while operating above 90°F, the assembly was maintained at 60 to 70°F by cooling coils embedded in the shield wall.

3. Instrumentation (see Fig. 11) - A negative high-voltage supply (HVP5-61511; range, 500-1500 v) powered the photomultiplier

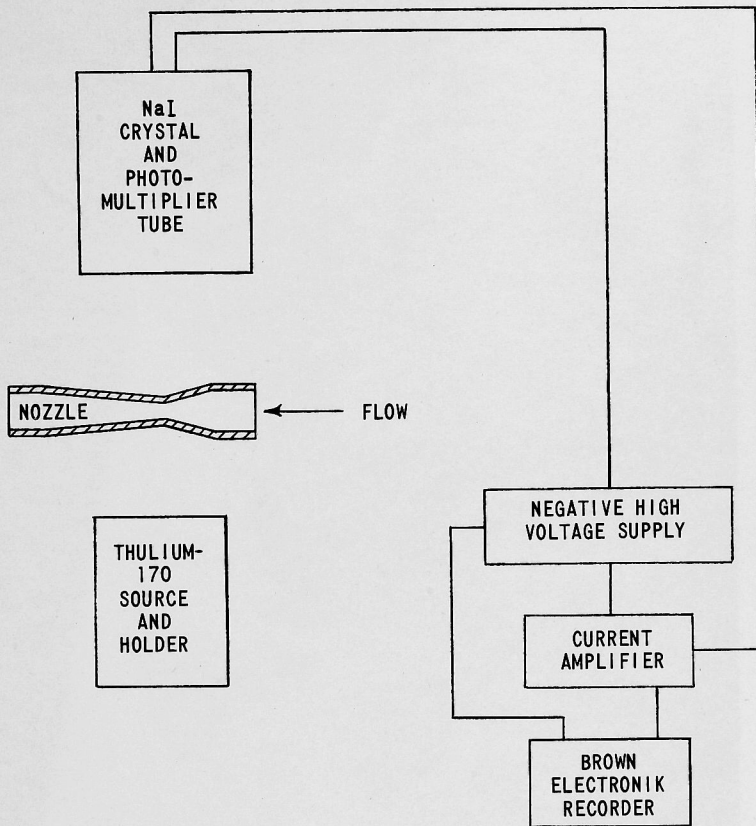


Fig. 6. Schematic Diagram of Gamma-Ray Attenuation Equipment - Elevation View

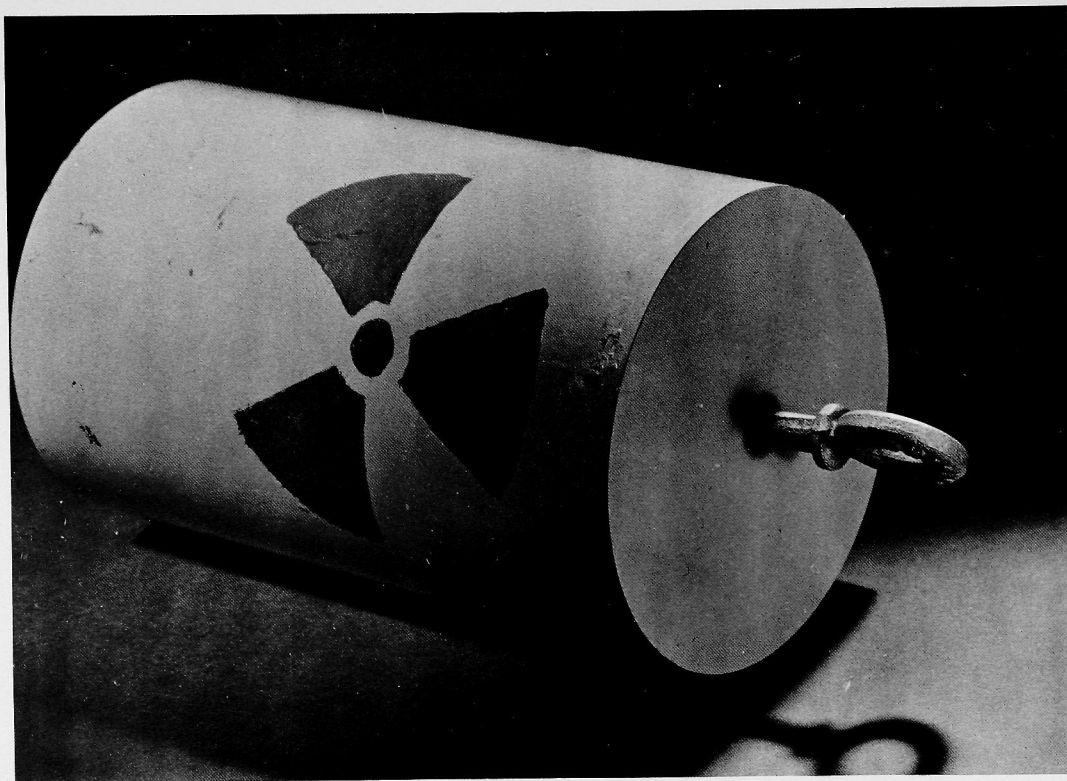


Fig. 7. Holder and Shield for Thulium-170 Source

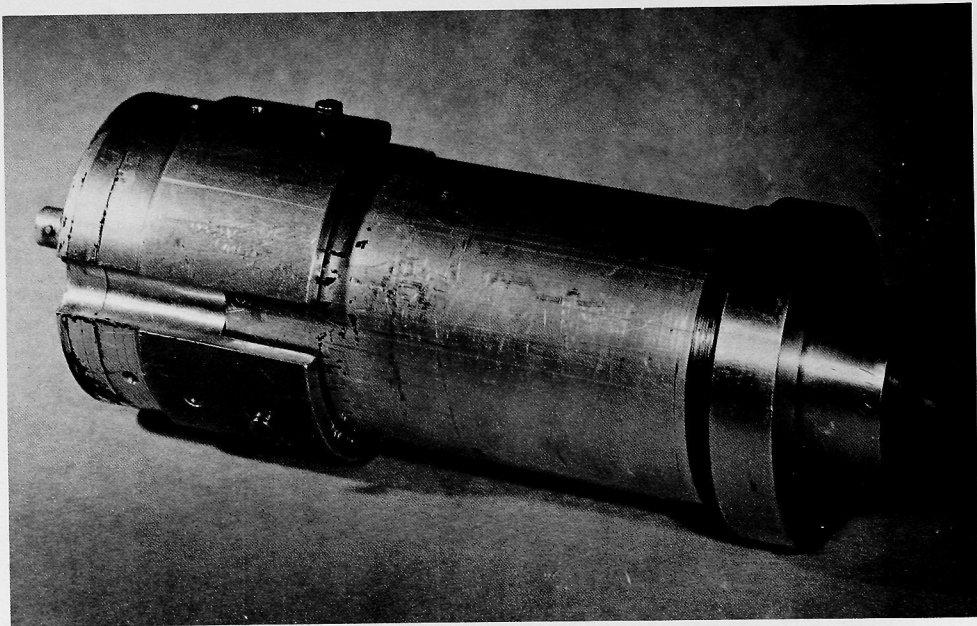


Fig. 8. Scintillation Crystal and Photomultiplier Tube Assembly

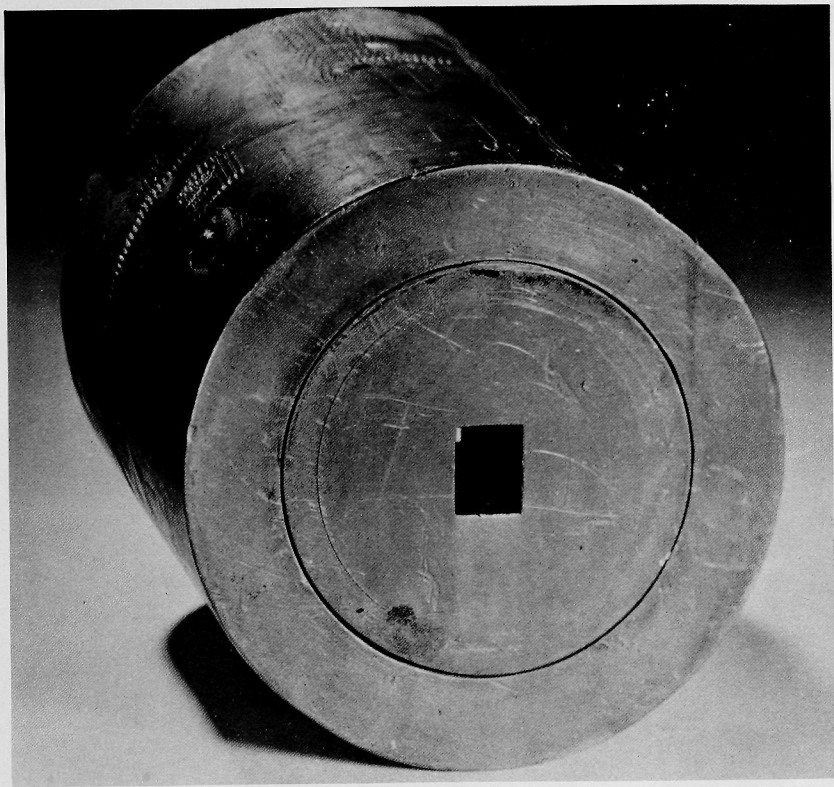


Fig. 9. Lead Shielding for Scintillation Crystal and Photomultiplier Tube Assembly



Fig. 10. $\frac{1}{16}$ by $\frac{1}{8}$ -in. Lead Window

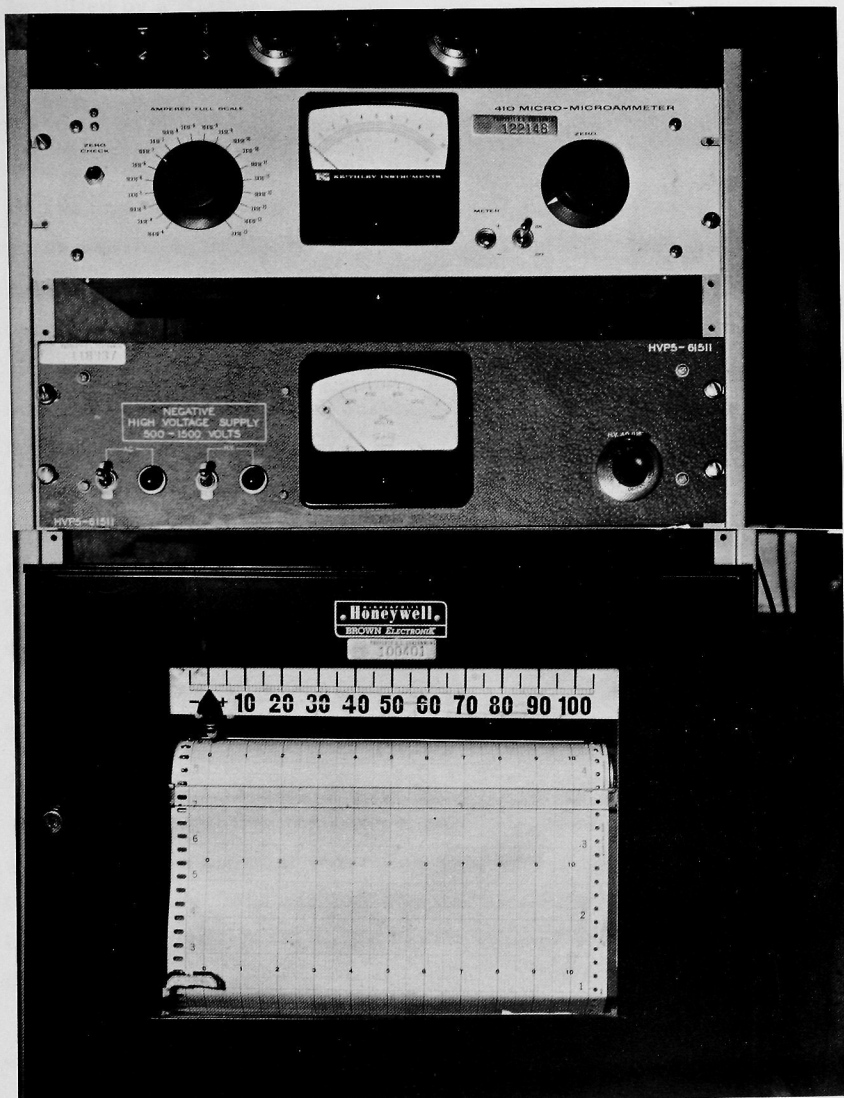


Fig. 11. Negative High-voltage Supply, Linear Current Amplifier, and Brown Elektronik Recorder

tube. The signal produced in the tube by the unattenuated radiation was amplified by a Kiethley current amplifier (scale range, $10 \times 10^{-4} - 3 \times 10^{-13}$ amp) and recorded on a Brown Electronik Recorder (153 x 16-V-II-III-156) having a $\frac{1}{4}$ -sec response time.

4. The Traversing Drive Mechanism - The traversing mechanism, pictured in Fig. 4, consisted of a two-way drive system. The source and tube assembly were mounted on separate aluminum blocks which were simultaneously driven horizontally along the nozzle length by lead screws through a set of worm gears by a constant-speed, 60-rpm Bodine motor. The 60-rpm motor was mounted on the back side (not shown in Fig. 4) of the upper vertical aluminum plate. The lead screws rotated through bushings on the aluminum plates. Thus, the plates remained stationary as the 60-rpm motor rotated, and the source and sink mounting blocks moved. The plates were suspended from wheels which moved on an overhead track. On the back side of each plate was fixed a rack driven by either a 10-rpm or a 25-rpm, constant-speed Bodine motor through a set of spur gears. This drive was used to traverse cross sections at various positions along the nozzle length. Positions along the nozzle length were located visually within $\pm \frac{1}{64}$ in. by a manually operated start and stop switch.

Experimental Procedure

A series of five tests were conducted, each of which consisted of maintaining a constant water flow rate while varying the quality of the total mixture. The settings of water flow rate investigated were: 0.155, 0.219, 0.303, 0.498, and 0.701 lb/sec, with qualities ranging from 0.56 to 14.3 per cent.

At the beginning of tests each day the water reservoir was filled with a fresh supply of tap water. The system manometer lines were purged, and the desired test conditions set by adjusting the air- and water-control valves. When it was determined that steady-state conditions were achieved, data were recorded and the two-phase void

reading was measured at the nozzle exit. Upon completion of the test, first water only and then air only was circulated through the loop, and the full and empty readings, respectively, were measured. When all of the tests in a series (constant water mass rate of flow) were completed as described above, the conditions were repeated individually for each of four other positions (1, 3, 4, and 9 in Fig. 3), and their respective void readings were recorded. Test conditions (water and air mass flow rates) were reproducible within ± 2.0 per cent.

Void records were not obtained at each of the five positions for the first test condition setting because difficulty was encountered in measuring corresponding test, empty, and full readings. This difficulty arose because with the system it was unable to repeat exactly a setting at a specified nozzle position once the location was changed. The latter would not have been harmful in a channel of constant cross-sectional area, but was in this investigation, since the area was continuously changing along the nozzle length. Void measurements were not obtained at any location other than the nozzle exit for the tests in which the water mass rates of flow were 0.155 and 0.219 lb/sec and part of the test in which the water mass rate of flow was 0.303 lb/sec.

CHAPTER III PROBLEM DISCUSSION AND ANALYTICAL DEVELOPMENT

As mentioned in the "Purpose of the Investigation" section of Chapter I, the object of the investigation was to study two-phase, two-component (air-water) flow in a converging-diverging nozzle. This study included the experimental determination of liquid and gas exit velocities, exit slip ratios, and exit liquid acceleration factors resulting from varying the mixture qualities. The acceleration factor is the ratio of the two-phase liquid exit velocity to the exit velocity that would be attained if only the liquid had been circulated through the nozzle for the same liquid mass rate of flow as the two-phase condition. It is thus a measure of how well the liquid is accelerated by passing a gas in conjunction with the liquid through the nozzle. In addition, velocities and slip ratios were investigated at various other positions along the nozzle length, specifically, positions i, 3, t, and 9 as shown in Fig. 3.

All determined values of velocity, slip ratio, and acceleration factor were average cross-sectional values based on an experimentally measured average cross-sectional void fraction, and no attempt was made to determine cross-sectional profiles of the aforementioned values.

Analytical Development - General

Mass cannot be created or destroyed in a continuum. The mass that flows into a system must eventually flow out of the system. Thus, the principle of conservation of mass is the foundation of the solutions for countless engineering applications. This principle is the basis for the development of the continuity equation which requires that the flow be steady and one-dimensional. Steady flow is defined as one in which all fluid properties, e.g., velocity, pressure, density, and temperature, at a position are independent of time. Thus, for velocity,

$$\frac{\delta V}{\delta \tau} = 0 \quad . \quad (1)$$

The assumption of steady flow for two-phase turbulent-flow nozzle application will be valid, in general, provided the definition of steady flow be modified to the following: steady flow is one in which all fluid properties, e.g., velocity, pressure, density, and temperature, are constant when taken as time-averaged values. Thus, the steady, one-dimensional continuity equation when applied to two-phase nozzles is

$$M_{in} = M_{out} \quad ; \quad (2)$$

$$(\rho_l A_l V_l + \rho_g A_g V_g)_{in} = (\rho_l A_l V_l + \rho_g A_g V_g)_{out} \quad . \quad (3)$$

For the liquid phase at any position,

$$M_l = \rho_l A_l V_l \quad . \quad (4)$$

For the gaseous phase at any position,

$$M_g = \rho_g A_g V_g \quad . \quad (5)$$

The void fraction α at any position is the ratio of the area of the gas phase to the area of the total mixture. Thus,

$$A_g = \alpha A \quad (6)$$

and

$$A_l = (1-\alpha)A \quad . \quad (7)$$

Combinations of Eqs. 4 and 7 and of Eqs. 5 and 6, respectively, give

$$M_l = \rho_l (1-\alpha) A V_l \quad (8)$$

and

$$M_g = \rho_g \alpha A V_g \quad . \quad (9)$$

By taking the ratio of Eqs. 8 and 9, we obtain

$$\frac{M_l}{M_g} = \left(\frac{\rho_l}{\rho_g} \right) \left(\frac{1-\alpha}{\alpha} \right) \left(\frac{V_l}{V_g} \right) \quad . \quad (10)$$

But, by definition,

$$M_g = xM \quad (11)$$

and

$$M_l = (1-x)M \quad (12)$$

Substitution of Eqs. 11 and 12 into 10 yields

$$\frac{1-x}{x} = \left(\frac{\rho_l}{\rho_g} \right) \left(\frac{1-\alpha}{\alpha} \right) \left(\frac{V_l}{V_g} \right) \quad (13)$$

We thereby obtain for the slip ratio k , the slip equation

$$k = \frac{V_g}{V_l} = \left(\frac{x}{1-x} \right) \left(\frac{1-\alpha}{\alpha} \right) \left(\frac{\rho_l}{\rho_g} \right) \quad (14)$$

From Eqs. 4, 7, and 12,

$$V_l = \frac{(1-x)M}{(1-\alpha)A\rho_l} \quad (15)$$

From Eq. 14,

$$V_g = kV_l \quad (16)$$

The acceleration factor A_F is

$$A_F = \frac{V_l}{V_{1\text{-phase}}} \quad (17)$$

where

$V_{1\text{-phase}}$ = velocity at any position that would be obtained for one-phase, liquid only, flow at the same liquid mass flow rate as for V_l .

Thus, liquid and air velocities, slip ratios, and acceleration factors can be readily determined at any position from Eqs. 14-17 provided the required values can be experimentally measured.

Measurement of the Void Fraction

As discussed in the "Literature Survey" section of Chapter I, numerous methods have been employed by various investigators to measure average cross-sectional void fractions experimentally. The most accurate and the most suitable method for this application is the gamma-ray-attenuation technique, based on the absorption of gamma rays emanating from a radioactive source, part of which are absorbed by a mixture flowing between the radiation source and a detection system. The detection system relays a signal which is amplified and recorded on an electronic recording device. A measurement is taken with the liquid-phase, gas-phase, and two-phase conditions present in the channel individually, and from these three measurements the average void fraction is determined.

The technique initially involved a "one-shot" method of determining the average void fraction. This method consisted of passing gamma rays through the whole channel cross section to a large lead detection window, but the method proved to be inaccurate. Petrick⁽⁵⁾ developed a more accurate "traversing" technique in which the source and detection equipment were traversed simultaneously past the test channel, and a trace was recorded for the cross section. In this case the detection window was a narrow, rectangular slit. Average local void fractions were determined from the traces, and from these the average cross-sectional void fraction was calculated by integrating across the cross section.

The gamma-ray-attenuation method was used extensively in this investigation. The "traversing" method rather than the "one-shot" method was employed.

Typical empty (gas phase only), full (liquid phase only), and two-phase tracings are shown in Fig. 12. From these tracings average

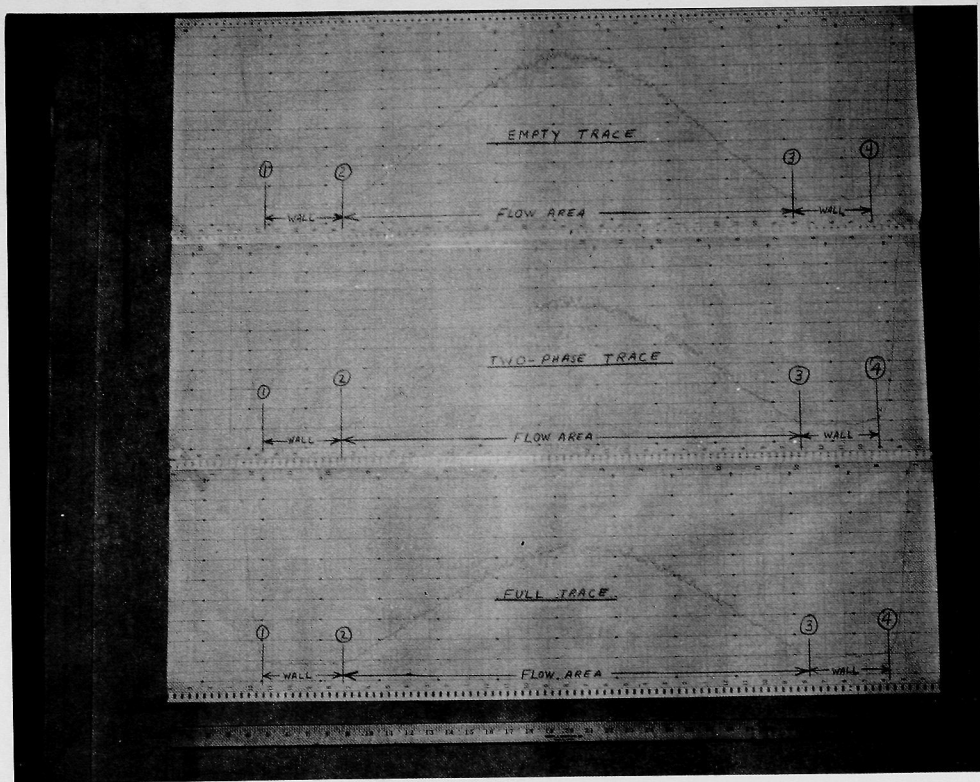


Fig. 12. Typical Empty, Full, and Two-phase Tracings

local and average cross-sectional void fractions were determined from the following relationships, respectively:

$$(\alpha_y)_n = \frac{\ln(E/E_\ell)_n}{\ln(E_g/E_\ell)_n} \quad (18)$$

and

$$\alpha = \frac{2}{\pi r^2} \sum_{n=1}^m (\alpha_y)_n (r^2 - y_n^2)^{1/2} (\Delta y_n) \quad , \quad (19)$$

where

$(\alpha_y)_n$ = average local void fraction at position y_n .

y_n = various positions along a nozzle cross section.

E = two-phase recorder reading.

E_g = gas-phase-only recorder reading.

E_ℓ = liquid-phase-only recorder reading.

α = average cross-sectional void fraction.

r = radius of the cross section traversed.

Δy_n = distance between y_n and y_{n+1} .

For the analytical development of Eqs. 18 and 19 and a more detailed discussion of the gamma-ray-attenuation method, see Appendix B. Equations 18 and 19 are Eqs. B-21 and B-30, respectively.

In this investigation the cross-sectional traces (see Fig. 12) were divided into 16 equal parts; thus $\Delta y_n = 2r/16$ in. The average local void fraction, $(\alpha_y)_n$, was obtained at each of the 16 subdivisions by Eq. 18, and the average cross-sectional void fraction was calculated by Eq. 19. Thus, Eqs. 14-19 were used for all calculations in this report.

CHAPTER IV DATA ANALYSIS, RESULTS, AND DISCUSSION

Data Analysis

Inspection of Eqs. 14-17 reveals that, in order to determine average values of slip ratio, air velocity, water velocity, and the acceleration factor for a specific two-phase condition, the following values must be determined either theoretically or experimentally:

1) mixture quality, 2) average cross-sectional void fraction, 3) liquid-phase density, 4) gaseous-phase density, and 5) total mass rate of flow.

Mixture quality and total mass rate of flow were determined by measuring the individual air and water mass rates of flow. The water flow rate was controllable at a constant value for each series of tests within $\pm 2\frac{1}{2}$ per cent. Maximum unsteady fluctuations occurred at low water flow rates and high air flow rates, and were of the order of ± 5 per cent.

Liquid- and gaseous-phase densities were obtained by measuring pressures and temperatures. Thermal and pressure equilibria were assumed to exist across a cross section. Maximum temperature variation in the nozzle between inlet and exit was 4°F. Thus, temperatures between the inlet and exit were assumed to be an arithmetic mean of the inlet and exit temperatures. The water density was obtained from steam tables⁽¹⁷⁾ at sub-cooled temperatures, and the air density was calculated from the perfect gas law, assuming that moist air closely follows the perfect gas relationship.

$$\rho = p/RT \quad .$$

The average local void fraction was obtained by the traversing technique with the gamma-ray-attenuation method. Two-phase test conditions, empty, and full tracings were recorded, and the average cross-sectional void fraction was calculated as described previously by means of Eq. 19. Theoretically, the empty and full readings should be recorded at the same temperature and pressure as the

corresponding two-phase test condition; however, for convenience, these readings were recorded at any temperature and pressure, since in the ranges tested the effects of pressure and temperature changes on empty and full readings were negligible. For a further discussion, numerical example, and experimental proof of the above statement, see Appendix D.

Thus, all unknown values of Eqs. 14-17 were determined experimentally, and average values of slip, air and water velocities, and acceleration factors were determined accordingly.

The greatest source of error in this investigation was in the determination of the void fractions. Flow rate measurements and pressure and temperature measurements were sufficiently accurate and, therefore, contributed little to any deviations from actual values. Thus, any inaccuracies in the calculated results were in most instances attributable to void measurements.

The principal influences in the measurement of void fractions that contributed in part to any deviations from the actual voids are:

1. human error in reading the recorded traces;
2. fluctuation in temperature of the photomultiplier tube and scintillation crystal;
3. fluctuation in temperature of the current amplifier and recorder, which continue to rise in temperature because of heating of component parts, resulting in recorder drift;
4. a variation in the supply voltage to the photomultiplier tube;
5. source decay over a period of time.

Influence 2 was almost completely eliminated by cooling coils in the crystal-tube assembly holder wall. Influence 3 was checked in part by periodically adjusting the zero drift. The variance of supply voltage was practically negligible, as it could be regulated to within ± 0.1 per cent. Source decay also had only a slight effect because of the frequency at which full and empty readings were measured.

Pressure Profiles

In all tests the nozzle exhausted into an atmospheric condition. Typical pressure profiles are shown in Figs. 13-16. In most of the conditions investigated the flow resembled the compressible type, that is, there was a considerable decrease in pressure after the throat. In a minor portion of the tests a flow resembling the incompressible type was encountered, that is, the pressure did not decrease to a value lower than the throat pressure after the throat but remained essentially constant and equal to atmospheric pressure. This condition is shown in Fig. 16. Incompressible-type flow was encountered at a water flow rate of 0.155 lb/sec at qualities less than approximately 3 per cent. This type of flow was not encountered at higher flow rates, but would have been had low enough qualities been investigated.

In the compressible-type flow regimes, the pressure decreased to a minimum at some location after the throat and then increased again to approximately atmospheric conditions at the exit. If optimum flow conditions had existed, the overexpansion would not have occurred, but the pressure would have continually decreased until it reached atmospheric pressure at the nozzle exit.

Slip Ratios along the Nozzle Length

As the air-water mixture flowed through the nozzle, the pressure continued to decrease until some location between the throat and exit was reached. Thus, the air density continued to decrease up to this point and then retained an almost constant density to the exit. Since water is essentially an incompressible fluid, its density remained practically constant throughout the expansion process. As the area decreased, the velocities increased in accordance with the continuity equation. Therefore, these two factors, air density and area changes, were the controlling factors for slip ratios along the nozzle length.

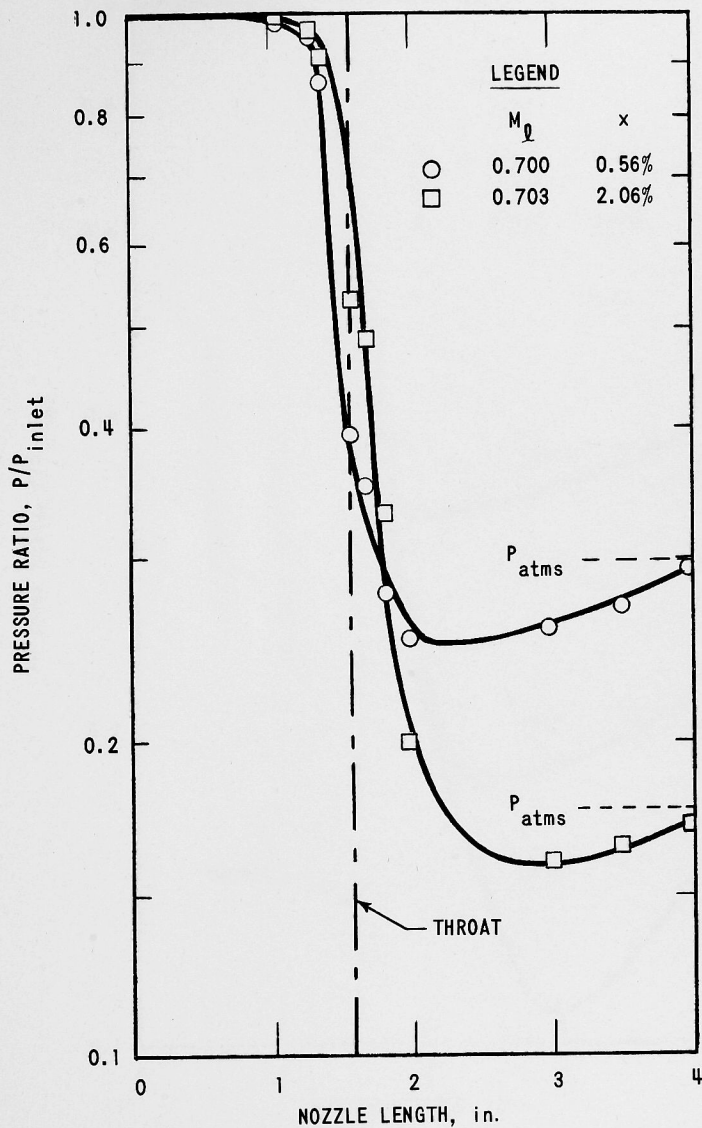


Fig. 13. Typical Compressible-type Pressure Profile; $M_l \approx 0.7$

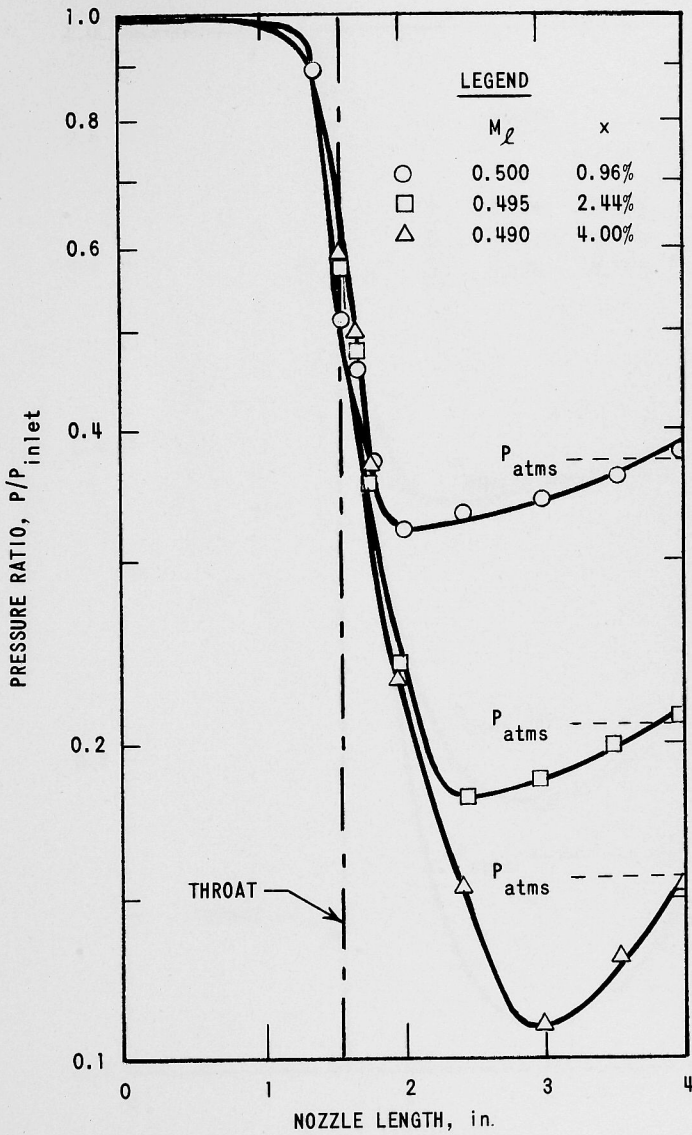


Fig. 14. Typical Compressible-type Pressure Profile; $M_\ell \approx 0.5$

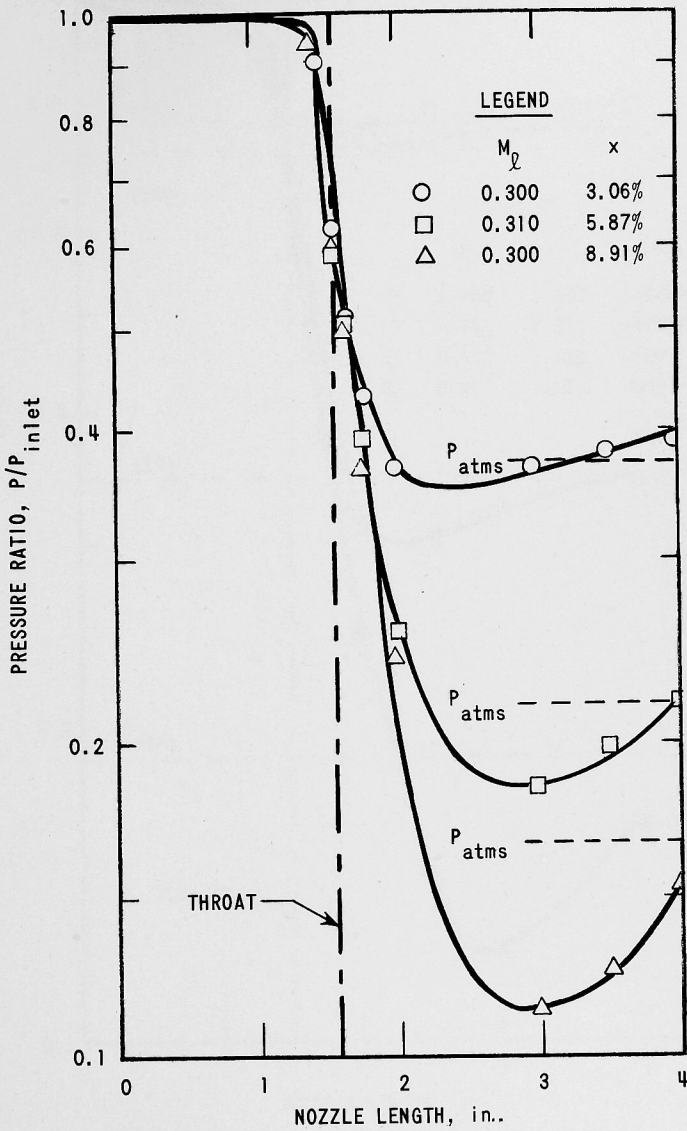


Fig. 15. Typical Compressible-type Pressure Profile; $M_\ell \cong 0.3$

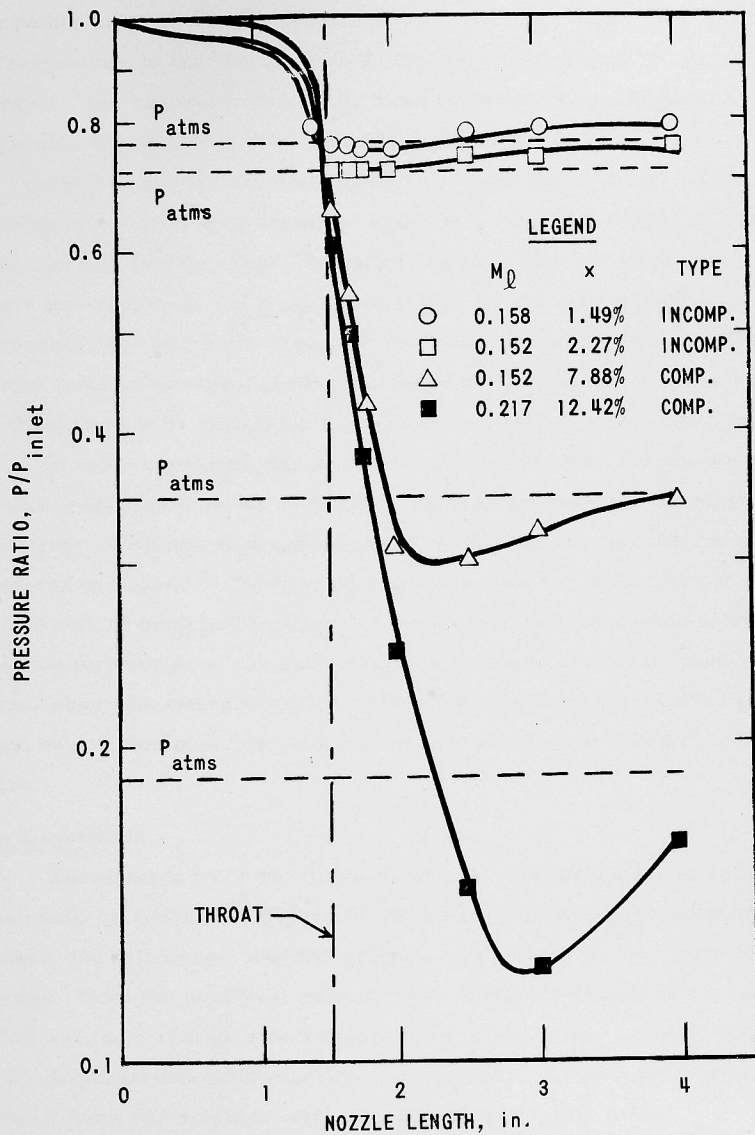


Fig. 16. Comparison of Compressible- and Incompressible-type Pressure Profiles

In Figs. 17-19 slip ratios are plotted versus the nozzle length, data points being in the positions i, 3, t, 9, and e as shown in Fig. 3 (corresponding to the distances 0, 1, throat, 2, and 4 in Figs. 17-19). Generally, the slip ratio increased from position i to 3. Figures 13-16 reveal that the pressure was essentially the same at positions i and 3 and, therefore, the air density remained essentially constant. Thus, the increase in slip ratio from position i to 3 was attributable to a decrease in void fraction (see Eq. 14) as the area changed to approximately one-fourth its value at the inlet (i). As the throat region was approached, the slip ratio tended to decrease. Note in Figs. 17-19 that the slip ratio at the throat generally tended to decrease as the quality was increased, thus indicating that the air accelerated the liquid phase.

In most instances, the slip ratio increased after the throat area and was a definite function of quality. No further attempt was made to investigate additional test conditions or to analyze further the results presented in Figs. 17-19 for positions other than the exit, since it was the position of principal interest. A more detailed discussion of the flow characteristics at the exit section will follow, but little more will be said about the characteristics within the nozzle. Figures 17-19 are shown only to demonstrate, to some extent, slip trends along the nozzle length.

Data Repetition

Three tests were re-run to determine how well the test conditions could be repeated. Figure 20 shows the nozzle length pressure profiles, the full lines being the original run and the dashed lines the re-runs. Note the excellent repeatability of water mass flow rate and quality settings. All pressures were repeatable within 2-3 psi. Figure 21 demonstrates void fraction comparisons. Re-run void fractions deviated from the original voids by an average of only 0.04.

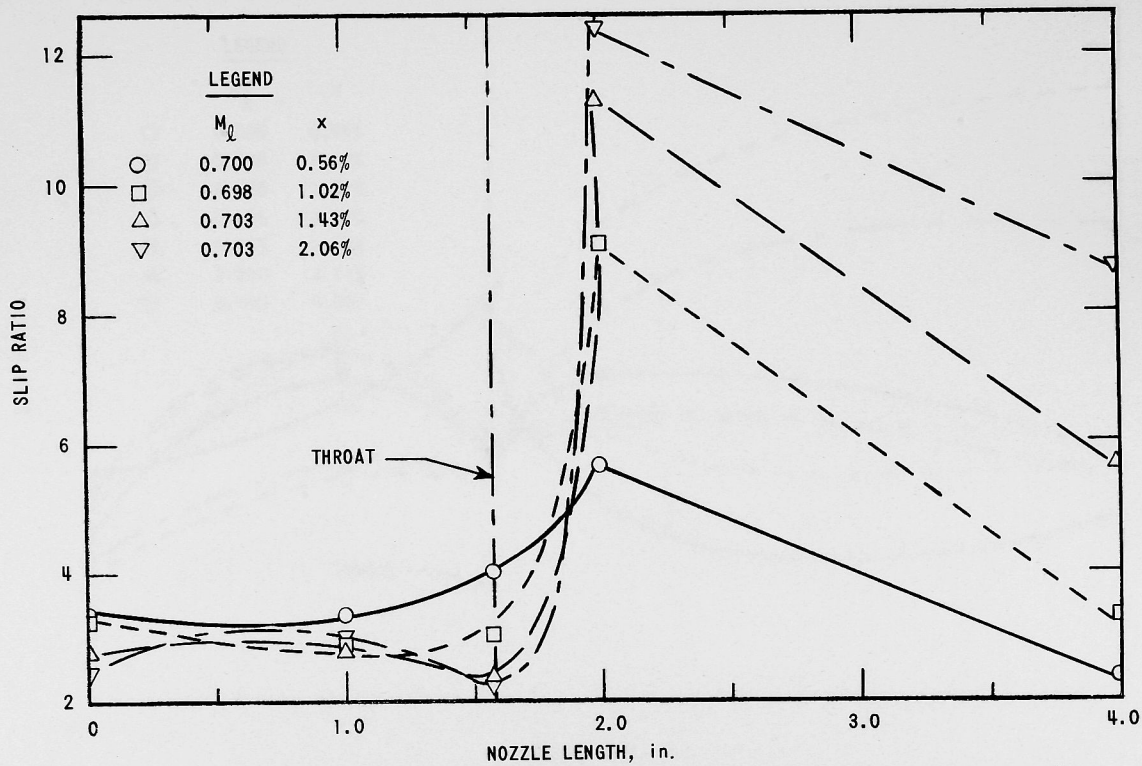


Fig. 17. Slip Ratios along the Nozzle Length; $M_l \cong 0.7$

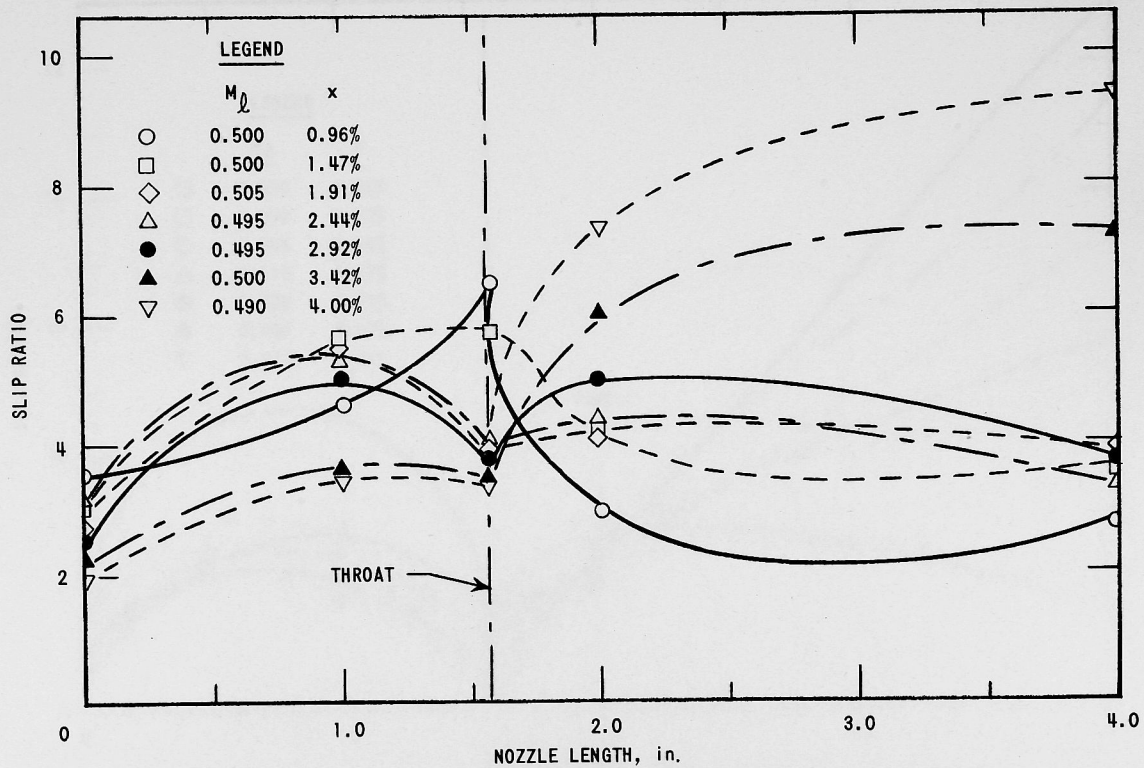


Fig. 18. Slip Ratios along the Nozzle Length; $M_\ell \approx 0.5$

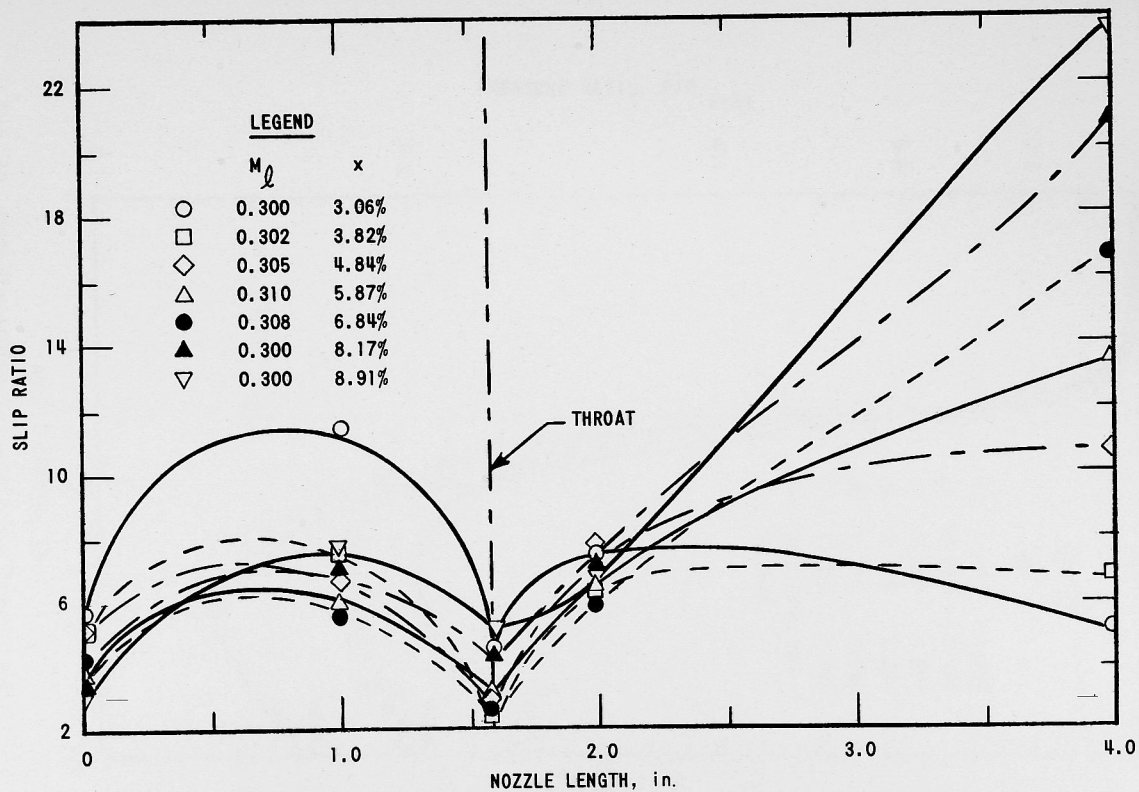


Fig. 19. Slip Ratios along the Nozzle Length; $M_\ell \approx 0.3$

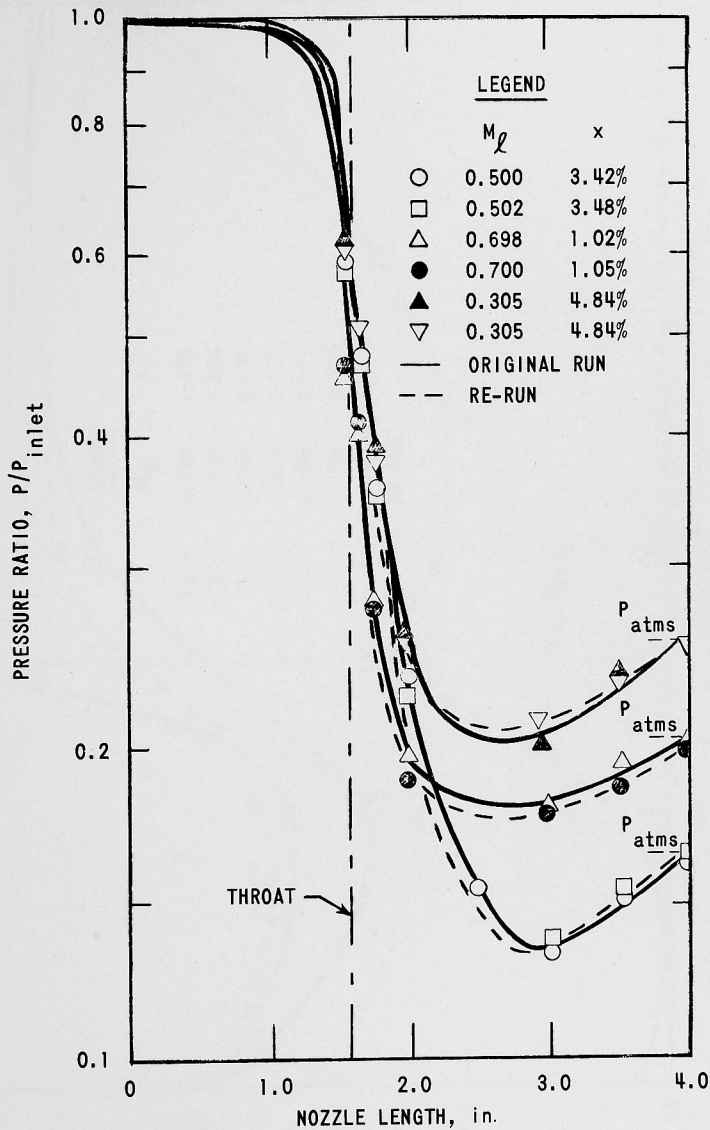


Fig. 20. Data Repetition Comparison - Pressure Profiles

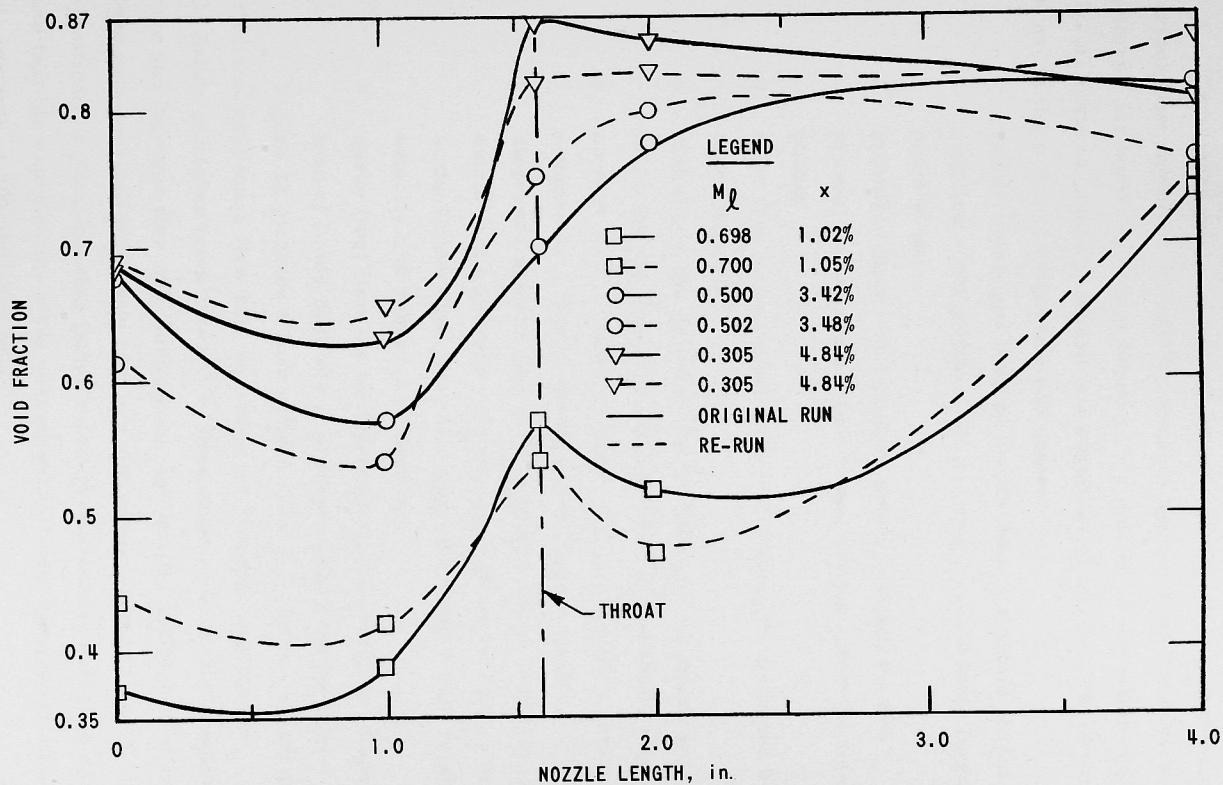


Fig. 21. Data Repetition Comparison - Void Fractions

Flow Mechanisms, Void Distribution, and Change of Flow Regime

Two-phase mixtures exhibit several modes of flow representing various flow regimes. Alves⁽¹⁸⁾ compiled the following list of flow patterns for horizontal pipes based on his studies of air-water and air-oil systems, and also on the investigations of others. These patterns, in the order of increasing gas content, are:

1. bubble flow - gas bubbles dispersed in the liquid phase;
2. plugflow - many bubbles of gas coalesce and form large plugs of gas;
3. stratified flow - an interface exists between the two phases, the lighter gaseous phase moving above the liquid phase;
4. wave flow - the aforementioned interface is disturbed by waves of liquid;
5. slug flow - the crests of the aforementioned waves periodically fill the whole channel thus forming periodic slugs;
6. annular flow - a core of high-velocity gas exists surrounded by a film of water adjacent to the walls;
7. dispersed annular flow - some dispersion of liquid droplets exists in the gaseous core and some gaseous bubbles exist in the liquid film. The core still maintains a high relative velocity (not reported by Alves);
8. spray (fog) flow - a homogeneous cross-sectional dispersion of liquid droplets is present in the gaseous phase.

Figure 22 pictures a flow pattern chart for various steam qualities and total mass flow rate densities for pipes as reported by O. Baker and taken from Sofer.⁽¹⁹⁾ This chart reveals that annular-type and fog-type flow are functions of high quality and high total mass flow rate density (mass flow rate per unit cross-sectional area). It is significant to point out that Baker's observations were visual in nature and that his experiments were performed with two-component steam-oil systems at 800 and 1500 psia.

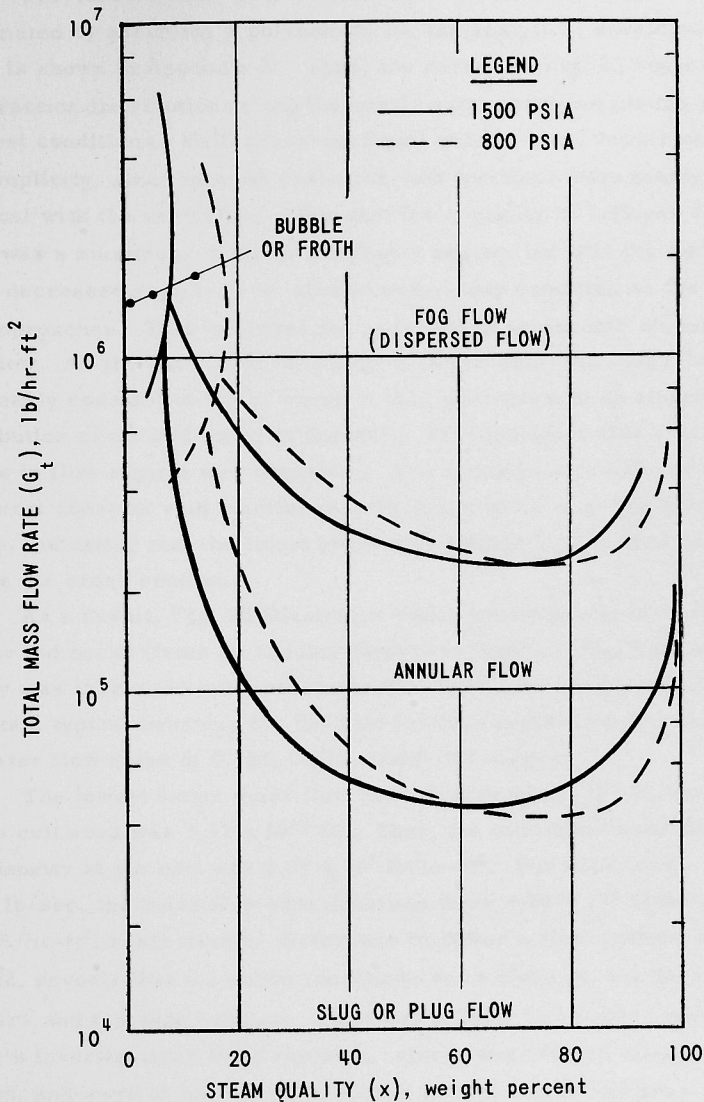


Fig. 22. Steam-Water System Flow Pattern Charts. Results of O. Baker, "Simultaneous Flow of an Oil and a Gas." Oil and Gas Journal 53 (12): 185 (July, 1954) as taken from Sofer.⁽¹⁹⁾

The void fraction distribution at the nozzle exit center was approximated by assuming a polynomial fit, the analytical development of which is shown in Appendix E. Thus, the curves in Fig. 23 represent void fraction distributions along the nozzle exit centerline for the specified test conditions. Half-cross-sectional values, only, were plotted for simplicity, since in most cases the void fractions were nearly symmetrical with the centerline. Note that for a quality of 1.49 per cent there was a maximum of air in the center region, but that the quantity of air decreased rapidly to an almost water-only condition as the wall was approached. This indicates the presence of an annular dispersed-type flow. As the quality increased to 6.14 per cent, the void fraction was nearly constant to 0.8 r, where it then decreased to an almost even distribution of air and water at the wall. This indicates that a possible change in flow regime was occurring. For a quality of 14.30 per cent an almost constant void fraction distribution existed over the whole radius, indicating that the liquid phase was almost evenly distributed across the cross section.

As a result, Fig. 23 illustrates that a possible change in flow regime did occur (from an annular dispersed type to a fog type) as the quality was increased for a constant water flow rate. Figure 23 represents a typical behavior for the void fraction centerline distribution for water flow rates of 0.155, 0.219, and 0.303 lb/sec.

The lowest water mass flow investigated was 0.155 lb/sec. The nozzle exit area was $1.37 \times 10^{-3} \text{ ft}^2$. Thus, the minimum mass flow rate density at the exit was $4.07 \times 10^5 \text{ lb/hr-ft}^2$. For 0.219 and 0.303 lb/sec, the mass flow rate densities were $5.75 \times 10^5 \text{ lb/hr-ft}^2$ and 7.97 lb/hr-ft^2 , respectively. Reference to Baker's flow-pattern chart, Fig. 22, reveals that the above conditions were close to, but not in, the annular- and fog-type regions. However, it must be recalled that Baker's investigations were visual in nature, were for an oil-steam system, and were at considerably higher temperatures and pressures than those investigated in this report. Note the considerable downshifting of the curves as the pressure was decreased from 1500 to 800 psia. If the curves downshift at least as much when the pressure

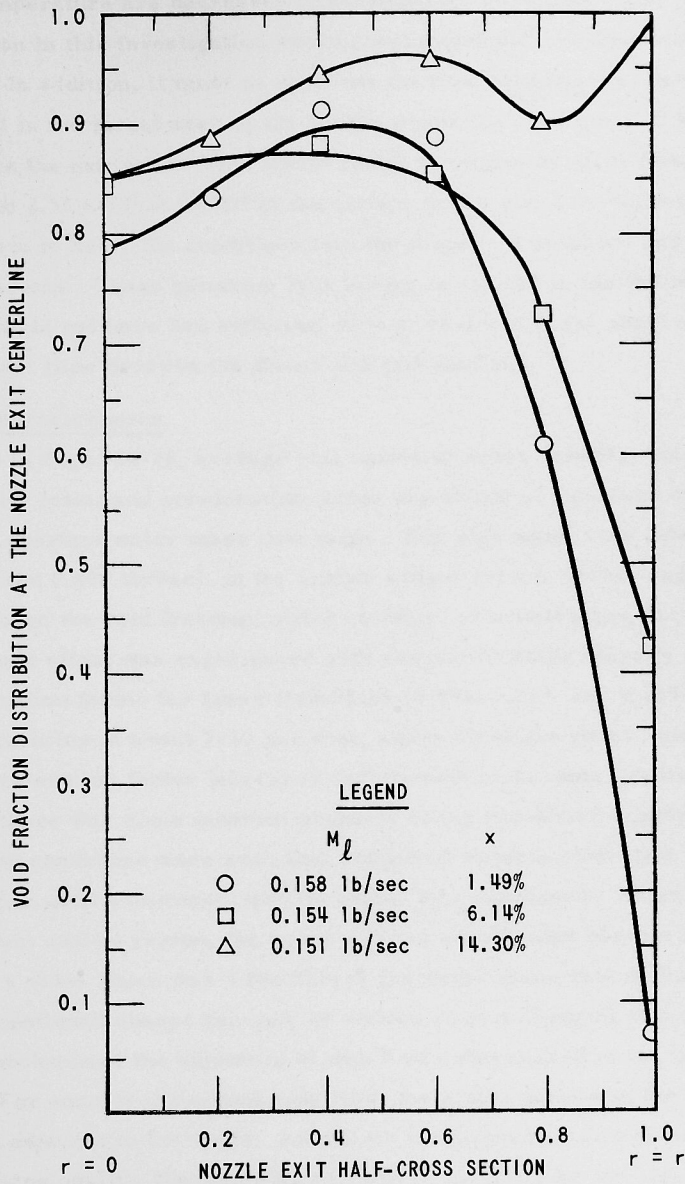


Fig. 23. Exit Half-cross-sectional Void Fraction Distribution

and temperature are decreased to atmospheric conditions, then the condition in this investigation would correspond with the flow chart.

In addition, it must be said that the flow patterns may have developed in the throat area of the nozzle where the area was $1/5.80$ as large as the exit area. This would result in minimum mass flow densities of 2.36×10^6 lb/hr-ft² at the throat, which would be more than sufficient to bring the conditions into the dispersed annular- and fog-type regions. These patterns, thus having developed in the throat region, might not have had sufficient time to re-form in the short amount of contact time between the throat and exit sections.

Exit Characteristics

In Figs. 24-28, average exit values of water velocity, void fraction, slip ratio, and acceleration factor are shown as functions of quality for constant water mass flow rates. For high water flow rates (0.701 and 0.498 lb/sec), in the quality ranges tested, quality had little effect upon the void fraction, water velocity, or acceleration factor. The same effect was experienced with respect to water velocity and acceleration factor for lower flow rates (0.303, 0.219, and 0.155 lb/sec) up to qualities of about 7-10 per cent, above which the water velocity and acceleration factor increased rapidly with increasing quality. Thus, there was some inherent property of the two-phase mixture whereby conditions were such that additional water acceleration did not occur until a minimum quality region was surpassed. Prior to this minimum quality region, the water was not accelerated above a limited value, a value which was a function of the water mass rate of flow. The aforementioned change can only be attributed to a changing two-phase flow mechanism, the existence of which was established in the last section. For annular dispersed-type flow, the major portion of the water flowed adjacent to the walls. As the air continued to accelerate with increasing quality, the water was forced to the walls by the high-velocity air, undergoing no additional acceleration. However, as more

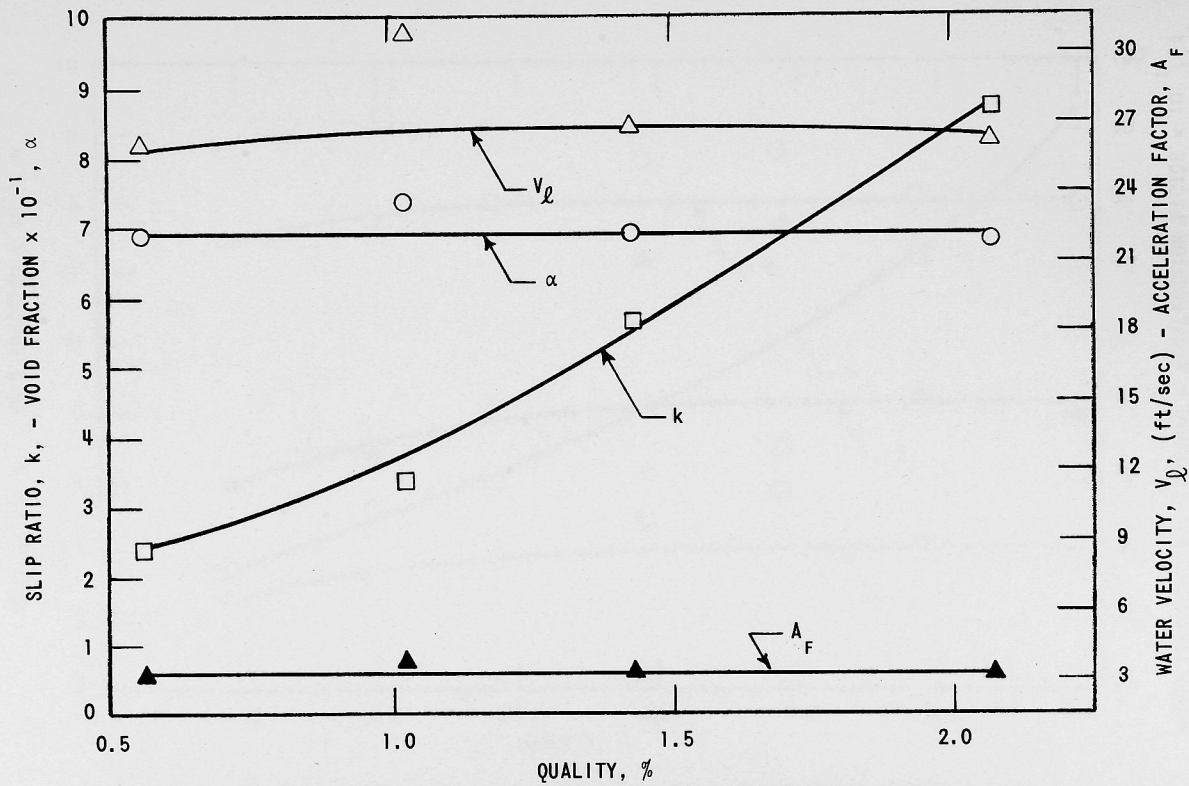


Fig. 24. Nozzle Exit Characteristics for Water Flow Rate = 0.701 lb/sec

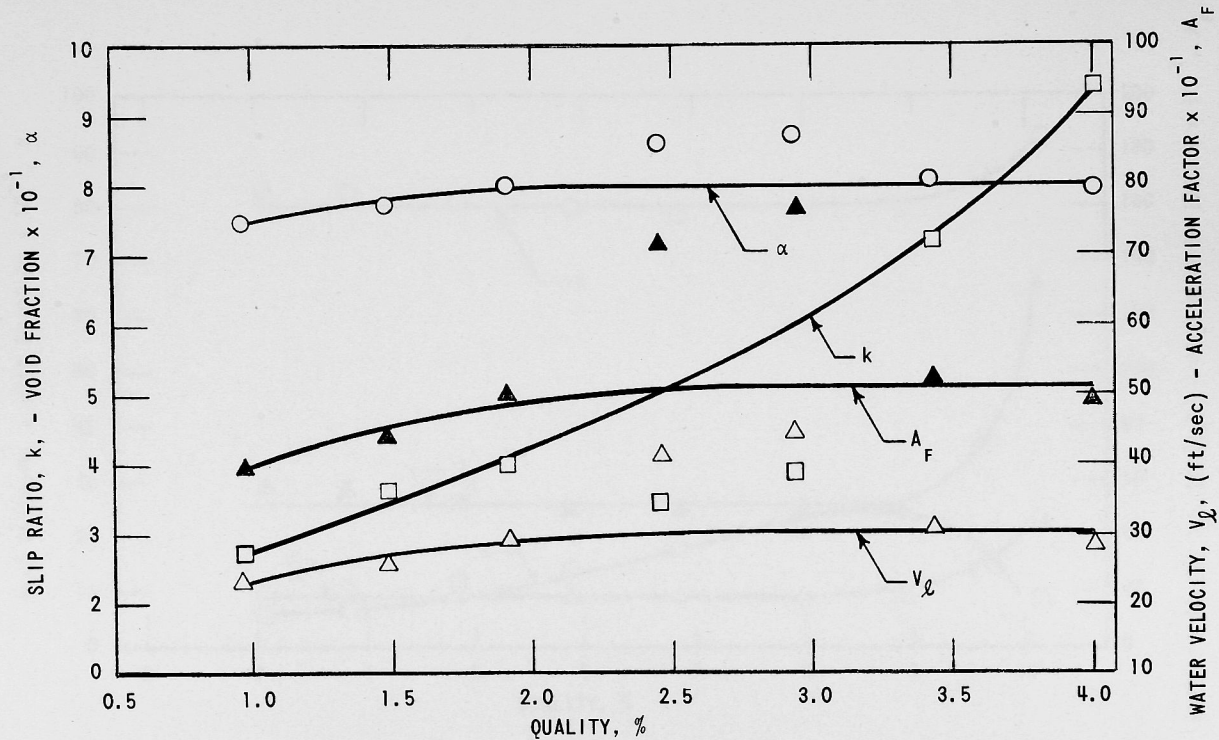


Fig. 25. Nozzle Exit Characteristics for Water Flow Rate = 0.498 lb/sec

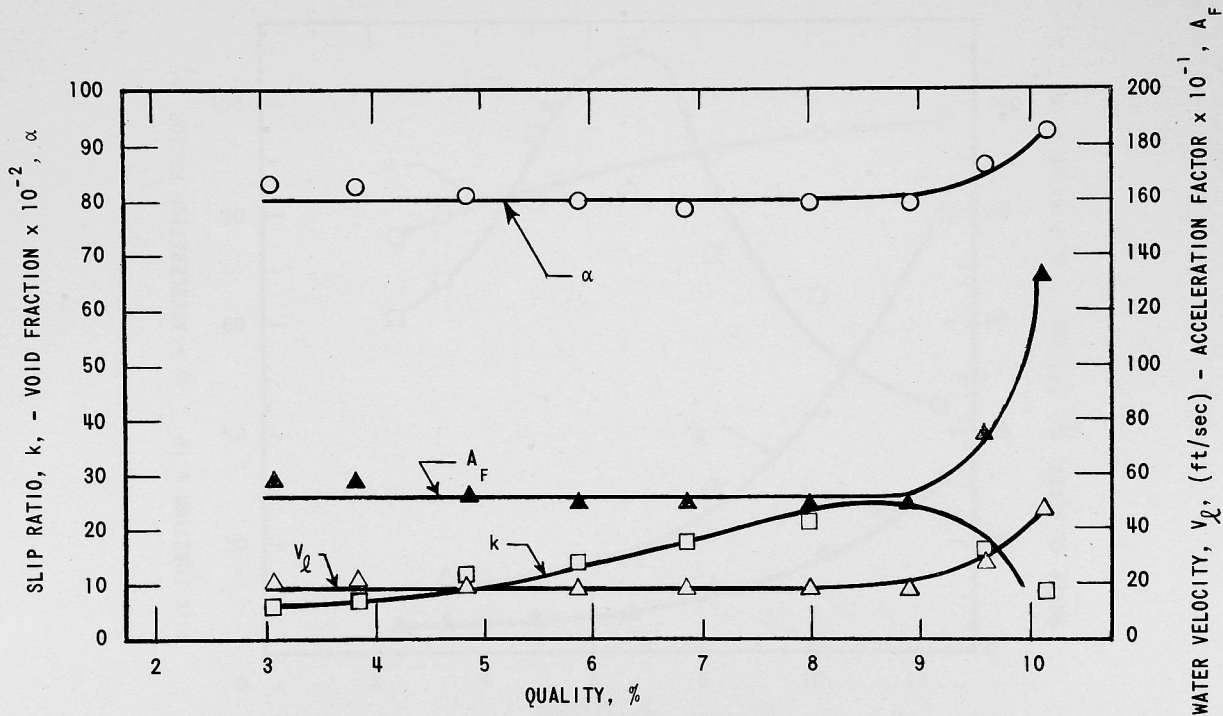


Fig. 26. Nozzle Exit Characteristics for Water Flow Rate = 0.303 lb/sec

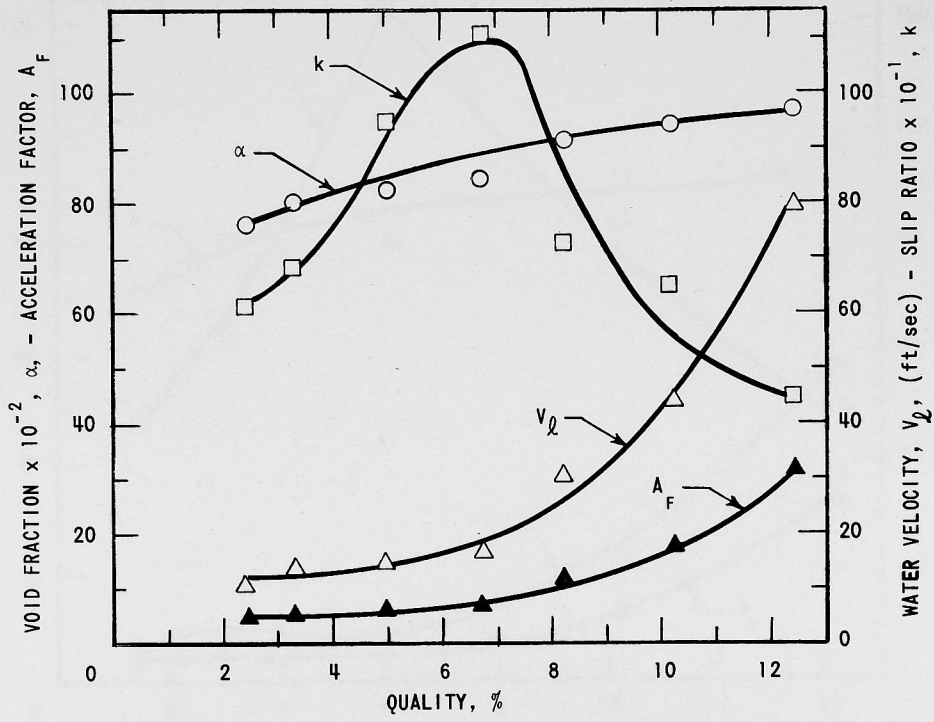


Fig. 27. Nozzle Exit Characteristics for Water Flow Rate = 0.219 lb/sec

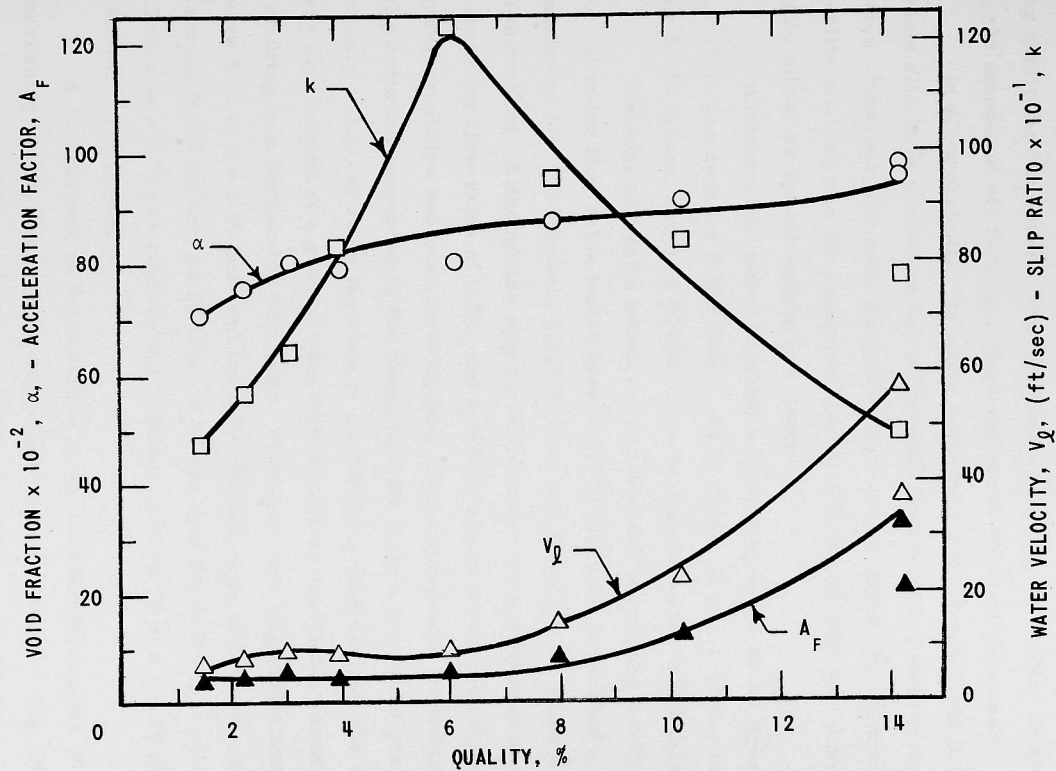


Fig. 28. Nozzle Exit Characteristics for Water Flow Rate = 0.155 lb/sec

air was injected into the mixture, the flow regime started to change and approached a fog-type pattern. The water now being more dispersed across the cross section continued to accelerate with increasing quality as the amount of water became lighter and lighter relative to the amount of air flowing. Thus, the water velocity increased.

In all probability, the water velocity for 0.701 and 0.498 lb/sec would also have increased had sufficiently high qualities been investigated. However, for each water flow rate investigated, the maximum quality attained was the maximum quality that the system would physically allow, as the air supply was limited.

Maximum exit water velocities occurring were: 47.20 ft/sec at $x = 10.15$ per cent for 0.303 lb/sec, 79.50 ft/sec at $x = 12.42$ per cent for 0.219 lb/sec, and 57.4 ft/sec at $x = 14.3$ per cent for 0.159 lb/sec.

The exit slip ratio increased rapidly with increasing quality for all water flow rates tested (see Figs. 24-28) until it reached a maximum for 0.303 lb/sec, 0.219 lb/sec, and 0.155 lb/sec, after which it decreased. Although the slip ratio did not reach a maximum and decrease for flow rates of 0.701 and 0.498 lb/sec, it would have if high-enough qualities had been investigated. This condition of maximum slip ratio corresponded to the changing flow regime discussed previously. Thus, at some instance in the changing flow regime, the water was accelerated at a greater rate than the air as the quality increased resulting in a decreasing slip ratio. Maximum exit slip ratios attained were 8.69 at $x = 2.06$ per cent for 0.701 lb/sec, 9.40 at $x = 4.00$ per cent for 0.498 lb/sec, 24.20 at $x = 8.91$ per cent for 0.303 lb/sec, 11.05 at $x = 6.72$ per cent for 0.219 lb/sec, and 12.30 at $x = 6.14$ per cent for 0.155 lb/sec.

A comparison of the variation of the acceleration factor with increasing quality for various water flow rates is shown in Fig. 29. Note that for all flow rates except 0.701 lb/sec, the acceleration factor had a limiting value prior to the flow regime change of approximately 5.2. Thus, for this nozzle the exit water velocity at which the changing

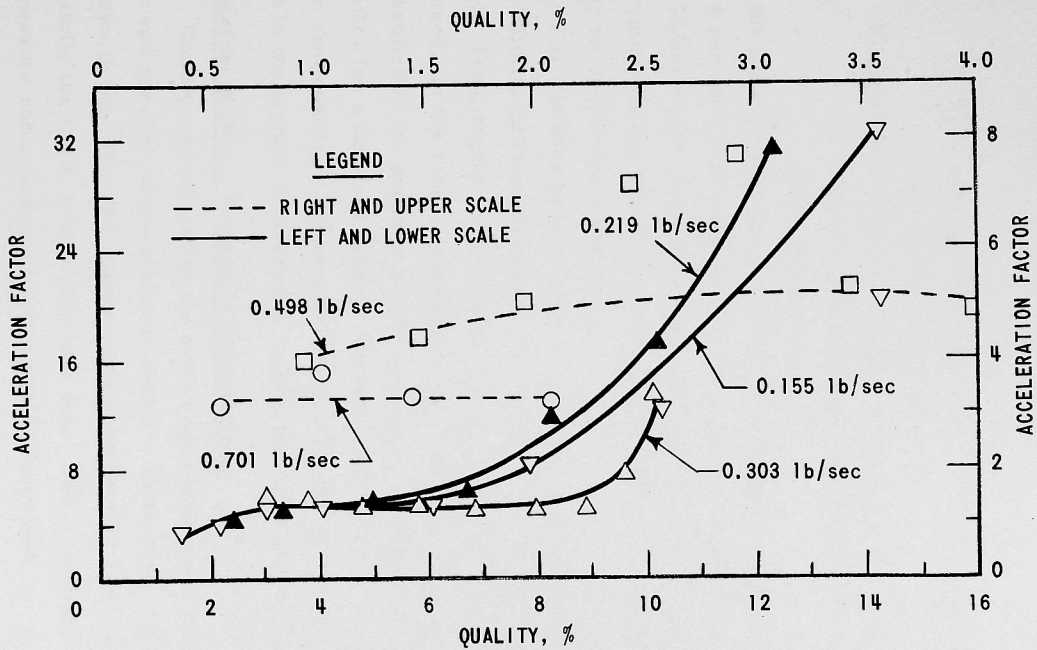


Fig. 29. Nozzle Exit Acceleration Factors

flow regime occurred can be predicted within ± 7.0 per cent for a flow rate of 0.155-0.498 lb/sec by the following relationship:

$$V_e' = 5.2 V_{1\text{-phase}}'$$

where

V_e' = average exit water velocity at which the change in flow regime occurred.

$V_{1\text{-phase}}'$ = exit water velocity that would be obtained if liquid only was flowing in the nozzle at the same water mass flow rate as V_e' .

Since the constant acceleration factor was obtained at qualities between 2 and 6 per cent, it is possible that the acceleration factor for 0.701 lb/sec would also have approached the value of 5.2 before the flow regime change occurred, since this flow rate was investigated only up to qualities of 2 per cent.

For qualities greater than 7-10 per cent, the acceleration factor was a definite function of quality, increasing radically with increasing quality. Thus, higher water velocities were obtained as the qualities increased. In the ranges investigated, the mass flow rate of 0.219 lb/sec resulted in the greatest acceleration factor and greatest exit liquid velocities for a constant quality. However, for values greater than 10 per cent quality, it appears as though 0.303 lb/sec possibly might result in the highest acceleration factors and liquid velocities.

Correlation of Data - Empirical Relationships

Quality was related to the exit to inlet pressure ratio, P_R , by a linear and parallel relationship for constant water mass rates of flow, as shown in Fig. 30. The slopes of the constant flow rate lines were essentially the same, within ± 1.33 per cent. For a constant flow rate, the pressure ratio decreased as the quality increased, or, in other words, as the quality increased the inlet pressure also increased, since the exit pressure was essentially atmospheric for all tests. The intercepts were obtained and fitted to a polynomial equation of the

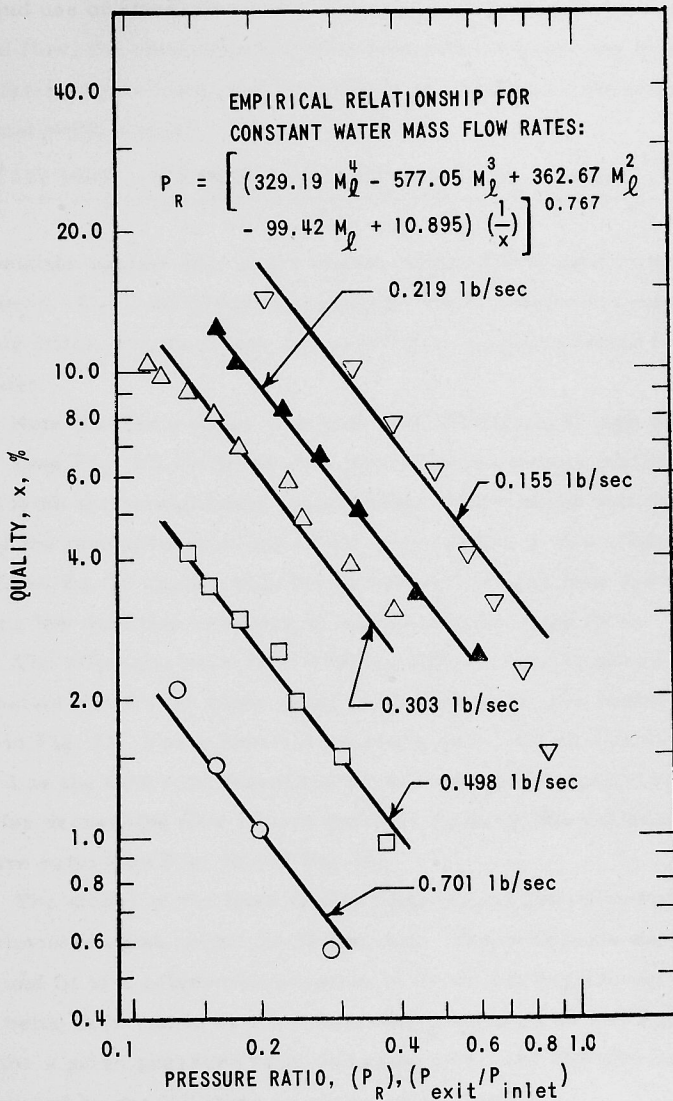


Fig. 30. Exit Quality-Pressure Ratio Correlation

fourth degree, the simultaneous equations being solved with a computer and use of standard matrix. Thus, for given water and air mass rates of flow, the corresponding inlet pressure (in psia) can be predicted for an atmospheric back-pressure application by the following empirical relationship:

$$P_R = \left(\frac{329.19M_\ell^4 - 577.05M_\ell^3 + 362.67M_\ell^2 - 99.42M_\ell + 10.895}{x} \right)^{0.767} \quad (20)$$

This equation applies only to the nozzle configuration used in this investigation. For a different configuration the constants and slope would probably differ, but the linear and parallel relationship would feasibly still exist.

Note that for a water flow rate of 0.155 lb/sec at high pressure ratios (see Fig. 30) the three data points for the lowest quality diverged from the straight-line relationship. These three test conditions were of the incompressible type discussed earlier in this chapter. Therefore, Eq. 20 applies only for compressible-type flow and is not valid for low qualities resulting in incompressible-type flow.

The slip ratio increased linearly with decreasing pressure ratio for constant water flow rates prior to the change in flow regime, as shown in Fig. 31. For a constant pressure ratio, the slip ratio increased as the flow rate decreased because the quality increased radically for decreasing flow rate in order to maintain the constant pressure ratio (see Fig. 30 and Eq. 14).

The slopes of the lines of slip ratio versus pressure ratio were approximately equal, within ± 1.56 per cent. The intercepts were obtained and fit to a polynomial equation of the fourth degree, the constants being determined by the simultaneous solution of five equations. Thus, for a given pressure ratio and mass flow rate, the slip ratio can be predicted by the following empirical relationship:

$$k = \left(\frac{580.13M_\ell^4 - 1016.25M_\ell^3 + 637.17M_\ell^2 - 172.84M_\ell + 18.314}{(P_R)^{1.64}} \right) \quad (21)$$

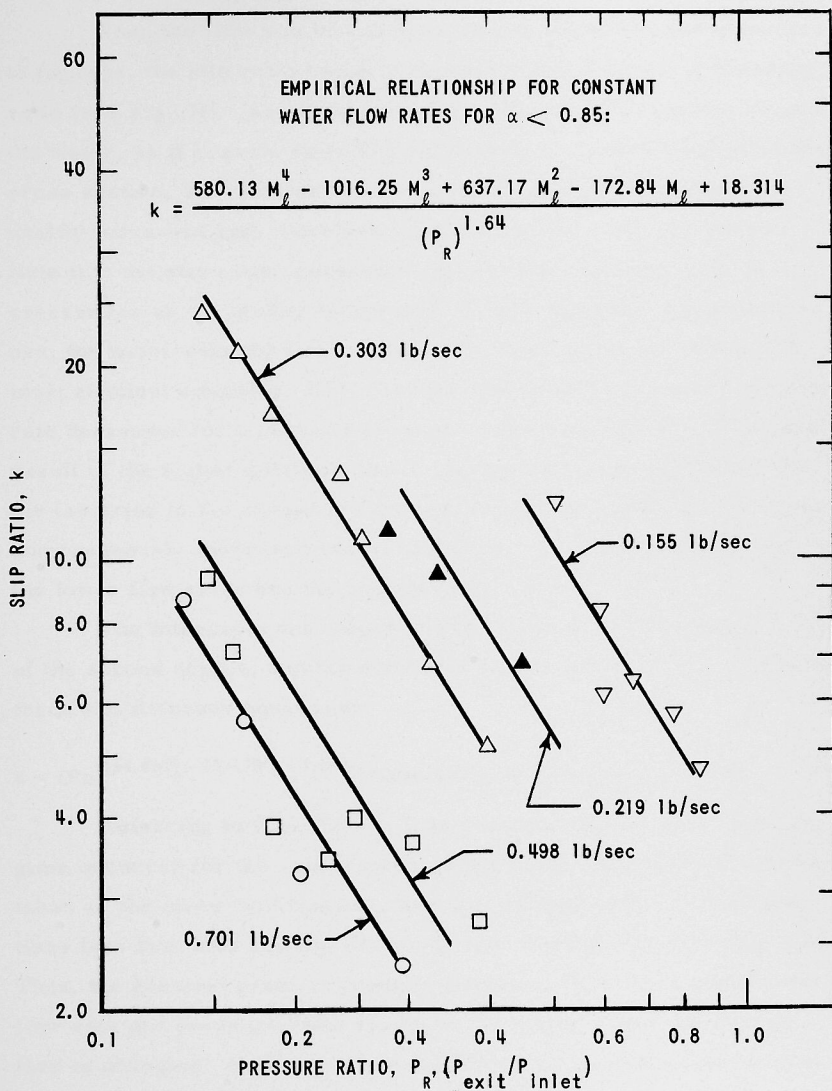


Fig. 31. Exit Slip Ratio-Pressure Ratio Correlation; $\alpha < 0.85$

This equation applies only to this nozzle configuration and only to conditions prior to the influence of the changing flow regime.

When the flow was changing its regime from annular dispersed to fog type, the slip ratio began to decrease with decreasing pressure ratio (see Fig. 32). As explained before, this situation existed because the water, as it became more homogeneously dispersed throughout the cross section, was accelerated at a greater rate than the air as the quality increased and, therefore, as the pressure ratio decreased. Note that the slip ratio approached unity as the pressure ratio decreased (or as the quality increased). If this desirable trend continues, the water velocity will eventually be equal to the air velocity, a most efficient condition. Note that the slip ratio decreased as the flow rate decreased for a constant pressure ratio (see Fig. 32). This was a result of the higher qualities now acting not merely to accelerate the air (as prior to the change in flow regime), but to accelerate the more homogeneously dispersed water, since for a constant pressure ratio the lower flow rates had the highest qualities (see Fig. 30).

The intercepts and slopes of Fig. 32 were fitted to polynomials of the second degree, and the constants obtained through the solution of three simultaneous equations:

$$k = (PR)^{(64.6M_w^2 - 15.23M_w + 1.84)}(772446.36M_w^2 - 287930.09M_w + 26096.29) \quad (22)$$

Referring to Figs. 26-28, it is seen that the change in flow regime occurred for the void fraction in the range 0.80-0.90. If 0.85 be taken as the mean void fraction, then Eq. 21 applies for all void fractions less than 0.85 and Eq. 22 for all void fractions greater than 0.85. Thus, the greatest error in predicting the slip ratio for a given water flow rate and pressure ratio arises in the region where the flow pattern is changing. However, these conditions can nevertheless be predicted with a reasonable amount of accuracy.

If both air and water mass rates of flow are known, the pressure ratio is calculated from Eq. 20 and the slip ratio from Eq. 22.

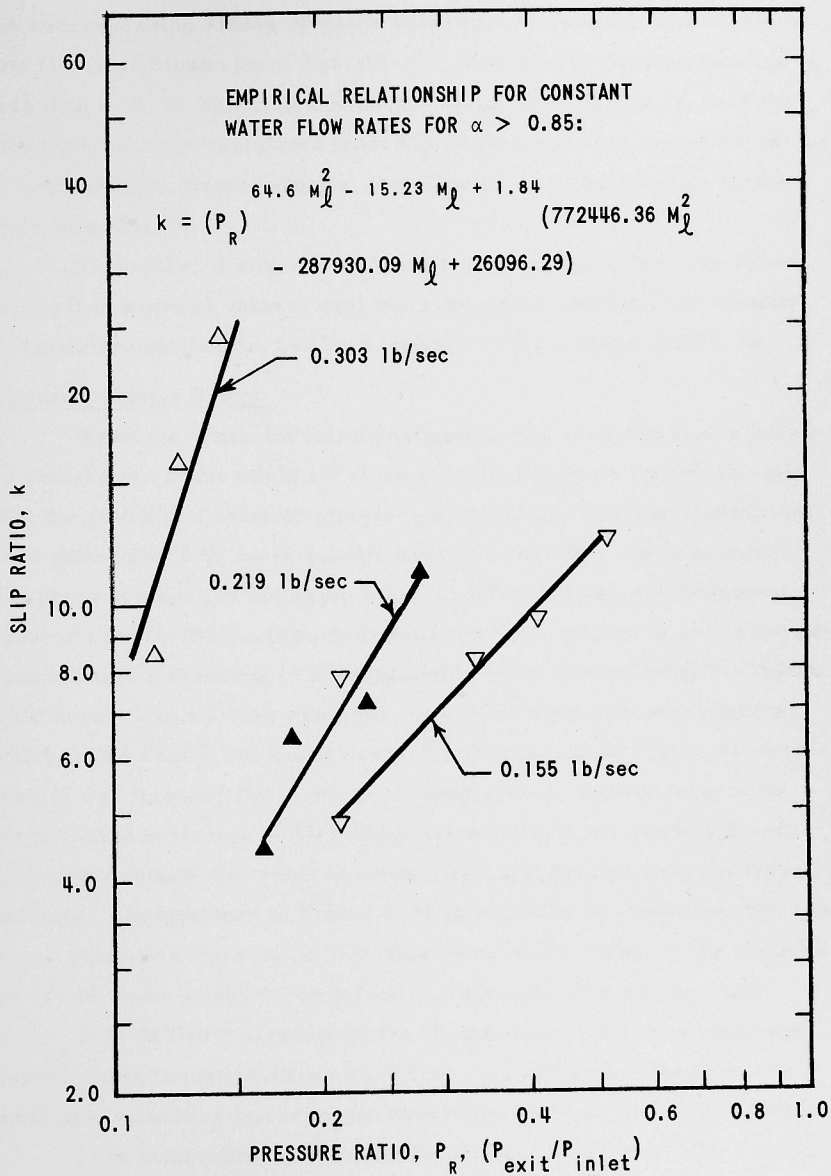


Fig. 32. Exit Slip Ratio-Pressure Ratio Correlation; $\alpha > 0.85$

The void fraction is determined by Eq. 14, and if it is greater than 0.85 the corresponding values of water velocity, air velocity, and acceleration factor are found from Eqs. 15-17. However, if the void fraction is less than 0.85, as calculated from the use of Eqs. 22 and 14, then the slip ratio must be calculated from Eq. 21, and the corresponding values of void fraction, water velocity, air velocity, and acceleration factor from Eqs. 14-17.

Therefore, if both air and water mass rates of flow are known, all desired average values: void fraction, water velocity, air velocity, and acceleration factor, can be predicted by Eqs. 14-17 and 20-22.

Optimum Nozzle Design

When the nozzle for this investigation was designed, it was intended that the air phase would accelerate the liquid phase to such an extent that the exit liquid velocity would be greater than it had been at the throat. This effect would be more readily accomplished by a one-component two-phase system (for the same inlet conditions as the two component system) because the liquid portion would continue to flash to gas as expansion occurred, resulting in more gas effectively to accelerate the liquid. This nozzle was initially designed for a one-component investigation, which is the reason for the long exit section as seen in Fig. 3. Nevertheless, it was intended for a two-component system so that, despite the large increase in area (5.81/1) from throat to exit, the air would sufficiently accelerate the water to an exit velocity greater than the throat velocity. Examination of Tables 1-21 in Appendix H shows that the exit water velocities were much less than those at the throat by as much as 14.7/1 in Table 16 for 0.308 lb/sec and a quality of 6.84 per cent.

It is difficult to compare the throat liquid velocities since the quality range investigated for each flow rate differed. However, the maximum velocities occurred for water flow rates equal to 0.303 lb/sec.

It is interesting to note that for a water flow rate of 0.498 lb/sec (Tables 1-7) the liquid velocity at position 9 actually did exceed the

velocity at the throat for lower qualities. Therefore, at least for certain conditions, the water is accelerated after the throat to a velocity exceeding the throat velocity. As a result, for a two-component two-phase system the optimum nozzle design would either be of the converging type or the converging-diverging type with only a short diverging portion.

A considerable amount of effort must be exerted to determine optimum design conditions. Experiments must be performed on both converging-type and converging-short-diverging-type nozzles. The latter would result in a small exit-to-throat area ratio as evidenced by the results at position 9 in this investigation, where the ratio was 1.5/1.

It must be pointed out that converging and converging-short diverging nozzles when exhausting into an atmospheric condition will result in lower throat and exit pressures than found in this investigation, and, thus, lower the air densities. This would tend to increase the slip ratio at the throat and exit, an undesirable condition. This possibly can be countered in part by increasing the nozzle back pressure. However, the effects of smaller exit area, varying air density and, hence, changing void fractions on exit velocities and slip ratios, can only be determined by additional experimentation.

Theoretical Models Used in Predicting Nozzle Characteristics

Attempts have been made at the University of California Radiation Laboratory^(10,11) to predict mass flow rate densities in nozzles by various flow models based on initial test conditions. The models and assumptions were:

1. Homogeneous model
 - a. slip ratio of unity
 - b. thermal equilibrium at a cross section
 - c. isentropic expansion
 - d. pressure equilibrium at a cross section

2. Separated phase model
 - a. thermal equilibrium at a cross section
 - b. isentropic expansion
 - c. pressure equilibrium at a cross section
 - d. liquid velocity behaves according to Bernoulli's equation
 - e. gas velocity behaves according to the energy equation.
3. Slip flow model
 - a. isentropic expansion
 - b. adiabatic expansion
 - c. pressure equilibrium at a cross section
 - d. a value for slip ratio can be assumed
4. Frozen composition model
 - a. isentropic expansion
 - b. gas expands adiabatically according to $pv^{1.3}$ equals a constant

Of these models, the homogeneous model proved to be the most useful. This model predicted mass flow rate densities within 15 per cent for qualities from 5 to 28 per cent; below this range predictions were in error by as much as 60 per cent. The pressure range that was investigated was 100-1300 psia. Although the investigation presented in this report showed that slip ratios much greater than unity existed for qualities between 1 and 15 per cent (see Figs. 24-28), nothing definite can be said with regard to the above system because of the much greater operating pressures.

Reese and Richard⁽⁷⁾ proposed an "isentropic flow model with no internal temperature differences" to predict liquid exit velocities. The assumptions they made are as follows:

1. perfect thermal mixing with no temperature differential between phases throughout expansion;
2. isentropic, adiabatic flow;
3. slip ratio equal to unity;

4. steady, one-dimensional flow so that the energy and continuity equations apply between nozzle inlet and exit.

They measured thrusts and calculated a liquid exit velocity, assuming all the thrust was a result of liquid momentum. They obtained very good results, their predicted velocities being within 88-90 per cent of the measured velocities for a helium-liquid nitrogen system. Either the two assumptions of slip equal to unity and thermal equilibrium were incorrect assumptions tending to offset one another, or slips very close to unity actually did exist for their system (inlet pressure of 500 psig).

Muir and Eichhorn⁽¹⁵⁾ also used the homogeneous model to predict nozzle exit characteristics. They investigated the bubble-flow region for an air-water system for inlet pressures up to 90 psia and qualities from 0.013 to 0.548 per cent, and found that for qualities from 0.013 to 0.154 per cent (the bubble-flow regime) slip ratios very close to unity (1.2-1.4) actually did exist. Thus, actual nozzle characteristics could be predicted quite accurately with the homogeneous model for bubble-type flow.

Nevertheless, no models have as yet been proposed that can reasonably predict nozzle exit characteristics for other than limited ranges. From the results presented in this investigation, models assuming a slip ratio of unity break down when attempting to predict nozzle characteristics for low-pressure, low-quality (at least up to 15 per cent) systems having a flow regime other than the bubble type.

Nozzle Efficiency

The purpose of this investigation was primarily to determine how well the liquid phase could be accelerated by the gaseous phase. Elliott⁽⁹⁾ has proposed a nozzle efficiency based on an isentropic, homogeneous expansion. A homogeneous expansion is one in which thermodynamic equilibrium is attained and no relative velocity exists between the liquid and gaseous phases. Using the steady-state energy equation and the First Law of Thermodynamics, Elliott derived the

following equations for the ideal liquid exit velocity and nozzle efficiency, respectively:

$$V_2 = \left[2x \frac{\bar{R}T_i}{\bar{M}} \ln\left(\frac{p_i}{p_e}\right) + 2v(p_i - p_e) \right]^{1/2} \quad (23)$$

and

$$\eta = \frac{(V_{\ell})_e^2}{(V_2)^2} \quad , \quad (24)$$

where

V_2 = ideal liquid exit velocity

x = quality

\bar{R} = universal gas content

\bar{M} = molecular weight of gas

T_i = nozzle inlet temperature, °F_{abs}

v = specific volume of liquid phase

p_i = pressure at the nozzle inlet

p_e = pressure at the nozzle exit

η = nozzle efficiency

$(V_{\ell})_e$ = actual two-phase liquid exit velocity.

For the analytical development of the above two equations, see Appendix F.

Elliott investigated air-hot water systems at inlet pressures of 500 psig and obtained efficiencies of 0.65-0.80. His measured liquid velocities were obtained by measuring the thrust and assuming it was a result of liquid momentum only. However, reference to Table 41 reveals that, for this investigation, nozzle efficiencies based on Elliott's ideal expansion were considerably lower. These efficiencies ranged from 0.10 to 2.80 per cent and differed radically in magnitude from the results obtained by Elliott. He was investigating larger ranges of working pressure, but was discharging into atmospheric conditions, and, therefore, the density effect upon slip ratios should have been no different for his results than for the results of this investigation.

Yet the slip ratios for this investigation at the nozzle exit were very much greater than unity (see Figs. 26-28). If Elliott's slip ratios were anywhere close to the magnitudes encountered in this investigation, then his assumption that the thrust was a result of liquid momentum only was very much in error, and would result in considerably lower exit liquid velocities than were reported, thus decreasing the actual nozzle efficiency.

Although the efficiency magnitudes in this investigation were small, definite trends were established. The efficiency for a constant water flow rate tended to decrease with increasing quality until it reached a minimum, at which it then began to increase with increasing quality, indicating that higher efficiencies were a function of low slip ratios. The slip ratio was tending toward unity as the quality was increased (above a limiting value) (see Figs. 26-28), and, hence, the efficiency would probably increase still more as even higher qualities were encountered; and more reasonable efficiencies might then be obtained.

Critical Mass Velocity and Critical Pressure

In a flow system there is no flow obtained until some pressure difference exists between the upstream and downstream positions. Therefore, for a constant-pressure system, there is no flow. As the pressure downstream is lowered to a value less than at some upstream location, flow begins. As this pressure differential is increased, the flow also increases until some condition where continuing to decrease the downstream condition (relative to a fixed upstream condition) no longer increases the flow rate. After this point the flow rate will remain constant regardless of how much the downstream pressure is lowered. A derivation of this maximum or critical flow is derived in Appendix G for a single-phase compressible fluid. The equation is

$$G_c = \left[-g_c \left(\frac{dp}{dv} \right) \right]^{1/2}, \quad (25)$$

where

G_C = the critical mass velocity for a one-phase compressible fluid

g_c = gravitational constant = 32.2 ft-lb_m/lb_F-sec²

v = specific volume

Attempts have been made to apply this equation to two-phase fluids by assuming a homogeneous model such that no relative velocities exist between the two phases and that the specific volume is additive. Thus, the homogeneous critical mass velocity is

$$G_H = \left[-g_c \left(\frac{dp}{dv} \right) \right]^{1/2}, \quad (26)$$

where

$$v = (1-x)v_\ell + xv_g \quad (27)$$

Previous investigators^(10,11,20) working with steam-water mixtures have reported that the homogeneous model leads to predicted values of mass velocities that are less than the measured mass velocities. They claimed that this was probably a result of slip between the phases or thermodynamic nonequilibrium, or both.

Some representative values were calculated in this investigation by the homogeneous model and the results are shown in Table 40. A sample calculation is shown in Appendix G. For all conditions the measured mass velocity was greater than mass velocity as predicted by the homogeneous theory. Since the system tested was essentially a constant-quality system, observed deviations from the homogeneous mass velocity were probably a result of slips not equal to unity at the nozzle throat (for slip magnitudes at the throat see Tables 1-39).

Faletti and Moulton⁽²⁰⁾ investigated a cylindrical-tube test section exhausting into an expansion chamber. Steam-water mixtures at qualities from 0 to 100 per cent and pressures from 0 to 100 psig were tested. They measured critical mass velocities and critical exit plane (throat) pressures by decreasing the pressure in the expansion chamber until a condition was attained in which continuing to lower the

pressure did not change the mass velocity and pressure profiles upstream. Figure 33 shows some of their results for a quality at the exit plane of 20.5 per cent. They measured the profiles into the expansion chamber with a pressure probe. Note that they observed an expansion past the exit plane. Also note that for an expansion chamber pressure setting of 20.0-21.5 psig the upstream pressure profiles was not quite coincident with the profiles of the other two pressure settings. Hence, this setting was probably the maximum back pressure at which continuing to decrease the back pressure (for a fixed inlet condition) would increase the mass velocity. Therefore, the critical mass velocity was obtainable at a maximum back pressure of about 20.0-21.5 psig. Continuing to decrease the back pressure (to 12.0 ± 0.5 psig and 1.9-2.0 psig) did not change the pressure profiles upstream. Thus, critical flow probably existed for all three settings shown. Note the extreme pressure gradient in the exit plane (throat) region.

Figure 34 shows a comparison for a typical run for this investigation with one of Faletti's runs. In this figure, the nozzle length is plotted so that the throat location corresponds to the location of Faletti's exit plane. Thus, the nozzle pressure profile behaved similarly to the cylindrical tube profile, the diverging section having similar effects to the expansion chamber of the cylindrical tube. Note the extreme pressure gradient at the nozzle throat. This leads to the conclusion that critical flow possibly may have existed for this nozzle test condition. If this is the case, the mass velocities are seriously limited in nozzle flow, and for a fixed inlet condition there is a maximum obtainable mass velocity, a mass velocity that cannot be exceeded by decreasing the nozzle back pressure below a certain limit. The trend of the nozzle pressure profile shown in Fig. 34 was typical of all compressible type conditions investigated in this report.

Fauske⁽²¹⁾ conducted tests similar to those of Faletti and Moulton, and reported similar results. He proposed a model which, at present, appears to be the most accurate model for predicting critical

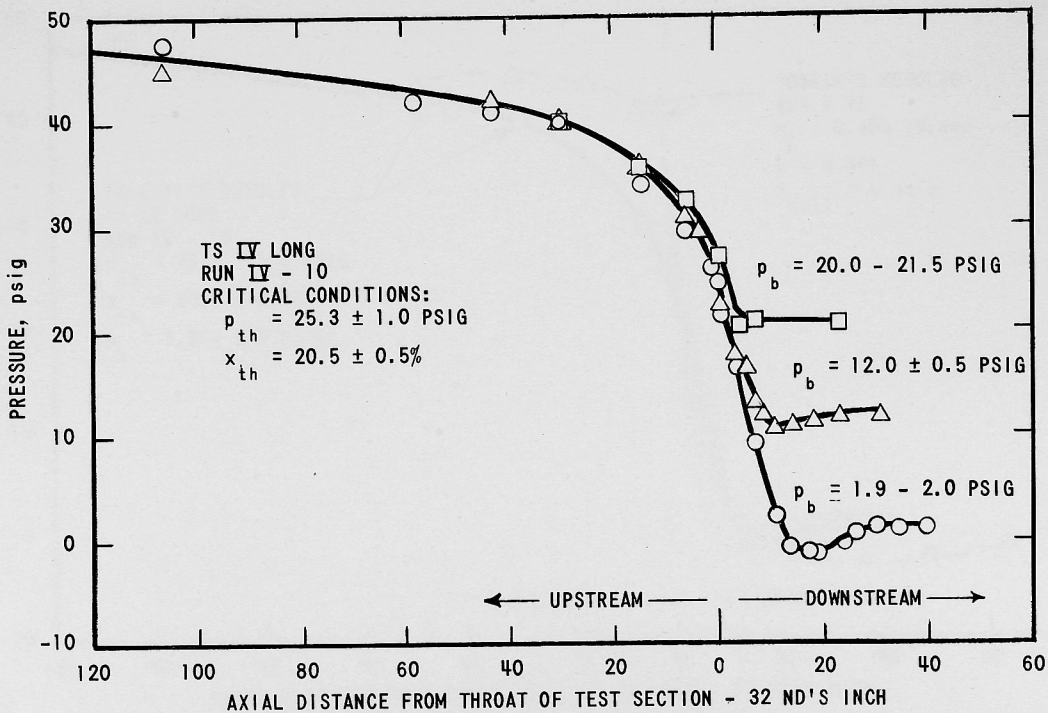


Fig. 33. Faletti and Moulton Results - Effect of Back Pressure on the Profile, 20.5% Steam

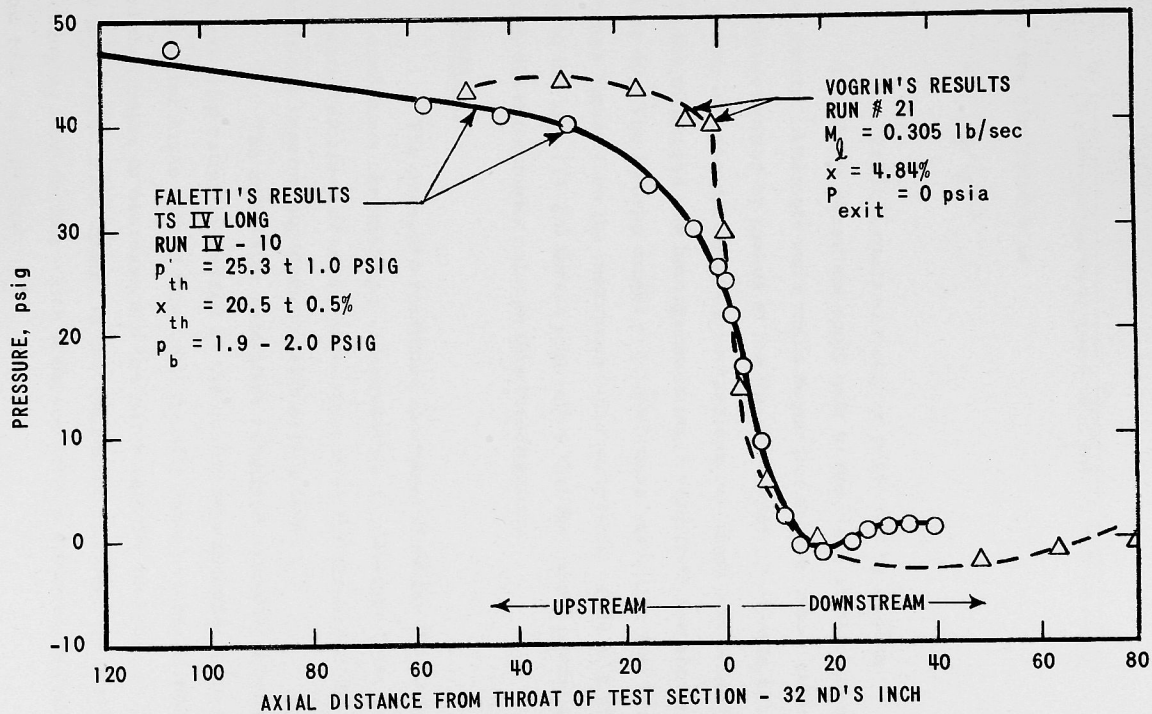


Fig. 34. Comparison of Vogrin and Faletti's Results

mass velocities in a cylindrical tube exhausting into an expansion chamber. This model leads to the equation

$$G_F = \left[\frac{-gck}{[(1-x+kx) \frac{dv_g}{dp} + [v_g(1+2kx-2x) + v_g(2kx-2k-2kx^2+k^2)] \frac{dx}{dp} + k [1+x(k-2) - x^2(k-1)] \frac{dv_g}{dp}]^{1/2}} \right] \quad (28)$$

where the slip ratio k is

$$k = (v_g/v_l)^{1/2} \quad (29)$$

and

G_F = critical mass velocity as predicted by Fauske.

The above equations apply only to the plane at which critical flow exists. Attempts were made to predict critical mass velocities in this investigation by means of the Fauske model. A sample calculation is shown in Appendix G, and a comparison for some test conditions with the measured and homogeneous mass velocities are shown in Table 40. The Fauske model predicted mass velocities that were 1.5 to 3 times higher than the measured mass velocities. This was primarily due to the high (14-25) throat slip ratios that the model predicted but which did not actually exist in this investigation.

Conclusions

1. The pressure continued to expand after the throat for the flow conditions resembling a compressible-family-type flow, but the pressure remained essentially constant after the throat for the flow conditions resembling incompressible-type flow.
2. The exit water velocities remained essentially constant and the exit slip ratios increased as the quality was increased for a constant water mass rate of flow until the slip ratio reached a maximum, and then began to decrease and the water velocity increase as the quality increased. This change in exit characteristics can be attributed to a changing flow regime which occurred from a dispersed annular-type flow to a fog-type flow.

3. For given water and air mass rates of flow, the pressure ratio (exit to inlet), exit water velocity, exit air velocity, exit slip ratio, and exit acceleration factor can be predicted from empirical relationships for a nozzle having the same configuration as the one tested in this investigation.

4. The slip ratio tended to approach a value of unity for high qualities (10-15 per cent), and it appeared as though this condition might be attained if the quality was increased still higher.

5. For a two-component, two-phase application, the optimum nozzle design is either a converging or a converging-short-diverging type. It is possible for some conditions to obtain higher water velocities at the exit of the converging-short-diverging nozzle than at the throat, provided the exit-to-throat area ratio is approximately in the range of 1-2 to 1.

6. Theoretical models assuming a slip ratio of unity, which in the past have been used for predicting nozzle exit characteristics, are generally valid for only limited ranges for nozzles exhausting to the atmosphere. Previously proposed models break down when attempting to predict nozzle exit characteristics for low-pressure, low-quality (at least up to approximately 15 per cent) systems having a flow regime other than the bubble type.

7. Radical pressure gradients in the throat region indicated the possibility that critical flow may have been present for the conditions tested. This means that the maximum mass velocities for the fixed upstream conditions had been obtained, and any decrease of the back pressure relative to the fixed upstream pressure would result in no additional mass velocity.

8. Very low efficiencies, based upon an isentropic, homogeneous model proposed by Elliott, were obtained and were probably due to very high slip ratios.

Suggested Further Considerations

The next step in two-component, two-phase study should be the investigation of converging and converging-short-diverging type nozzles. In addition, the effects of varying the nozzle back pressure should be considered to determine the effects on slip ratio, and also to determine if critical flow actually did exist. It is suggested that future studies also be conducted with higher ranges of working pressure to determine whether slip ratios close to unity actually do exist.

Investigations should also be conducted with one-component, two-phase systems, as greater exit liquid velocities would probably result for the same inlet conditions as for the two-component system.

APPENDIX A
FLOW RATE DETERMINATION

Two orifices, one to measure air flow and the other to measure the water flow, were constructed and installed according to ASME specifications.⁽¹⁶⁾ The air orifice, which had vena-contracta taps, was not calibrated, but its characteristics were calculated by means of ASME experimental values for the flow coefficient K' and the expansion factor Y . The working equation used was

$$M_g = 0.525K'YD^2\gamma_1^{1/2}(p_1 - p_2)^{1/2} \text{ lb sec}^{-1} \quad (\text{A-1})$$

where

$$K' = C/(1 - \beta^4)^{1/2}$$

$$C = \text{discharge coefficient} = \frac{\text{actual weight flow}}{\text{theoretical weight flow}}$$

$$\beta = \text{orifice diameter/pipe diameter}$$

$$Y = \text{expansion factor}$$

$$D = \text{orifice diameter}$$

$$\gamma_1 = \text{specific weight at orifice inlet}$$

$$p_1 = \text{pressure (psia) at orifice inlet}$$

$$p_2 = \text{pressure (psia) at orifice exit}$$

$$0.525 = \text{constant to establish proper units.}$$

The flow rate through the water orifice, which had flanged taps, was calculated by the above equation. In addition, the water orifice was calibrated by measuring various flow rates with a weight tank over a time interval, and recording the corresponding pressure drop in in. of mercury for high flow rates and in. of fluid of specific gravity 2.95 for low flow rates. The calculated and calibrated flow rates agreed within 2 per cent for flow rates greater than 0.75 lb/sec, but differed radially for lower flow rates.

APPENDIX B
ANALYTICAL DEVELOPMENT -
GAMMA-RAY-ATTENUATION METHOD

Radiation upon passing through the thickness of a substance is reduced in intensity by a factor μ per in. It can be assumed that the intensity of radiation of a collimated beam of monoenergetic radiation can be represented by the following relationship:

$$I = I_0 e^{-\mu y} \quad , \quad (B-1)$$

where

I = intensity of radiation at a position y

I_0 = intensity of radiation at a position $y = 0$

μ = linear absorption coefficient per in.

y = depth of radiation penetration in in.

Further,

$$\mu = N_0 \rho \sigma / A \quad , \quad (B-2)$$

where

N_0 = Avogadro's number

A = atomic weight of penetrated substance

σ = microscopic cross section

ρ = density of penetrated substance.

But N_0 , σ , and A remain constant for a specific substance. Therefore,

$$\mu = c \rho \quad , \quad (B-3)$$

where

$c = N_0 \sigma / A =$ mass absorption coefficient.

Before proceeding with the analysis, the following assumptions must be made: 1) that the gamma ray is monoenergetic, 2) the gas-liquid media can be represented by layers perpendicular to the direction of radiation, and 3) only the radiation passing through the liquid-gas

media impinges upon the scintillation crystal. The first assumption was fulfilled by the insertion of a $\frac{1}{32}$ -in. steel plate between source and nozzle as discussed in Chapter II. Thus, only the high-energy (84-kev) beam of the thulium source impinges upon the scintillation crystal. Assumptions 2 and 3 were not necessarily true, but in all probability conditions very close to these actually did exist.

Figure 35 shows a typical nozzle cross sectional area as seen by the gamma rays passing through a $\frac{1}{16}$ -in. lead detection window. The liquid film with gaseous core does not represent an actual test condition, but is shown in this manner merely for analysis purposes. The gas phase, liquid phase, and wall thicknesses are y_g , y_l , and y_w , respectively.

Combining Eqs. B-1 and B-3,

$$I = I_0 e^{-c\rho y} \quad (B-4)$$

For a three-layer substance as shown in Fig. 35, Eq. B-4 becomes

$$I = I_0 e^{-c_g \rho_g y_g} e^{-c_l \rho_l y_l} e^{-c_w \rho_w y_w} \quad (B-5)$$

but as seen in Fig. 35

$$y_g = y_4 \quad ; \quad y_l = y_2 - y_4 \quad (B-6)$$

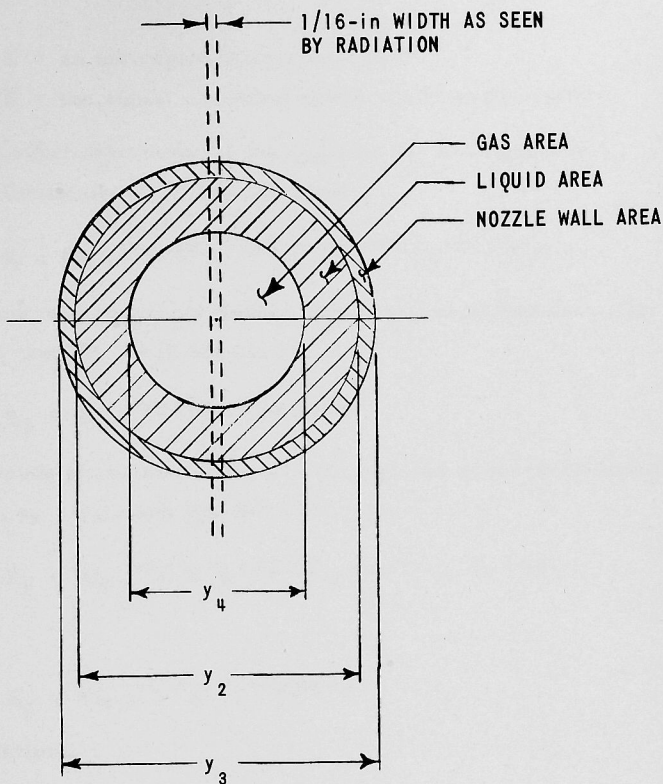
Combining Eqs. B-5 and B-6,

$$I = I_0 e^{-c_g \rho_g y_4} e^{-c_l \rho_l (y_2 - y_4)} e^{-c_w \rho_w y_w} \quad (B-7)$$

and

$$I = I_0 e^{-y_4(c_g \rho_g - c_l \rho_l)} e^{-c_l \rho_l y_2} e^{-c_w \rho_w y_w} \quad (B-8)$$

If the current amplifier of the detecting equipment is a linear amplifier, then the intensity of the radiation impinging upon the scintillation crystal is proportional to the signal received by the electronic recorder. Thus, the recorder signal is proportional to the radiation intensity as received by the crystal detector by the following relationship:



THICKNESSES AS SEEN BY RADIATION

1. GAS THICKNESS: $y_g = y_4$
2. LIQUID THICKNESS: $y_l = y_2 - y_4$
3. WALL THICKNESS: $y_w = y_3 - y_2$

Fig. 35. Gas, Liquid, and Wall Thicknesses as Seen by Radiation through $\frac{1}{16}$ -in. Lead Window in a Typical Nozzle Cross Section

$$E = KI \quad , \quad (B-9)$$

where

K = an instrumentation constant

E = the signal recorded by the electronic recorder.

For a further discussion of the constant K , see Appendix C.

Combining Eqs. B-8 and B-9,

$$E = KI_0 e^{-y_4(c_g \rho_g - c_l \rho_l)} e^{-c_l \rho_l y_2} e^{-c_w \rho_w y_w} \quad . \quad (B-10)$$

If a liquid only is passed through the cross-sectional area (that is, $y_4 = 0$), then Eq. B-10 becomes

$$E_l = KI_0 e^{-c_l \rho_l y_2} e^{-c_w \rho_w y_w} \quad . \quad (B-11)$$

If a gaseous phase only is passed through the cross-sectional area (that is, $y_4 = y_2$), then Eq. B-10 becomes

$$E_g = KI_0 e^{-y_2(c_g \rho_g - c_l \rho_l)} e^{-c_l \rho_l y_2} e^{-c_w \rho_w y_w} \quad . \quad (B-12)$$

Thus,

$$E_g = KI_0 e^{-c_g \rho_g y_2} e^{-c_w \rho_w y_w} \quad . \quad (B-13)$$

By definition,

$$\alpha = \frac{y_g}{y_g + y_l} = \frac{y_4}{y_4 + y_2 - y_4} = \frac{y_4}{y_2} \quad . \quad (B-14)$$

Therefore,

$$y_4 = \alpha y_2 \quad . \quad (B-15)$$

Combining Eqs. B-10 and B-15,

$$E = KI_0 e^{-\alpha y_2(c_g \rho_g - c_l \rho_l)} e^{-c_l \rho_l y_2} e^{-c_w \rho_w y_w} \quad . \quad (B-16)$$

Combining Eqs. B-11 and B-16,

$$E = E_l e^{-\alpha y_2(c_g \rho_g - c_l \rho_l)} \quad . \quad (B-17)$$

Dividing Eq. B-13 by B-11,

$$E_g/E_\ell = e^{-y_2(c_g \rho_g - c_\ell \rho_\ell)} \quad . \quad (\text{B-18})$$

Combining Eqs. B-17 and B-18,

$$E = E_\ell (E_g/E_\ell)^\alpha \quad . \quad (\text{B-19})$$

Taking the natural logarithm of both sides of Eq. B-19,

$$\ln E = \ln E_\ell + \alpha \ln (E_g/E_\ell) \quad . \quad (\text{B-20})$$

Therefore,

$$\alpha = \frac{\ln (E/E_\ell)}{\ln (E_g/E_\ell)} \quad , \quad (\text{B-21})$$

where

α = average void fraction

E = "two-phase" recorder reading

E_ℓ = "liquid only" recorder reading

E_g = "gas only" recorder reading.

Thus, the void fraction can be readily determined by measuring each of three conditions: 1) "two-phase" test condition, 2) "liquid phase only" condition (full reading), and 3) "gaseous phase only" condition (empty reading).

The above analysis gives the average local void fraction, or the average void fraction for the "one-shot" technique. However, in the "traversing" technique the source and detector crystal and tube are traversed across the cross section, and a trace of the distribution is recorded by the recording equipment. This procedure is repeated for the empty, full, and two-phase readings. Sample traces are shown in Fig. 12. The traces are aligned by matching corresponding positions 1, 2, 3, and 4 as shown in that figure. The cross section is divided into 16 equal portions, and the average local void fractions are determined by Eq. B-21 at each subdivision. A weighting factor is applied to each

division, and then the average void fraction is the sum of the products of the local void fractions and their corresponding weighting factors. The weighting factor is the ratio of the subdivision area to the total cross-sectional area. This method will now be shown analytically.

The actual void fraction $\bar{\alpha}$ is the ratio of the gas area to the total cross-sectional area:

$$\bar{\alpha} = \frac{\text{gas area}}{\text{total cross-sectional area}} \quad . \quad (\text{B-22})$$

From Fig. 36,

$$\bar{\alpha} = \text{gas area}/\pi r^2 \quad (\text{B-23})$$

and

$$\text{gas area} = \int_{y=-r}^{y=r} \psi(y) dy \quad . \quad (\text{B-24})$$

The average local void fraction between y and $y + dy$ is

$$\alpha_y = \psi(y)/\phi_y \quad (\text{B-25})$$

and

$$\psi(y) = \alpha_y \phi(y) \quad , \quad (\text{B-26})$$

but

$$\phi(y) = 2(r^2 - y^2)^{1/2} \quad . \quad (\text{B-27})$$

Therefore,

$$\text{gas area} = 2 \int_{y=-r}^{y=r} \alpha_y (r^2 - y^2)^{1/2} dy \quad . \quad (\text{B-28})$$

Combining Eqs. B-23 and B-28,

$$\alpha = \frac{2}{\pi r^2} \int_{y=-r}^{y=r} \alpha_y (r^2 - y^2)^{1/2} dy \quad . \quad (\text{B-29})$$

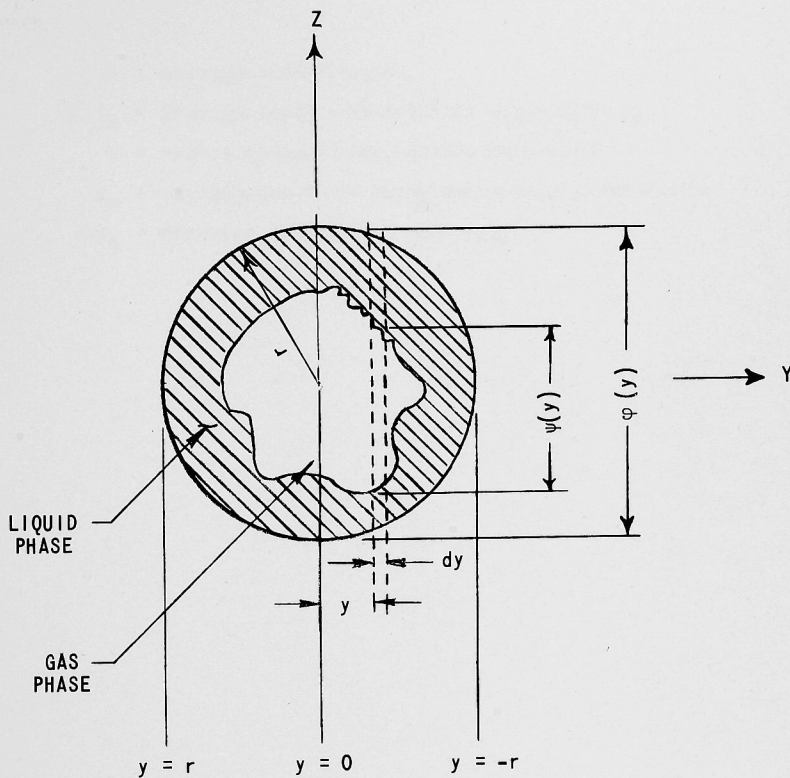


Fig. 36. Two-phase Cross Section; Annular Distribution Shown for Analysis Simplicity Only

Replacing the integral sign with a summation gives the average void fraction of the whole cross-sectional area:

$$\alpha = \frac{2}{\pi r^2} \sum_{n=1}^m (\alpha_y)_n (r^2 - y_n^2)^{1/2} (\Delta y_n) \quad , \quad (\text{B-30})$$

where

- α = average void fraction
- $(\alpha_y)_n$ = average local void fraction at position y_n
- r = radius of the cross section traversed
- y_n = various positions along the nozzle cross section
- Δy_n = distance between y_n and y_{n+1} .

APPENDIX C
DETERMINATION OF INSTRUMENTATION CONSTANT K

It was established in the derivation of the void fraction relationship that the recorder electromotive force E was proportional to the intensity I impinging upon the scintillation crystal. From Eq. B-9,

$$E = KI \quad . \quad (B-9)$$

However, Hooker and Popper⁽²²⁾ have given a detailed discussion of what this constant K includes. The following is a summary of their discussion.

The light output of the scintillation crystal is proportional to the amount of unattenuated radiation impinging upon the crystal:

$$\phi_v = f_1(T)\phi \quad , \quad (C-1)$$

where

ϕ_v = amount of visible light

ϕ = impinging radiation = IA

$f_1(T) = \phi_v/\phi$ = conversion efficiency of the scintillation crystal.

The conversion efficiency can be assumed to be constant over the range of fluxes involved, but its value is a function of temperature. The output current of the photomultiplier tube is governed by the following relationship:

$$i = k_1 f_2(T) (v_h)^7 \phi_v \quad , \quad (C-2)$$

where

i = output current of photomultiplier tube

k_1 = a constant representing the fraction of the total light received from the crystal

$f_2(T)$ = the product of the temperature-dependent photomultiplier tube conversion efficiency and conversion units

v_h = negative supply voltage to the photomultiplier tube.

The current signal is fed from the photomultiplier tube through the linear current amplifier whose output voltage E is

$$E = k_2 i \quad , \quad (C-3)$$

where

K_2 = transfer characteristic of the current amplifier.

Combining Eqs. C-1, C-2, and C-3,

$$E = k_1 k_2 f_2(T) (v_h)^7 f_1(T) A I \quad . \quad (C-4)$$

Therefore,

$$K = k_1 k_2 f_1(T) f_2(T) A (v_h)^7 \quad . \quad (C-5)$$

APPENDIX D
AN ANALYSIS OF DENSITY EFFECT ON FULL AND EMPTY
READINGS FOR VOID FRACTION DETERMINATION

The measurements of the empty and full readings for determination of the void fraction should theoretically be taken at the same pressure and temperature of the corresponding two-phase test run. In this investigation, empty and full readings were taken, and all test runs were conducted at essentially the same temperature, approximately equal to the ambient air temperature. Thus, temperature had only a negligible effect on both liquid and gaseous phase densities. Since water is essentially an incompressible fluid in the range tested (10 to 150 psia), pressure also had only a negligible effect on liquid densities. Therefore, the full reading for a specific test does not require the same liquid pressures and temperatures as were obtained in the corresponding test condition, that is, the full reading could be obtained for any subcooled condition in the above-stated pressure range.

However, the gaseous phase density changes radically with change in system pressure. Assuming that moist air follows closely the perfect gas law, the density, then, will change according to the ratio of initial to final pressure. From Eq. B-13,

$$E_g = KI_0 e^{-c_g \rho_g Y_2} e^{-c_w \rho_w Y_w} \quad (B-13)$$

Application of the above equation to two conditions, one at $p_1 = 10$ psia and the other at $p_2 = 150$ psia (these two pressures covered the range tested in this experiment), yields

$$E_{g_1} = K_1 I_0 e^{-(c_g \rho_g Y_2)_1} e^{-c_w \rho_w Y_w} \quad (D-1)$$

and

$$E_{g_2} = K_2 I_0 e^{-(c_g \rho_g Y_2)_2} e^{-c_w \rho_w Y_w} \quad (D-2)$$

The ratio of Eq. D-1 to D-2 gives

$$\frac{E_{g_1}}{E_{g_2}} = \frac{K_1 e^{-(c_g \rho_g y_2)_1}}{K_2 e^{-(c_g \rho_g y_2)_2}} \quad (D-3)$$

But $K_1 = K_2$, since K is an instrumentation constant, and $c_{g_1} = c_{g_2}$, since the mass absorption coefficient is not affected by density change. It is, however, affected by the energy level of the radioactive source. From Grodstein,⁽²³⁾ we obtain for an energy level of 84 keV

$$c_{g_1} = c_{g_2} = 0.159 \text{ cm}^2/\text{gr} = 0.0778 \text{ ft}^2/\text{lb}$$

The densities at 80°F are

$$\rho_1 = \frac{P_1}{RT_a} = \left(\frac{10}{53.35} \right) \left(\frac{144}{540} \right) = 0.0498 \text{ lb/ft}^3$$

and

$$\rho_2 = 0.0498 \left(\frac{150}{10} \right) = 0.748 \text{ lb/ft}^3$$

In view of the above, Eq. D-3 becomes

$$\frac{E_{g_1}}{E_{g_2}} = \frac{e^{-[(0.0778)(0.0498)y_2]}}{e^{-[(0.0778)(0.748)y_2]}} \quad (D-4)$$

At the nozzle inlet, the cross-sectional inlet diameter, $y_2 = 1.0002 \text{ in.} = 0.0835 \text{ ft}$. Thus,

$$\frac{E_{g_1}}{E_{g_2}} = \frac{e^{-(0.0778)(0.0498)(0.0835)}}{e^{-(0.0778)(0.748)(0.0835)}} \quad (D-5)$$

and

$$\frac{E_{g_1}}{E_{g_2}} = \frac{e^{(-323.516 \times 10^{-6})}}{e^{(-485.923 \times 10^{-6})}} \quad (D-6)$$

Both the numerator and the denominator are approximately equal to 1.00 since

$$\lim_{z \rightarrow 0} (e^z) = 1.00 \quad . \quad (D-7)$$

Therefore,

$$E_{g_1}/E_{g_2} \cong 1.00 \quad . \quad (D-8)$$

Equations D-5 to D-8 apply to the nozzle inlet condition. The inlet condition has the largest diameter, y_2 , as shown in Fig. 3. Therefore, at any other position in the nozzle, the ratio E_{g_1}/E_{g_2} in Eq. D-8 will become more exact. As a result, for this nozzle in the pressure range specified (and in even a much greater range), the empty reading is a negligible function of system pressure.

In accordance with the above analysis, the empty and full measurements can be obtained at any system pressure and subcooled temperature (and, therefore, any system density) regardless of the corresponding test conditions. An experiment was performed with the thulium-170 sink and the photomultiplier tube source at fixed positions while varying the system empty pressures. A similar procedure was performed while varying the system full pressures. In both instances it was observed that the system pressure had no effect on the recorder reading.

APPENDIX E
 DETERMINATION OF THE TRUE VOID FRACTION DISTRIBUTION
 ALONG THE NOZZLE CENTERLINE

The following analysis was developed by Haywood et al.⁽²⁴⁾ and Schwarz,⁽²⁵⁾ and was obtained from a report by Petrick.⁽²⁶⁾

It was assumed that the void fraction at any radius r can be closely approximated by a polynomial equation such that

$$\alpha_r = a\left(\frac{r}{R}\right)^2 + b\left(\frac{r}{R}\right)^4 + c\left(\frac{r}{R}\right)^6 + d \quad , \quad (\text{E-1})$$

where a , b , c , and d are arbitrary constants, α_r is the void fraction at some position r , and the remainder of the symbols are designated in Fig. 37.

At any chord at a distance z from the center, the average void fraction is

$$\alpha_z = \int_0^Y \alpha_r \frac{dy}{Y} \quad , \quad (\text{E-2})$$

with

$$r = (y^2 + z^2)^{1/2} \quad . \quad (\text{E-3})$$

Combining Eqs. E-1, E-2, and E-3,

$$\alpha_z = \frac{a}{YR^2} \int_0^Y (y^2 + z^2) dy + \frac{b}{YR^4} \int_0^Y (y^2 + z^2)^2 dy + \frac{c}{YR^6} \int_0^Y (y^2 + z^2)^3 dy + \frac{d}{Y} \int_0^Y dy \quad . \quad (\text{E-4})$$

Performance of the indicated integration yields

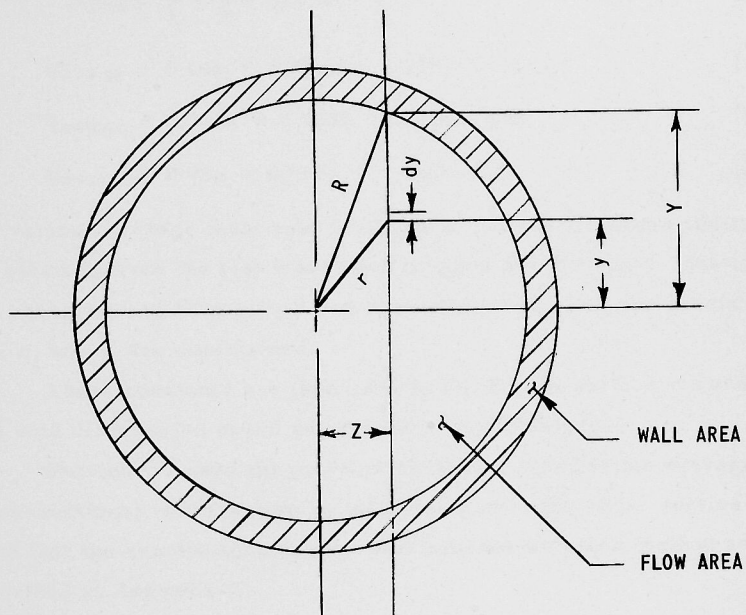


Fig. 37. Cross Section of a Circular Channel

$$\alpha_z = \frac{a}{R^2} \left(\frac{Y^2}{3} + z^2 \right) + \frac{b}{R^4} \left(\frac{Y^4}{5} + \frac{2}{3} Y^2 z^2 + z^4 \right) + \frac{c}{R^6} \left(\frac{Y^6}{7} + \frac{3}{5} Y^4 z^2 + Y^2 z^4 + z^6 \right) + d \quad . \quad (\text{E-5})$$

Evaluation of Eq. E-5 at $z = 0$, $z = 0.4R$, $z = 0.6R$, and $z = 0.8R$ yields

$$\alpha_{z=0} = \frac{a}{3} + \frac{b}{5} + \frac{c}{7} + d \quad ; \quad (\text{E-6})$$

$$\alpha_{z=0.4R} = 0.44a + 0.256b + 0.1799c + d \quad ; \quad (\text{E-7})$$

$$\alpha_{z=0.6R} = 0.573a + 0.365b + 0.255c + d \quad ; \quad (\text{E-8})$$

$$\alpha_{z=0.8R} = 0.76a + 0.587b + 0.465b + d \quad . \quad (\text{E-9})$$

The various average local void fractions at each of the above positions are obtained from the test traces and plugged into the above equations. The equations are then solved simultaneously and, thus, the constants a , b , c , and d are determined.

These constants are then used in Eq. E-1 at various r 's and the true void distribution at the centerline is thus obtained.

Petrick⁽²⁶⁾ used the polynomial fit to determine the average cross-sectional void fraction by integrating over the cross section and found that the results agreed very well with the weighted method as described in Appendix B.

APPENDIX F
ANALYTICAL DEVELOPMENT OF ELLIOTT'S NOZZLE EFFICIENCY

Elliott⁽¹⁾ has proposed a liquid metal cycle for the production of electrical power, as shown in Fig. 38. Essentially, the cycle consists of a vapor accelerating a liquid metal in a two-phase converging-diverging nozzle, a separation process, and the use of the kinetic energy and the high electrical conductivity of the liquid metal to produce electrical power in the magnetohydrodynamic generator.

The following analysis was taken in part from Elliott's unpublished notes,⁽⁹⁾ in which he derived an ideal two-phase, two-component liquid exit velocity. The ideal velocity is based upon an isentropic, homogeneous expansion, and is calculated by means of the First Law of Thermodynamics and the energy equation. The term homogeneous means no relative velocity between liquid and air phases, and also that thermodynamic equilibrium exists.

The First Law of Thermodynamics in differential form for a reversible process is

$$dQ = du + p(dv) \quad , \quad (F-1)$$

where

- Q = heat energy
- u = specific internal energy
- p = pressure
- v = specific volume;

but,

$$u = h - pv \quad , \quad (F-2)$$

where

- h = specific enthalpy.

Differentiating Eq. F-2, there is obtained

$$du = dh - p(dv) - v(dp) \quad . \quad (F-3)$$

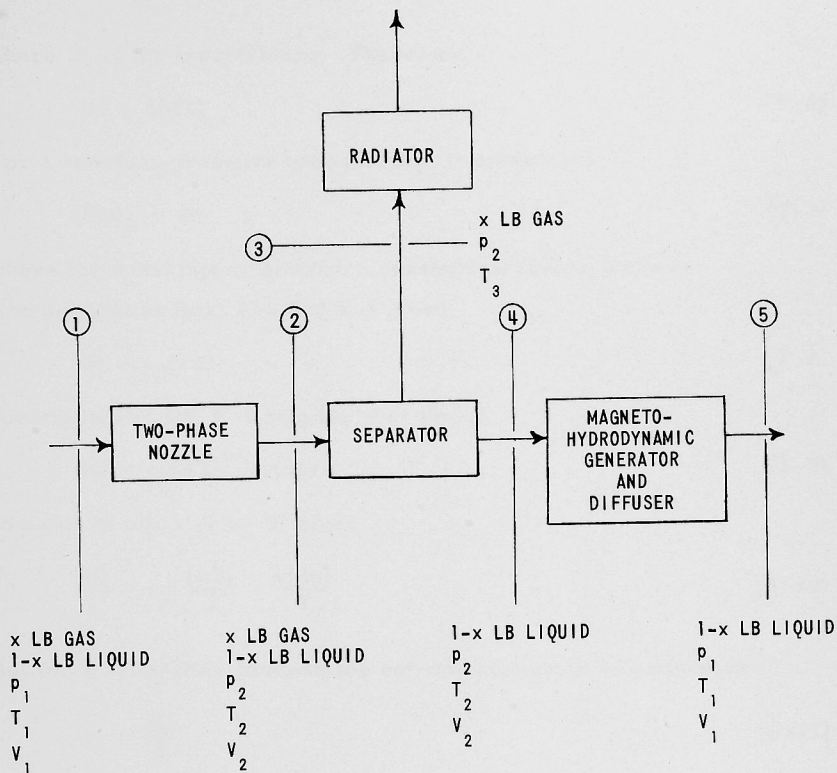


Fig. 38. Elliott's Schematic Diagram for a Two-Component Power Conversion Cycle

Combination of Eqs. F-1 and F-3 gives

$$dQ = dh - v(dp) \quad . \quad (F-4)$$

The heat capacity c is defined as

$$c = \frac{dQ}{dT} \quad , \quad (F-5)$$

where T is the temperature. Therefore,

$$dQ = c(dT) \quad . \quad (F-6)$$

For a constant-pressure process, Eq. F-4 becomes

$$(dQ)_p = dh \quad , \quad (F-7)$$

where the subscript p denotes a constant-pressure process.

Combination of Eqs. F-6 and F-7 gives

$$dh = c_p(dT) \quad . \quad (F-8)$$

Substitution of Eq. F-8 into Eq. F-4 yields

$$dQ = c_p(dT) - v(dp) \quad . \quad (F-9)$$

Division of Eq. F-9 by T gives

$$\frac{dQ}{T} = c_p \frac{(dT)}{T} - \frac{v(dp)}{T} \quad . \quad (F-10)$$

But for a reversible process the entropy change ds is defined as

$$ds = \frac{dQ}{T} \quad . \quad (F-11)$$

Therefore,

$$ds = c_p \frac{(dT)}{T} - \frac{v(dp)}{T} \quad . \quad (F-12)$$

For an ideal gas,

$$\frac{v}{T} = \frac{\bar{R}}{Mp} \quad , \quad (F-13)$$

where

M = molecular weight of the gas

\bar{R} = universal gas constant.

Therefore,

$$ds = c_p \left(\frac{dT}{T} \right) - \frac{\bar{R}}{M} \left(\frac{dp}{p} \right) .$$

Integrating between two state points (1 and 2) and assuming c_p is a constant, there is obtained the entropy change for an ideal gas in a reversible process:

$$\Delta s = s_2 - s_1 = c_p \ln \left(\frac{T_2}{T_1} \right) - \frac{\bar{R}}{M} \ln \left(\frac{p_2}{p_1} \right) . \quad (\text{F-14})$$

For an incompressible fluid, Eq. F-6 becomes

$$dQ = c_v(dT) , \quad (\text{F-15})$$

where the subscript v refers to a constant-volume process. Division of Eq. F-15 by T gives

$$\frac{dQ}{T} = c_v \frac{(dT)}{T} . \quad (\text{F-16})$$

Combination of Eqs. F-11 and F-16 yields

$$ds = c_v \frac{(dT)}{T} . \quad (\text{F-17})$$

Integration between state points 1 and 2 and the assumption that c_v remains constant throughout the interval gives

$$\Delta s = s_2 - s_1 = c_v \ln \left(\frac{T_2}{T_1} \right) . \quad (\text{F-18})$$

Thus, Eqs. F-14 and F-18 represent the entropy changes for the gas and liquid phases, respectively.

By definition, the enthalpy for an ideal gas is

$$dh = c_p(dT) . \quad (\text{F-19})$$

Integration over state points 1 and 2, assuming c_p to be constant, yields

$$\Delta h = h_2 - h_1 = c_p (T_2 - T_1) \quad . \quad (F-20)$$

From Eqs. F-4 and F-6,

$$dQ = c(dT) = dh - v(dp) \quad . \quad (F-21)$$

For an incompressible fluid

$$dh = c_v(dT) + v(dp) \quad . \quad (F-22)$$

Integration over state points 1 and 2 gives

$$dh = h_2 - h_1 = c_v(T_2 - T_1) + v(p_2 - p_1) \quad . \quad (F-23)$$

Thus, Eqs. F-20 and F-23 represent enthalpy changes for gas and liquid phases, respectively.

Figure 38 is based on the flow of a two-phase medium into and out of a converging-diverging nozzle. For two-component flow, the total entropy change through the nozzle is

$$\Delta s = x(\Delta s)_g + (1 - x)(\Delta s)_\ell \quad ,$$

where

$$\Delta s = s_2 - s_\ell$$

g = a subscript representing the gas phase

ℓ = a subscript representing the liquid phase.

Therefore, from Eqs. F-14 and F-18,

$$\Delta s = x c_p \ln \left(\frac{T_2}{T_1} \right) - x \frac{\bar{R}}{M} \ln \left(\frac{p_2}{p_1} \right) + (1 - x) c_v \ln \left(\frac{T_2}{T_1} \right) \quad . \quad (F-24)$$

But for the ideal nozzle the entropy is assumed to be constant throughout the flow process. Therefore,

$$x c_p \ln \left(\frac{T_2}{T_1} \right) - \frac{x \bar{R}}{M} \ln \left(\frac{p_2}{p_1} \right) + (1 - x) c_v \ln \left(\frac{T_2}{T_1} \right) = 0 \quad . \quad (F-25)$$

The total enthalpy change through the nozzle is

$$\Delta h = h_2 - h_1 = x(\Delta h)_g + (1 - x)(\Delta h)_l \quad . \quad (\text{F-26})$$

Combination of Eqs. F-20, F-23, and F-26 gives

$$\Delta h = x c_p(T_2 - T_1) + (1 - x) c_v(T_2 - T_1) + (1 - x) v(p_2 - p_1) \quad . \quad (\text{F-27})$$

Solution of Eq. F-25 for T_2/T_1 yields

$$\ln\left(\frac{T_2}{T_1}\right) = \frac{x \bar{R}/M}{x c_p + (1 - x) c_v} \ln\left(\frac{p_2}{p_1}\right) \quad . \quad (\text{F-28})$$

Taking the anti-log of Eq. F-28, there is obtained

$$\frac{T_2}{T_1} = \left(\frac{p_2}{p_1}\right)^{\frac{x \bar{R}/M}{x c_p + (1 - x) c_v}} \quad . \quad (\text{F-29})$$

For values of x of practical interest (that is, for low quality), the exponent is very small and T_2/T_1 can reasonably be expressed by the first two terms of the series expansion. Thus,

$$\frac{T_2}{T_1} = 1 + \frac{x \bar{R}/M}{x c_p + (1 - x) c_v} \ln\left(\frac{p_2}{p_1}\right) \quad . \quad (\text{F-30})$$

Combination of Eqs. F-27 and F-30 gives

$$\Delta h = v(1 - x)(p_2 - p_1) + \frac{x \bar{R} T_1}{M} \ln\left(\frac{p_2}{p_1}\right) \quad . \quad (\text{F-31})$$

But, from the steady-state energy equation for nozzle flow, if it be assumed that the inlet velocity is negligible and that no relative velocity exists between the liquid and gas phases,

$$\frac{V_2^2}{2} = -\Delta h = -(h_2 - h_1) \quad . \quad (\text{F-32})$$

Therefore,

$$\frac{V_2^2}{2} = v(1 - x)(p_1 - p_2) + \frac{x \bar{R} T_1}{M} \ln\left(\frac{p_1}{p_2}\right) \quad (\text{F-33})$$

and

$$\frac{V_2^2}{2} = x \left[\frac{\bar{R}T_1}{M} \ln \left(\frac{p_1}{p_2} \right) - v(p_1 - p_2) \right] + v(p_1 - p_2) \quad . \quad (F-34)$$

Assuming values of $p_1 = 150$ psia and $p_2 = 15$ psia, and that the liquid phase is water, we obtain

$$v(p_1 - p_2) = \frac{(150-15)}{62.4} \left(\frac{144}{778} \right) = 0.4 \text{ Btu/lb}_m \quad .$$

Also assuming that the gas phase is air ($M = 28.97$) and that $T_1 = 50^\circ\text{F} = 510^\circ\text{R}$, then we obtain

$$\frac{\bar{R}T_1}{M} \ln \left(\frac{p_1}{p_2} \right) = \frac{1545(510)}{28.97(778)} \ln \left(\frac{150}{15} \right) = 84 \text{ Btu/lb}_m \quad .$$

Therefore, $v(p_1 - p_2)$ is small compared with $(\bar{R}T_1/M) \ln(p_1/p_2)$ and can be neglected. Eq. F-34 then becomes

$$\frac{V_2^2}{2} = \frac{x\bar{R}T_1}{M} \ln \left(\frac{p_1}{p_2} \right) + v(p_1 - p_2) \quad . \quad (F-35)$$

Thus,

$$V_2 = \left[2x \frac{\bar{R}T_1}{M} \ln \left(\frac{p_1}{p_2} \right) + 2v(p_1 - p_2) \right]^{1/2} \quad . \quad (F-36)$$

Elliott used this equation to define his ideal liquid exit velocity. He further defined a nozzle efficiency as the ratio of the two-phase liquid kinetic energy to the ideal liquid kinetic energy. Therefore,

$$\eta = \frac{\frac{1}{2} M_\ell (V_\ell)_e^2}{\frac{1}{2} M_\ell V_2^2} = \frac{(V_\ell)_e^2}{V_2^2} \quad . \quad (F-37)$$

Sample Calculations:

For test #39, $M_\ell = 0.217$ lb/sec, $x = 12.42\%$, $T_1 = 534^\circ\text{R}$, $p_1 = 79.0$ psia, $p_e = 12.9$ psia, and $(V_1)_e = 79.50$ ft/sec. From Eq. F-36,

$$V_2 = [2(0.1242)(53.35)(534)(32.2)\ln(79/12.9) \\ + 2(32.2)(144)(0.01616)(79-12.9)]^{1/2} ,$$

where

$$\bar{R}/M = R_{\text{air}} = \text{gas constant for air} = 53.35 \text{ ft}\cdot\text{lb}_f/\text{lb}_m\cdot^\circ\text{R} .$$

Conversion factors:

$$1 \text{ lb}_f\text{-sec}^2 = 32.2 \text{ ft lb}_m$$

$$1 \text{ ft}^2 = 144 \text{ in.}^2$$

$$V_2 = (41.3 \times 10^4 + 1.01 \times 10^4)^{1/2}$$

$$V_2 = 643 \text{ ft/sec}$$

$$\eta = (V_e)^2 / (V_2)^2$$

$$\eta = \frac{(79.50)^2}{(643)^2}$$

$$\eta = 0.0153 = 1.53\% .$$

APPENDIX G
CRITICAL MASS VELOCITY

The following is a derivative of the equation for the critical mass velocity for a single-phase compressible fluid.

The continuity equation is

$$M = AV/v \quad , \quad (G-1)$$

where

v = specific volume.

But

$$G = M/A = V/v \quad , \quad (G-2)$$

where

G = mass velocity = $\text{lb}_m/\text{ft}^2\text{-sec}$

or

$$V = Gv \quad . \quad (G-3)$$

Differentiation of Eq. G-3 with respect to p yields

$$\frac{dV}{dp} = (v) \frac{dG}{dp} + G \frac{dv}{dp} \quad . \quad (G-4)$$

But, at the maximum mass velocity, G does not change with increasing p . Therefore,

$$\frac{dG}{dp} = 0 \quad (G-5)$$

and

$$\frac{dV}{dp} = G_c \left(\frac{dv}{dp} \right) \quad , \quad (G-6)$$

where

G_c = critical mass velocity for a single-phase compressible fluid.

The mechanical energy balance can be written as

$$\frac{g}{g_c} dz + dF + \frac{V}{g_c}(dV) + v(dp) = dW \quad . \quad (G-7)$$

For no elevation change, friction losses, or shaft work,

$$\frac{V}{g_c}(dV) + v(dp) = 0 \quad (G-8)$$

or

$$\frac{dV}{dp} = -\frac{v}{V} g_c \quad . \quad (G-9)$$

Substitution into Eq. G-6 yields

$$\frac{-v}{V} g_c = G_c \frac{dv}{dp} \quad ; \quad (G-10)$$

but

$$G = V/v \quad .$$

Therefore,

$$G_c = \left[-g_c \left(\frac{dp}{dv} \right) \right]^{1/2} \quad . \quad (G-11)$$

For the homogeneous model,

$$G_H = \left[-g_c \left(\frac{dp}{dv} \right) \right]^{1/2} \quad , \quad (G-12)$$

where

$$v = (1 - x)v_\ell + xv_g \quad . \quad (G-13)$$

For calculation purposes, Eq. G-12 can be approximated by

$$G_H = \left[-g_c \left(\frac{\Delta P}{\Delta v} \right) \right]^{1/2} \quad . \quad (G-14)$$

The homogeneous mass velocity will now be calculated for test run #6 for which $M_{\ell} = 0.500$ lb/sec, $x = 3.42$ per cent, $t_{avg} = 68^{\circ}\text{F}$, and $p_t = 52.8$ psia. This will be done by calculating $\Delta p/\Delta v$ as the fluid passes through the throat region for a change in pressure from 51.8 to 53.8 psia. Thus, determining v_{ℓ} from the steam tables, v_g from the perfect gas law, and v from Eq. G-14, we find

p (psia)	51.8	53.8
v_{ℓ} (lb_m/ft^3) ⁻¹	0.017288	0.017308
v_g (lb_m/ft^3) ⁻¹	3.7764	3.6360
v (lb_m/ft^3) ⁻¹	0.145850	0.141067

$$\Delta p = 53.8 - 51.8 = 2 \text{ psia}$$

$$\Delta v = 0.141067 - 0.145850 = -0.004783 \text{ ft}^3/\text{lb}_m$$

Substitution into Eq. G-14 gives

$$G_H = \left[\frac{(-32.2)(2)(144)}{-0.004783} \right]^{1/2} = 1380 \text{ lb}_m/\text{ft}^2\text{-sec}$$

The area at the throat section is $0.236 \times 10^{-3} \text{ ft}^2$. Therefore, the measured mass velocity is

$$G_m = \frac{M}{A} = \frac{0.500}{0.236 \times 10^{-3}} = 2119 \text{ lb}_m/\text{ft}^2\text{-sec.}$$

At the throat, at $p_t = 52.8$ psia,

$$v_{\ell} = 0.017298 \text{ ft}^3/\text{lb}_m$$

$$v_g = 3.7049 \text{ ft}^3/\text{lb}_m$$

$$\Delta v_g = 3.6360 - 3.7764 = 0.1404 \text{ ft}^3/\text{lb}_m$$

$$\Delta v = 0.017308 - 0.017288 = 0.000020 \text{ ft}^3/\text{lb}_m$$

$$\frac{\Delta v_g}{\Delta p} = \frac{-0.1404}{2} = -0.0702$$

$$\frac{\Delta v_{\ell}}{\Delta p} = \frac{0.000020}{2} = 0.000010$$

Therefore, by the Fauske model, with the aid of Eq. 29 we find

$$k = \left(\frac{v_g}{v_l} \right)^{1/2} = \left(\frac{3.7049}{0.017298} \right)^{1/2} = 14.63 \quad .$$

For a constant-quality system Eq. 28 becomes

$$G_F = \left[\frac{-g_c k}{[(1-x+kx)x] dv_g/dp + [1+x(k-2) - x^2(k-1)] (k) dv_l/dp} \right]^{1/2}$$

Approximating

$$\frac{dv_g}{dp} \text{ by } \frac{\Delta v_g}{\Delta p}$$

and

$$\frac{dv_l}{dp} \text{ by } \frac{\Delta v_l}{\Delta p} \quad ,$$

we find

$$G_F = \left[\frac{-(32.2)(144)(14.63)}{[1 - 0.0342 + 14.63(0.0342)] (0.0342)(-0.0702) + [1 + 0.0342(12.63) - (0.0342)^2(13.63)] (14.63)(0.000010)} \right]^{1/2}$$

$$= 6950 \text{ lb}_m/\text{ft}^2\text{-sec} \quad .$$

APPENDIX H
TABULATED DATA AND RESULTS

Tables 1 through 39 contain the tabulated data required to calculate water velocity, slip ratio and acceleration factor. Void fractions were measured only at positions: i, 3, t, 9, and e for runs 1 through 21, and only at the nozzle exit (e) for runs 22 through 39. The pressure profile along the nozzle length was recorded for all runs except 22, 23, 27, 30, 31, and 32.

Table 40 represents mass velocities for various test runs and shows a comparison of the experimentally measured mass velocities to those calculated by the homogeneous and Fauske models.

Table 41 shows the nozzle efficiencies for all tests. The efficiency was calculated based on Elliotts' homogeneous model.

Table 1. Run No. 1; $M \ell$, 0.500 lb/sec; x, 0.96%

Pos.	p psia	p/p _i	t F	α	V _W ft/sec	k	A _F
i	38.4	1.000	62.5	0.462	2.74	3.54	
2	40.7	1.000					
3	39.1	1.000		0.392	9.37	4.64	
4	37.7	0.982					
5	34.5	0.989					
t	19.9	0.518		0.473	64.80	6.50	1.91
7	17.7	0.461					
8	14.3	0.372					
9	12.4	0.323		0.760	94.40	2.97	
10	12.9	0.336					
11	13.3	0.346					
12	14.1	0.367					
e	14.7	0.383	64.5	0.745	23.10	2.72	3.93

Table 2. Run No. 2; M_ℓ , 0.500 lb/sec; x , 1.47%

Pos.	P psia	p/P _i	t F	α	V _W ft/sec	k	A _F
i	48.4	1.000	61.0	0.544	3.18	3.10	
2	49.1	1.000					
3	48.3	0.998		0.405	9.60	5.42	
4	47.3	0.977					
5	44.0	0.909					
t	26.6	0.550		0.539	73.80	5.71	
7	22.6	0.467					
8	16.9	0.350					
9	12.9	0.267		0.770	98.70	4.15	
10	12.6	0.261					
11	13.2	0.273					
12	13.8	0.285					
e	14.6	0.301	62.0	0.773	25.85	3.60	4.40

Table 3. Run No. 3; M_ℓ , 0.505 lb/sec; x , 1.91%

Pos.	P psia	p/P _i	t F	α	V _W ft/sec	k	A _F
i	59.9	1.000	63.5	0.590	3.63	2.73	
2	60.6	1.000					
3	60.0	1.000		0.422	9.97	5.39	
4	58.0	0.968					
5	54.6	0.911					
t	33.8	0.564		0.640	95.70	3.92	
7	28.2	0.471					
8	21.2	0.354					
9	14.7	0.245		0.795	112.00	4.13	
10	12.7	0.212					
11	13.1	0.218					
12	13.9	0.232					
e	14.8	0.247	65.5	0.801	29.74	3.96	5.02

Table 4. Run No. 4; M_l , 0.495 lb/sec; x , 2.44%

Pos.	p psia	p/Pi	t F	α	V_W ft/sec	k	A_F
i	68.6	1.000	69.0	0.584	3.51	3.17	
2	70.1	1.000					
3	69.5	1.000		0.450	10.25	5.37	
4	67.4	0.983					
5	63.3	0.923					
t	39.5	0.576		0.661	99.50	3.96	
7	33.3	0.485					
8	24.5	0.357					
9	16.4	0.239		0.810	118.50	4.36	
10	12.3	0.179					
11	12.6	0.184					
12	13.5	0.197					
e	14.6	0.213	70.0	0.861	41.68	3.39	7.18

Table 5. Run No. 5; M_l , 0.495 lb/sec; x , 2.92%

Pos.	p psia	p/Pi	t F	α	V_W ft/sec	k	A_F
i	76.9	1.000	65.0	0.648	4.14	2.58	
2	78.8	1.000					
3	77.6	1.000		0.485	10.95	4.98	
4	75.9	0.988					
5	71.5	0.930					
t	45.1	0.586		0.680	105.00	3.81	
7	37.6	0.489					
8	27.4	0.356					
9	17.5	0.228		0.800	112.00	5.20	
10	12.0	0.157					
11	11.9	0.155					
12	12.8	0.167					
e	14.2	0.185	67.0	0.870	44.70	3.83	7.69

Table 6. Run No. 6; M_ℓ , 0.500 lb/sec; x , 3.42%

Pos.	p psia	p/P _i	t F	α	V _W ft/sec	k	A _F
i	89.5	1.000	67.0	0.685	4.67	2.21	
2	91.1	1.000					
3	89.6	1.000		0.568	13.20	3.65	
4	87.2	0.974					
5	83.5	0.933					
t	52.8	0.590		0.698	112.50	3.52	
7	43.0	0.480					
8	32.2	0.360					
9	20.8	0.232		0.774	100.20	6.03	
10	13.0	0.145					
11	11.5	0.129					
12	12.4	0.139					
e	14.1	0.158	69.0	0.180	30.80	7.18	5.24

Table 7. Run No. 7; M_ℓ , 0.490 lb/sec; x , 4.00%

Pos.	p psia	p/P _i	t F	α	V _W ft/sec	k	A _F
i	96.1	1.000	69.5	0.730	5.37	1.95	
2	98.7	1.000					
3	96.7	1.000		0.605	14.18	3.44	
4	93.2	0.970					
5	89.5	0.930					
t	56.9	0.592		0.718	118.50	3.51	3.56
7	47.5	0.495					
8	35.8	0.372					
9	22.4	0.233		0.757	91.80	7.35	
10	13.6	0.142					
11	11.4	0.119					
12	12.1	0.126					
e	14.1	0.147	70.5	0.795	28.10	9.40	4.88

Table 8. Run No. 8; M_{ℓ} , 0.700 lb/sec; x , 0.56%

Pos.	p psia	p/p _i	t F	α	V _W ft/sec	k	A _F
i	47.0	1.000	70.0	0.311	2.99	3.32	
2	47.7	1.000					
3	46.9	0.996		0.308	11.60	3.36	
4	44.7	0.953					
5	40.3	0.859					
t	18.6	0.396		0.485	92.40	4.02	1.94
7	16.6	0.353					
8	13.1	0.299					
9	11.9	0.253		0.512	65.30	5.63	
10	-	-					
11	12.3	0.262					
12	12.7	0.271					
e	13.7	0.292	71.0	0.684	26.00	2.35	3.16

Table 9. Run No. 9; M_{ℓ} , 0.698 lb/sec; x , 1.02%

Pos.	p psia	p/p _i	t F	α	V _W ft/sec	k	A _F
i	67.3	1.000	70.5	0.364	3.23	3.28	
2	68.2	1.000					
3	67.7	1.000		0.384	12.85	2.98	
4	64.1	0.954					
5	58.9	0.875					
t	31.6	0.470		0.568	109.80	3.02	2.32
7	27.3	0.405					
8	18.9	0.280					
9	13.2	0.196		0.514	65.20	9.04	
10	-	-					
11	11.9	0.177					
12	12.7	0.189					
e	13.7	0.204	71.5	0.735	30.80	3.28	3.76

Table 10. Run No. 10; M_l , 0.703 lb/sec; x , 1.43%

Pos.	p psia	p/p _i	t F	α	V _W ft/sec	k	A _F
i	83.7	1.000	69.0	0.434	3.67	2.76	
2	86.1	1.000					
3	84.6	1.000		0.423	13.90	2.84	
4	81.4	0.975					
5	75.7	0.905					
t	43.1	0.515		0.632	130.00	2.38	2.72
7	35.2	0.420					
8	25.7	0.307					
9	16.6	0.198		0.485	62.20	11.30	
10	-	-					
11	11.9	0.142					
12	12.6	0.151					
e	14.0	0.167	71.0	0.692	26.80	5.62	3.24

Table 11. Run No. 11; M_l , 0.703 lb/sec; x , 2.06%

Pos.	p psia	p/p _i	t F	α	V _W ft/sec	k	A _F
i	103.1	1.000	67.0	0.492	4.12	2.56	
2	106.1	1.000					
3	103.5	1.000		0.452	14.77	3.00	
4	100.0	0.970					
5	94.1	0.912					
t	55.0	0.533		0.675	149.00	2.24	3.12
7	49.7	0.480					
8	34.0	0.330					
9	20.6	0.200		0.502	64.50	12.37	
10	-	-					
11	11.5	0.112					
12	12.2	0.118					
e	13.9	0.135	69.0	0.680	26.00	8.69	3.14

Table 12. Run No. 12; M_{ℓ} , 0.300 lb/sec; x , 3.06%

Pos.	p psia	p/P _i	t F	α	V _W ft/sec	k	A _F
i	38.3	1.000	67.0	0.640	2.46	5.65	
2	39.5	1.000					
3	39.0	1.000		0.463	6.38	11.37	
4	38.5	1.000					
5	35.9	0.937					
t	24.4	0.637		0.780	93.00	4.46	4.56
7	19.7	0.514					
8	16.8	0.439					
9	14.2	0.371		0.785	63.50	7.42	
10	-	-					
11	14.3	0.373					
12	14.8	0.386					
e	15.3	0.400	67.5	0.830	20.70	5.15	5.87

Table 13. Run No. 13; M_{ℓ} , 0.302 lb/sec; x , 3.82%

Pos.	p psia	p/P _i	t F	α	V _W ft/sec	k	A _F
i	45.7	1.000	62.5	0.670	2.70	5.17	
2	46.5	1.000					
3	45.6	0.999		0.583	8.27	7.33	
4	44.9	0.984					
5	42.7	0.935					
t	28.4	0.622		0.839	127.50	2.39	6.21
7	23.4	0.513					
8	18.4	0.402					
9	13.2	0.289		0.845	88.60	6.65	
10	-	-					
11	13.4	0.294					
12	14.2	0.311					
e	14.8	0.324	63.5	0.826	20.60	6.85	5.81

Table 14. Run No. 14; M_{ℓ} , 0.305 lb/sec; x , 4.84%

Pos.	p psia	p/p _i	t F	α	V _W ft/sec	k	A _F
i	56.7	1.000	66.0	0.685	2.85	5.20	
2	57.2	1.000					
3	56.7	1.000		0.628	9.34	6.72	
4	55.8	0.985					
5	52.9	0.934					
t	35.3	0.624		0.865	154.00	2.83	7.42
7	29.0	0.512					
8	22.3	0.393					
9	15.0	0.265		0.850	92.30	7.55	
10	-	-					
11	11.6	0.205					
12	13.5	0.238					
e	14.5	0.256	70.0	0.804	18.30	10.78	5.11

Table 15. Run No. 15; M_{ℓ} , 0.310 lb/sec; x , 5.87%

Pos.	p psia	p/p _i	t F	α	V _W ft/sec	k	A _F
i	65.9	1.000	70.0	0.738	3.48	4.10	
2	67.1	1.000					
3	66.4	1.000		0.652	10.15	6.13	
4	63.8	0.970					
5	62.2	0.946					
t	40.2	0.610		0.860	151.00	3.08	7.17
7	33.5	0.509					
8	26.2	0.397					
9	17.0	0.258		0.870	108.50	6.69	
10	-	-					
11	11.9	0.181					
12	13.1	0.199					
e	14.3	0.217	70.0	0.796	17.80	13.60	4.90

Table 16. Run No. 16; M_l , 0.308 lb/sec; x , 6.84%

Pos.	p psia	p/P _i	t F	α	V _W ft/sec	k	A _F
i	74.1	1.000	72.0	0.743	3.55	4.20	
2	76.6	1.000					
3	76.0	1.000		0.678	10.90	5.63	
4	73.8	0.995					
5	71.3	0.962					
t	46.8	0.633		0.878	173.00	2.67	8.25
7	38.4	0.518					
8	29.5	0.398					
9	18.8	0.254		0.902	143.00	5.17	
10	-	-					
11	10.6	0.143					
12	11.9	0.161					
e	13.7	0.185	72.5	0.795	17.60	16.90	4.87

Table 17. Run No. 17; M_l , 0.300 lb/sec; x , 8.17%

Pos.	p psia	p/P _i	t F	α	V _W ft/sec	k	A _F
i	81.8	1.000	72.5	0.780	4.00	3.77	
2	83.1	1.000					
3	82.8	1.000		0.656	9.89	6.90	
4	81.1	0.993					
5	77.4	0.946					
t	50.7	0.620		0.835	123.00	4.26	6.04
7	44.4	0.543					
8	31.7	0.388					
9	20.3	0.248		0.888	111.00	7.40	
10	-	-					
11	10.2	0.125					
12	11.5	0.141					
e	13.4	0.164	71.0	0.795	17.10	21.00	4.85

Table 18. Run No. 18; M_{ℓ} , 0.300 lb/sec; x , 8.91%

Pos.	p psia	p/P _i	t F	α	V _W ft/sec	k	A _F
i	88.4	1.000	74.0	0.807	4.61	3.26	
2	90.0	1.000					
3	88.6	1.000		0.647	9.74	7.42	
4	87.6	0.993					
5	83.4	0.945					
t	54.2	0.612		0.810	108.00	5.21	5.3
7	44.9	0.508					
8	33.9	0.383					
9	21.5	0.243		0.890	124.00	6.93	
10	-	-					
11	9.9	0.112					
12	10.6	0.120					
e	12.8	0.145	73.5	0.795	17.20	24.20	4.88

Table 19. Run No. 19; M_{ℓ} , 0.502 lb/sec; x , 3.48%

Pos.	p psia	p/P _i	t F	α	V _W ft/sec	k	A _F
i	87.1	1.000	70.0	0.610	3.81	3.22	
2	89.6	1.000					
3	87.8	1.000		0.537	12.40	4.33	
4	84.8	0.964					
5	81.1	0.930					
t	50.9	0.585		0.752	138.00	2.85	4.05
7	42.1	0.483					
8	30.8	0.354					
9	19.5	0.224		0.798	113.00	5.72	
10	-	-					
11	11.5	0.132					
12	12.6	0.145					
e	14.1	0.162	70.0	0.745	23.10	10.68	3.91

Table 20. Run No. 20; M_{ℓ} , 0.700 lb/sec; x , 1.05%

Pos.	p psia	p/p _i	t F	α	V _W ft/sec	k	A _F
i	67.6	1.000	68.0	0.438	3.58	2.44	
2	68.7	1.000					
3	67.6	1.000		0.422	13.80	2.62	
4	65.0	0.962					
5	59.3	0.878					
t	31.5	0.466		0.540	103.80	3.49	2.18
7	28.2	0.418					
8	18.3	0.270					
9	12.6	0.187		0.469	59.80	11.60	
10	-	-					
11	11.6	0.172					
12	12.4	0.183					
e	13.6	0.201	68.0	0.750	32.90	3.18	3.98

Table 21. Run No. 21; M_{ℓ} , 0.305 lb/sec; x , 4.84%

Pos.	p psia	p/p _i	t F	α	V _W ft/sec	k	A _F
i	56.9	1.000	76.0	0.680	2.80	5.25	
2	58.0	1.000					
3	57.4	1.000		0.657	10.14	5.83	
4	55.5	0.972					
5	54.6	0.962					
t	34.5	0.606		0.817	113.50	3.19	2.07
7	28.7	0.509					
8	21.4	0.376					
9	14.6	0.257		0.819	76.40	9.65	
10	-	-					
11	12.3	0.217					
12	13.4	0.236					
e	14.4	0.254	73.0	0.852	24.10	7.67	6.70

Table 22. Run No. 22; M_l , 0.301 lb/sec; x , 10.15%

Pos.	p psia	p/Pi	t F	α	V_W ft/sec	k	A_F
i	102.5	1.000					
2							
3							
4							
5							
t							
7							
8							
9							
10							
11							
12							
e	12.1	0.118	71.5	0.925	47.20	8.50	13.30

Table 23. Run No. 23; M_l , 0.303 lb/sec; x , 9.60%

Pos.	p psia	p/Pi	t F	α	V_W ft/sec	k	A_F
i	98.5						
2							
3							
4							
5							
t							
7							
8							
9							
10							
11							
12							
e	12.4	0.126	69.5	0.867	26.8	15.95	7.52

Table 24. Run No. 24; $M \rho$, 0.158 lb/sec; x , 1.49%

Pos.	p psia	p/P _i	t F	α	V _W ft/sec	k	A _F
i	19.0	1.000					
2	18.1	0.954					
3	18.0	0.948					
4	17.4	0.917					
5	15.0	0.790					
t	14.5	0.763					
7	14.5	0.763					
8	14.4	0.757					
9	14.4	0.757					
10	14.9	0.785					
11	15.0	0.790					
12	-	-					
e	15.2	0.800	67.5	0.709	6.39	4.70	3.43

Table 25. Run No. 25; $M \rho$, 0.152 lb/sec; x , 2.27%

Pos.	p psia	p/P _i	t F	α	V _W ft/sec	k	A _F
i	20.0	1.000					
2	19.1	0.956					
3	19.0	0.950					
4	19.2	0.962					
5	18.2	0.910					
t	14.5	0.725					
7	14.5	0.725					
8	14.5	0.725					
9	14.5	0.725					
10	14.9	0.745					
11	14.9	0.745					
12	-	-					
e	15.2	0.761	68.0	0.756	7.31	5.68	4.07

Table 26. Run No. 26; M_l , 0.156 lb/sec; x , 3.11%

Pos.	p psia	p/P _i	t F	α	V _W ft/sec	k	A _F
i	23.9	1.000					
2	23.1	0.968					
3	22.6	0.947					
4	22.4	0.940					
5	21.4	0.898					
t	16.9	0.708					
7	14.5	0.607					
8	14.7	0.615					
9	14.5	0.607					
10	14.8	0.620					
11	14.8	0.620					
12							
e	15.1	0.633	69.0	0.805	9.40	6.40	5.13

Table 27. Run No. 27; M_l , 0.156 lb/sec; x , 4.05%

Pos.	p psia	p/P _i	t F	α	V _W ft/sec	k	A _F
i	26.6						
2							
3							
4							
5							
t							
7							
8							
9							
10							
11							
12							
e	15.8	0.595	66.0	0.790	8.73	8.30	4.77

Table 28. Run No. 28; M_l , 0.154 lb/sec; x , 6.14%

Pos.	p psia	p/P _i	t F	α	V _W ft/sec	k	A _F
i	35.1	1.000					
2	35.6	1.000					
3	34.6	0.987					
4	34.2	0.975					
5	32.5	0.927					
t	22.9	0.653					
7	18.7	0.534					
8	16.1	0.460					
9	13.6	0.388					
10	13.7	0.391					
11	14.2	0.405					
12	-	-					
e	14.7	0.420	70.0	0.805	9.27	12.30	5.12

Table 29. Run No. 29; M_l , 0.152 lb/sec; x , 7.88%

Pos.	p psia	p/P _i	t F	α	V _W ft/sec	k	A _F
i	42.1	1.000					
2	41.6	0.988					
3	41.6	0.988					
4	40.1	0.954					
5	39.6	0.940					
t	27.5	0.653					
7	23.0	0.546					
8	18.1	0.430					
9	13.1	0.312					
10	12.8	0.304					
11	13.5	0.321					
12	-	-					
e	14.5	0.344	69.0	0.877	14.50	9.52	8.10

Table 30. Run No. 30; M_ℓ , 0.158 lb/sec; x , 10.3%

Pos.	p psia	p/p _i	t F	α	V _W ft/sec	k	A _F
i	44.7						
2							
3							
4							
5							
t							
7							
8							
9							
10							
11							
12							
e	14.9	0.331	68.5	0.917	22.30	8.35	12.00

Table 31. Run No. 31; M_ℓ , 0.155 lb/sec; x , 14.3%

Pos.	p psia	p/p _i	t F	α	V _W ft/sec	k	A _F
i	64.6						
2							
3							
4							
5							
t							
7							
8							
9							
10							
11							
12							
e	13.7	0.212	73.5	0.950	36.60	7.74	20.10

Table 32. Run No. 32; M_ℓ , 0.151 lb/sec; x , 14.3%

Pos.	p psia	p/P _i	t F	α	V _W ft/sec	k	A _F
i	64.6						
2							
3							
4							
5							
t							
7							
8							
9							
10							
11							
12							
e	13.7	0.212	71.5	0.969	57.4	4.83	32.4

Table 33. Run No. 33; M_ℓ , 0.218 lb/sec; x , 2.46%

Pos.	p psia	p/P _i	t F	α	V _W ft/sec	k	A _F
i	26.4	1.000					
2	25.6	0.970					
3	25.0	0.950					
4	24.9	0.944					
5	23.6	0.894					
t	17.8	0.675					
7	14.6	0.554					
8	14.8	0.561					
9	14.6	0.554					
10	15.0	0.568					
11	15.5	0.587					
12	-	-					
e	15.9	0.602	70.0	0.760	10.65	6.12	4.16

Table 34. Run No. 34; M_ℓ , 0.223 lb/sec; x , 3.31%

Pos.	P psia	p/P _i	t F	α	V _W ft/sec	k	A _F
i	33.6	1.000					
2	32.5	0.968					
3	31.5	0.940					
4	31.8	0.942					
5	29.6	0.870					
t	21.5	0.640					
7	17.7	0.527					
8	15.6	0.465					
9	14.0	0.416					
10	14.3	0.426					
11	14.8	0.440					
12	-	-					
e	15.1	0.450	70.0	0.802	13.23	6.85	5.05

Table 35. Run No. 35; M_ℓ , 0.218 lb/sec; x , 5.02%

Pos.	P psia	p/P _i	t F	α	V _W ft/sec	k	A _F
i	44.2	1.000					
2	43.6	0.989					
3	43.1	0.978					
4	42.1	0.955					
5	39.6	0.897					
t	28.1	0.636					
7	22.4	0.507					
8	18.4	0.417					
9	13.8	0.313					
10	13.4	0.303					
11	13.8	0.313					
12	-	-					
e	14.8	0.335	71.5	0.822	14.40	9.48	5.64

Table 36. Run No. 36; M_ℓ , 0.221 lb/sec; x , 6.72%

Pos.	P psia	P/P _i	t F	α	V _W ft/sec	k	A _F
i	53.8	1.000					
2	51.3	0.955					
3	51.1	0.950					
4	49.5	0.920					
5	48.0	0.894					
t	32.4	0.602					
7	27.6	0.513					
8	21.4	0.398					
9	14.5	0.270					
10	12.3	0.229					
11	13.4	0.249					
12	-	-					
e	14.9	0.277	70.0	0.842	16.45	11.05	6.34

Table 37. Run No. 37; M_ℓ , 0.219 lb/sec; x , 8.25%

Pos.	p psia	p/P _i	t F	α	V _W ft/sec	k	A _F
i	61.6	1.000					
2	60.5	0.984					
3	59.9	0.973					
4	59.4	0.964					
5	56.1	0.912					
t	37.3	0.605					
7	31.6	0.572					
8	24.0	0.390					
9	15.9	0.258					
10	11.3	0.184					
11	12.1	0.196					
12	-	-					
e	14.2	0.231	70.5	0.914	29.9	7.21	11.60

Table 38. Run No. 38; M_l , 0.217 lb/sec; x , 10.20%

Pos.	p psia	p/Pi	t F	α	V_W ft/sec	k	A_F
i	73.3	1.000					
2	72.7	0.991					
3	71.5	0.977					
4	69.5	0.950					
5	68.4	0.934					
t	44.0	0.601					
7	37.0	0.505					
8	27.3	0.373					
9	17.8	0.243					
10	11.1	0.153					
11	10.4	0.142					
12	-	-					
e	13.3	0.181	73.0	0.942	44.00	6.45	17.20

Table 39. Run No. 39; M_l , 0.217 lb/sec; x , 12.42%

Pos.	p psia	p/Pi	t F	α	V_W ft/sec	k	A_F
i	79.0	1.000					
2	78.6	0.997					
3	77.4	0.981					
4	76.5	0.970					
5	71.9	0.912					
t	48.5	0.615					
7	39.7	0.503					
8	30.4	0.386					
9	19.5	0.247					
10	11.6	0.147					
11	9.6	0.122					
12	-	-					
e	12.9	0.164	74	0.968	79.50	4.47	14.90

Table 40. Mass Velocities

Run No.	M_{ℓ} lb/sec	X %	Pt psia	G_M lb/ft ² -sec	G_H lb/ft ² -sec	G_F lb/ft ² -sec
1	0.500	0.96	19.9	2119	990	4400
3	0.505	1.91	33.8	2140	1200	
6	0.500	3.42	52.8	2119	1380	6950
9	0.698	1.02	31.6	2960	1546	
13	0.302	3.82	28.4	1280	710	2380
16	0.308	6.84	46.8	1305	876	
20	0.700	1.05	31.5	2960	1500	4960
24	0.158	1.49	14.5	645	578	
26	0.156	3.11	16.9	675	470	1800
29	0.152	7.88	27.5	645	476	
34	0.223	3.31	21.5	945	574	
37	0.219	8.25	37.3	928	626	
38	0.217	10.20	44.0	910	672	2600

Table 41. Nozzle Efficiencies Based on Elliott's Model

Run No.	M_ℓ lb/sec	X %	T_i °F _{abs}	P_i psia	P_e psia	V_ℓ ft/sec	V_2 ft/sec	η %
1	0.500	0.96	522.5	38.4	14.7	23.10	142	2.56
2	0.500	1.47	521.0	48.4	14.6	25.85	192	1.83
3	0.505	1.91	523.5	59.9	14.8	29.74	235	1.61
4	0.495	2.44	529.0	68.6	14.6	41.68	276	2.28
5	0.495	2.92	525.0	76.9	14.2	44.70	314	2.00
6	0.500	3.42	527.0	89.5	14.1	30.80	354	0.76
7	0.490	4.00	529.5	96.1	14.1	28.10	390	0.52
8	0.700	0.56	530.0	47.0	13.7	26.00	161	2.62
9	0.698	1.02	530.5	67.3	13.7	30.80	194	2.50
10	0.703	1.43	529.0	83.7	14.0	26.80	238	1.28
11	0.703	2.06	527.0	103.1	13.9	26.00	297	0.87
12	0.300	3.06	527.0	38.3	15.3	20.70	233	0.79
13	0.302	3.82	522.5	45.7	14.8	20.60	287	0.52
14	0.305	4.84	526.0	56.7	14.5	18.30	353	0.27
15	0.310	5.87	530.0	65.9	14.3	17.80	411	0.18
16	0.308	6.84	532.0	74.1	13.7	17.60	471	0.14
17	0.300	8.17	532.5	81.8	13.4	17.10	530	0.10
18	0.300	8.91	534.0	88.4	12.8	17.20	567	0.09
19	0.502	3.48	530.0	87.1	14.1	23.10	356	0.43
20	0.700	1.05	528.0	67.6	13.6	32.90	196	2.80
21	0.305	4.84	536.0	56.9	14.4	24.10	356	0.46
22	0.301	10.15	531.5	102.5	12.1	47.20	632	0.56
23	0.303	9.60	529.5	98.5	12.4	26.80	605	0.19
24	0.158	1.49	527.5	19.0	15.2	6.39	81	0.62
25	0.152	2.27	528.0	20.0	15.2	7.31	109	0.45
26	0.156	3.11	529.0	23.9	15.1	9.40	165	0.33
27	0.156	4.05	526.0	26.6	15.8	8.73	200	0.19
28	0.154	6.14	530.0	35.1	14.7	9.27	316	0.09
29	0.152	7.88	529.0	42.1	14.5	14.50	396	0.14
30	0.158	10.30	528.5	44.7	14.9	22.30	555	0.16
31	0.155	14.30	533.5	64.6	13.7	36.60	638	0.34
32	0.151	14.30	531.5	64.6	13.7	57.40	638	0.81
33	0.218	2.46	530.0	26.4	15.9	10.65	155	0.47
34	0.223	3.31	530.0	33.6	15.1	13.23	225	0.35
35	0.218	5.02	531.5	44.2	14.8	14.40	322	0.20
36	0.221	6.72	530.0	53.8	14.9	16.45	403	0.18
37	0.219	8.25	530.5	61.6	14.2	29.90	478	0.40
38	0.217	10.20	533.0	73.3	14.3	44.00	560	0.63
39	0.217	12.42	534.0	79.0	12.9	79.50	643	1.53

BIBLIOGRAPHY

1. Elliott, D. G., A Two-fluid Magnetohydrodynamic Cycle for Nuclear-Electric Power Conversion, California Institute of Technology JPL-TR-32-116 (June 30, 1961).
2. McManus, H. N., Jr., An Experimental Investigation of Film Characteristics in Horizontal Annular Two-phase Flow, ASME Publication No. 57-A-144 (1957).
3. Griffith, P., Clark, J. A., and Rohsenow, W. M., Void Volumes in Sub-cooled Boiling Systems, Office of Naval Research, N5 ori-07894-TR-12 (1958).
4. Johnson, H. A., and Abou-Sabe, A. H. A., Heat Transfer and Pressure Drop for Turbulent Flow of Air-Water Mixtures in a Horizontal Pipe, ASME Trans., 74, 977-987 (1952).
5. Petrick, M., Two-phase Air-Water Flow Phenomena, ANL-5787 (March 1958).
6. Richardson, B. L., Some Problems in Horizontal Two-phase Two-component Flow, ANL-5949 (1959).
7. Reese, B. A., and Richard, L. P., Equilibrium between Phases in Converging-Diverging Nozzles, American Rocket Society Reprint No. 1714-61, presented at ARS Propellants, Combustion and Liquid Rockets Conference, Palm Beach, Florida (April 26-28, 1961).
8. Richard, L. P., The Effect of Initially Large Internal Temperature Difference, and Condensibility of the Gas on the Exit Velocity for Two-phase Flow of a Liquid and a Gas in a Nozzle, Unpublished Masters Thesis, Purdue University (Aug 1959).
9. Elliott, D. G., Comparison between Single Component and Two-component Two-phase Magnetohydrodynamic Power Conversion System, Unpublished notes, Purdue Jet Propulsion Laboratory (Nov 9, 1962).
10. Neusen, L. F., Optimizing of Flow Parameters for the Expansion of Very Low-quality Steam, UCRL-6152 (Jan 25, 1962).
11. Maneely, D. J., A Study of the Expansion Process of Low-quality Steam through a De-Laval Nozzle, UCRL-6230 (Jan 25, 1962).

12. Brown, R. A., Flashing Expansion of Water through a Converging-Diverging Nozzle, UCRL-6665-T (Oct 24, 1961).
13. Fiedler, R. A., Shock Location during Two-phase Flow in an Overexpanded Nozzle, UCRL-6678 (Nov 1, 1961).
14. Hering, R., and Vogrin, J. A., Two-phase Air-Water Study in a Converging-Diverging Nozzle, Unpublished ANL paper.
15. Muir, J. F., and Eichhorn, R., Compressible Flow of an Air-Water Mixture through a Vertical, Two-dimensional Converging-Diverging Nozzle, Report #FLD 10, M.E. Dept., Princeton University, Princeton, N. J. (March 1, 1963).
16. Fluid Meters, Their Theory and Application, ASME Research Publication, 5th Edition (1959).
17. Keenan, J. H., and Keyes, F. G., Thermodynamic Properties of Steam, 1st Edition, John Wiley and Sons, Inc., New York (April 1957).
18. Alves, G. E., Co-current Liquid-Gas Flow in a Pipe-line Conductor. Chem. Eng. Progress, 50, 449 (1954).
19. Sofer, G. A., Fog Coolant Technology and Its Application to Nuclear Reactors, Design Eng., 1464 (April 20, 1962).
20. Faletti, D. W., and Moulton, R. W., Two-phase Critical Flow of Steam-Water Mixtures, A.I.Ch.E. J., 247-253 (March 1963).
21. Fauske, H. K., Contribution to the Theory of Two-phase, One-component Critical Flow, ANL-6633 (Oct 1962).
22. Hooker, H. H., and Popper, G. F., A Gamma-ray Attenuation Method for Void Fraction Determination in Experimental Boiling Heat Transfer Facilities, ANL-5766 (Nov 1958).
23. Grodstein, G. W., X-ray Attenuation Coefficients from 10 Kev to 100 Mev, National Bureau of Standards Publication No. 583.
24. Haywood, R. W., Knights, G. A., Middleton, G. E., and Thorn, J. R. S., Experimental Study of the Flow Conditions and Pressure Drop of Steam-Water Mixtures at High Pressures in Heated and Unheated Tubes, Paper presented at the Institution of Mechanical Engineers (March 1961).

25. Schwarz, K., Investigation of the Distribution of Specific Gravity, The Water and Steam Velocities and the Frictional Pressure Drop in Vertical and Horizontal Boiler Tubes, V.D.I., Forschung auf dem Gebiete des Ingenieurwesens. V.D.I. Forschungs B.20, No. 445, P. I. (1954).
26. Petrick, M., A Study of Vapor Carryunder and Associated Problems, ANL-6581 (July 1962).
27. Zucrow, M. J., Aircraft and Missile Propulsion. 1st Edition, John Wiley and Sons, Inc., New York (1958).

NOMENCLATURE

Symbol	Description	Units	Symbol	Description	Units
A	Total cross-sectional area	in. ²	P _R	Pressure ratio, P _{exit} /P _{inlet}	-
A _g	Gaseous portion of total cross-sectional area	in. ²	r	Radius of cross section	in.
A _F	Average cross-sectional acceleration factor	-	t	Temperature	F
A _l	Liquid portion of total cross-sectional area	in. ²	T	Temperature	Fabs
c	Mass absorption coefficient	in. ² -lb ⁻¹	V	Average cross-sectional velocity	ft-sec ⁻¹
E	Electronic recorder reading for a two-phase mixture	mv	V _H	Homogeneous nozzle exit velocity	ft-sec ⁻¹
E _g	Electronic recorder reading for gaseous phase only	mv	v	Specific volume	ft ³ -lb _m ⁻¹
E _l	Electronic recorder reading for liquid phase only	mv	x	Quality - ratio of gaseous mass to total mixture mass	-
G	Mass velocity	lb _m -ft ⁻² -sec ⁻¹	y	A measurement of distance or thickness	in.
G _c	Critical mass velocity	lb _m -ft ⁻² -sec ⁻¹	Greek Symbols		
G _F	Critical mass velocity predicted by Fauske	lb _m -ft ⁻² -sec ⁻¹	α	Average cross-sectional void fraction	-
G _H	Homogeneous model mass velocity	lb _m -ft ⁻² -sec ⁻¹	α	Actual cross-sectional void fraction	-
G _m	Measured mass velocity	lb _m -ft ⁻² -sec ⁻¹	α _y	Average local void fraction at a position y	-
g _c	Gravitational constant	ft-lb _m -lb _f ⁻¹ -sec ⁻²	η	Nozzle efficiency	-
H	Manometer Height	in.	μ	Linear absorption coefficient	in. ⁻¹
I	Intensity of radiation at a position y	r-hr ⁻¹	ρ	Density	lb _m -ft ⁻³
I ₀	Intensity of radiation at a position y = 0	r-hr ⁻¹	τ	Time	sec
k	Average cross-sectional slip ratio	-	φ(y)	Thickness of gas phase at a position y	in.
K	Instrumentation constant	-	ψ(y)	Thickness of mixture at a position y	in.
M	Total mass flow rate - liquid plus gaseous mass rate of flow	lb-sec ⁻¹	Subscripts		
M _g	Mass rate of flow of gas	lb-sec ⁻¹	e	Refers to nozzle exit location	
M _l	Mass rate of flow of liquid	lb-sec ⁻¹	g	Refers to gaseous phase	
p	Pressure	psia	i	Refers to nozzle inlet condition	
			l	Refers to liquid phase	
			n	Nozzle location	
			t	Refers to nozzle throat condition	
			2,3,4,5, 7,8,9,10, 11,12	Refer to a specific location along the nozzle length as shown in Fig. 3	

ARGONNE NATIONAL LAB WEST



3 4444 0008831 0

X